

**SYNTHESIS, CHARACTERIZATION AND STUDIES OF
COBALT CORROLES**

Thesis Submitted to the **Delhi Technological University**

for the Award of the Degree of

DOCTOR OF PHILOSOPHY

IN

CHEMISTRY

By

JYOTI

(2K18/Ph.D/AC/02)

Under the Supervision of

Prof. SUDHIR G. WARKAR

and

Prof. ANIL KUMAR



DEPARTMENT OF APPLIED CHEMISTRY

DELHI TECHNOLOGICAL UNIVERSITY

Delhi-110042 (INDIA)

2023

©DELHI TECHNOLOGICAL UNIVERSITY-2023
ALL RIGHTS RESERVED

This Thesis is dedicated

To my Parents

Mr. and Mrs. Dalal

To my siblings

Asha & Devender

To my Husband

Mr. Samit Malik

*Thanks for your endless sacrifices, love, support and
prayers*



**DEPARTMENT OF APPLIED CHEMISTRY
DELHI TECHNOLOGICAL UNIVERSITY
Delhi-110042 (INDIA)**

DECLARATION

I declare that the research work reported in the thesis entitled “**Synthesis, Characterization and Studies of Cobalt Corroles**” for the award of degree of *Doctoral of Philosophy* in Chemistry has been carried out by me under the supervision of **Prof. Sudhir G. Warkar** and **Prof. Anil Kumar**, Department of Applied Chemistry, Delhi Technological University, India.

The research work embodied in this thesis, except where otherwise indicated, is my original research. This thesis has not been submitted by me in part or full to any other University for the award of any degree or diploma. This thesis does not contain other person's data, graphs or other information, unless specifically acknowledged.

Jyoti

Candidate

2K18/Ph.D/AC/02

Prof. Sudhir G. Warkar

Supervisor

Prof. Anil Kumar

Co-Supervisor

Prof. Anil Kumar

Head of Department

Applied Chemistry, DTU



**DEPARTMENT OF APPLIED CHEMISTRY
DELHI TECHNOLOGICAL UNIVERSITY
Delhi-110042 (INDIA)**

CERTIFICATE

This is to certify that the Ph.D. thesis entitled “**Synthesis, Characterization and Studies of Cobalt Corroles**” submitted to Delhi Technological University, Delhi, for the award of Doctoral of Philosophy in Chemistry, is based on original research work carried out by me, under the supervision of **Prof. Sudhir G. Warkar** and **Prof. Anil Kumar**, Department of Applied Chemistry, Delhi Technological University, Delhi, India. It is further certified that the work embodied in this thesis has neither partially or fully submitted to any other university or institution for the award of any degree or diploma.

Jyoti

Candidate

2K18/Ph.D/AC/02

This is to certify that the above statement made by the candidate is correct to the best of our knowledge.

Prof. Sudhir G. Warkar

Supervisor

Prof. Anil Kumar

Co-Supervisor

Prof. Anil Kumar

Head of Department

Applied Chemistry, DTU

ACKNOWLEDGEMENTS

This thesis is a compilation of my years of hard work, commitment, and discipline towards research. A lot of people helped me get over this obstacle and made it possible for me to reach my goal. It fills my heart with unspeakable joy to express my gratitude to everyone who contributed in one way or another to the successful accomplishment of my Ph.D. thesis.

First and foremost, I would like to express my sincere gratitude to my research supervisors, **Prof. Sudhir G. Warkar** and **Prof. Anil Kumar**, for their consistent guidance and encouragement throughout my PhD. I can't thank them enough for their continuous support, valuable comments, suggestions, and vast expertise in making this research meaningful. I found great value in the way that they have guided me in both my professional and personal lives. This experience of finishing the research work under their supervision has been tremendously rewarding and will undoubtedly assist me in achieving my goals in the years to come.

I am grateful to **Prof. Yogesh Singh**, former Honourable Vice-Chancellor, and **Prof. S. Indu**, Honourable Vice-Chancellor, Delhi Technological University, for providing all the facilities to carry out this research. Also, I thank **Prof. Archana Rani**, former Head, Department of Applied Chemistry, DTU, for providing me with the necessary help in my research work. I wish to express my sincere thanks to all the faculty members of the Department of Applied Chemistry at DTU for their assistance and support during my research work and professional growth. Also, I am thankful to the non-teaching staff of the Department of Applied Chemistry, DTU, particularly Mr. Raju, Mr. Umesh, and Mrs. Mohini.

I offer my sincere thanks to **Dr. Natalia Fridman**, Technion, Israel Institute of Technology, for helping me solve my crystal data and to **Prof. Muniappan Sankar**, IIT Roorkee, for allowing me to perform the CV experiment in his lab.

I would like to take this opportunity to express my gratitude to the Department of Chemistry, **Rajdhani College** and **Maharishi Dayanand University**. It is from these institutions that I received my graduate and postgraduate degrees, respectively. In addition, I would like to express my deepest gratitude and thankfulness to the **Council for Scientific and Industrial Research (CSIR)** for supplying financial help in the form of JRF and SRF.

My special thanks to Mange Ram Mangyan and Harendar Mor for their genuine care and endless moral support at DTU. This journey would not have been easier without them. I also offer my thanks to my labmates Sourav, Sachin, Shikha, Deepali, Indu, Ritika, and Atul.

I count myself extremely fortunate to have such wonderful people all around me who have consistently served as a ray of hope even at the worst moments of my life. I want to offer a particularly heartfelt thanks to my best friends, Dr. Ishana Kathuria, Deepak Yogi, Yogesh Gagneja, Sumit Kaushik and Shweta Malik, for their never-ending support and affection, which has always made me feel special and kept me going in difficult times.

I cannot find words to express my gratitude to my family. I am indebted to my parents for everything they have done for me. They have been a significant contributor to the success of my research career thus far. For my whole life, **Mr. Dharmpal Dalal**, my father, has been my true inspiration. He has been my source of a positive attitude

towards life. **Mrs. Sunita Dalal**, my mother, has always been an emotional support for me throughout my life. I especially thank her for wishing for such kind of education for me and raising me to be a kind person. My siblings, **Devender** and **Asha**, have always been a source of unconditional love and support for me.

I would like to heartiest thanks to my loving husband, **Mr. Samit Malik**. I appreciate his love, concern, and all kinds of support whenever I need it. I thank him for being patient during my tough time. My Ph.D. journey would have never been possible without his affection, care, and patience. Thank you so much for standing by my side as a helping hand when time gets more laborious. I am heartfully thankful to my in-laws for giving me moral support, encouragement, and time. They have brought a new source of strength and stability into my life.

Above all, I owe almighty God for answering my prayers, for providing me with divine guidance, wisdom, health and strength, and for being the source of everything. I am grateful for the person I am today and the person I may become tomorrow.

(Jyoti)

LIST OF ABBREVIATIONS

HER	:	Hydrogen evolution reaction
OER	:	Oxygen evolution reaction
ORR	:	Oxygen reduction reaction
HCl	:	Hydrochloric acid
DFT	:	Density functional theory
CV	:	Cyclic Voltammetry
UV-Vis	:	Ultra violet-visible
NMR	:	Nuclear magnetic resonance spectroscopy
HRMS	:	High resolution mass spectroscopy
HOMO	:	Highest occupied molecular orbital
LUMO	:	Lowest unoccupied molecular orbital
DCM	:	Dichloromethane
FMO	:	Frontier molecular orbital
LoD	:	Limit of detection
TLC	:	Thin layer chromatography
λ	:	Wavelength (nm)
QY	:	Quantum yield
μM	:	Micro molar
THF	:	Tetrahydrofuran

ϵ	:	Molar extinction coefficient
A	:	Absorbance
TPFCor	:	Tris(2,3,4,5,6-pentafluorophenyl)corrole
py	:	Pyridine
PPh ₃	:	Triphenylphosphine
TFA	:	Trifluoro acetic acid
E _{1/2}	:	Half wave potential
SHE	:	Simple Hydrogen Electrode
Co(tpfc)	:	Cobalt tripentafluorophenyl corrole

LIST OF CONTENTS

<i>Declaration</i>	<i>i</i>
<i>Certificate</i>	<i>ii</i>
<i>Acknowledgements</i>	<i>iii</i>
<i>List of Abbreviations</i>	<i>vi</i>
<i>List of Tables</i>	<i>xi</i>
<i>List of Schemes</i>	<i>xii</i>
<i>List of Figures</i>	<i>xiii</i>
<i>Abstract</i>	<i>xvi</i>
CHAPTER 1: INTRODUCTION.....	1-43
1.1. General Introduction	1
1.2. Sites of substitution.....	2
1.3. Cobalt corroles synthesis	3
1.4. Structure and spectral characterization of cobalt corroles	8
1.4.1 ¹ H-NMR Spectroscopy	8
1.4.2 UV-Visible Spectroscopy	9
1.4.3 X-Ray Crystallography	13
1.5. Applications of cobalt corroles	16
1.5.1. Oxygen Reduction Reaction	18
1.5.2. Hydrogen Evolution Reaction.....	21
1.5.3. Oxygen Evolution Reaction.....	25
1.5.4. Cobalt Corroles As Sensors	30
<i>References</i>	<i>35-43</i>
CHAPTER 2: SCOPE OF THE WORK	44-45

**CHAPTER 3: SYNTHESIS, STRUCTURAL CHARACTERIZATION AND
BINDING ABILITY OF A₂B COBALT(III) CORROLES WITH
PYRIDINE..... 46-73**

3.1. Introduction.....	46
3.2. Experimental section.....	47
3.2.1. Instrumentation	47
3.2.2. Binding Constant Determination	48
3.2.3. Chemicals.....	48
3.2.4. Synthesis	48
3.3. Results and discussion	58
3.3.1. Synthesis	58
3.3.2. NMR Spectroscopy	59
3.3.3. Single-crystal X-ray structure of Co-2	59
3.3.4. UV-Visible spectroscopy of Co-(1 to 5)	62
3.4. Conclusion	69
<i>References</i>	70-73

**CHAPTER 4: STUDY THE INTERACTION OF ANIONS WITH A₂B
COBALT CORROLES IN NON-AQUEOUS MEDIUM..... 74-95**

4.1. Introduction.....	74
4.2. Experimental section.....	74
4.3. Results and discussion	76
4.3.1. UV-Visible response of Co-(1-5) towards solvents.....	76
4.3.2. Colorimetric response of Co-(1-5) towards anions	79
4.3.3. UV-Visible response of Co-(1-5) towards anions	80
4.4. Limit of detection of Cyanide, Fluoride and Acetate Anions	89
4.5. Conclusion	92
<i>References</i>	94-95

**CHAPTER 5: ELECTROCHEMICAL AND THEORETICAL INSIGHTS OF
COBALT CORROLES..... 96-117**

5.1. Introduction.....	96
------------------------	----

5.2. Experimental section.....	97
5.2.1. Materials	97
5.2.2. Instrumentation	97
5.2.3. Synthesis of the Complexes	99
5.3. Result and discussion.....	101
5.3.1. Synthesis	101
5.3.2. NMR Spectroscopy	102
5.3.3. X-ray Crystallography	102
5.4. DFT studies.....	104
5.5. Electrochemistry	105
5.6. HER activity analysis.....	107
5.7. Conclusion	111
<i>References</i>	<i>112-117</i>
CHAPTER 6: CONCLUSION AND FUTURE PROSPECTS.....	118-119
6.1. Conclusion	188
6.2. Future prospects	119
<i>List of Publications</i>	<i>120</i>
<i>Conferences and Workshops</i>	<i>121</i>
<i>About the Author</i>	<i>122</i>

LIST OF TABLES

Table No.	Title	Page No.
3.1	Comparison of Selected bond distances (\AA) of Co-2 with previously reported dipyridine-cobalt corrole complexes.	62
3.2	UV-Vis spectral bands of Co-(1-5) in (a) 10^{-6} M DCM (b) 10^{-5} pyridine (c) 10^{-5} benzonitrile solution.	65
3.3	Pyridine binding constants for cobalt corroles in CH_2Cl_2 .	67
4.1	Binding constant and limit of detection for addition of different anion on position six of mono-pyridine cobalt corrole Co-1 , Co-3 and Co-4	84
4.2	UV-Visible spectral data of Co-(1) and Co-(3-4) summarizing λ_{max} values of initial and final steps of titration with anions.	85
4.3	UV-Visible spectra at 10^{-5} M concentration of the bis-X adducts in CH_3CN solvent of Co-(1) and Co-(3-4) .	90
5.1	Half wave and peak potentials of Co-(1-5) ($E_{1/2}$ or E_p (in V) vs SHE) for two oxidations and three reduction processes in CH_2Cl_2 containing 0.1 M TBAP.	110

LIST OF SCHEMES

Scheme No.	Title	Page No.
1.1	Synthesis of cobalt-corrole from Free base corrole and Co ^{II} salt.	4
1.2	Synthesis of free base corroles via the Biladiene-a,c route.	5
1.3	Synthesis of Triphenylphosphine ligated β -substitued cobalt corroles via [2+2] approach.	6
1.4	Synthesis of A ₂ B corrole.	7
1.5	The two and four-electron pathway of oxygen reduction reaction.	18
1.6	Catalytic Pathways followed by Co ^{III} -corroles during hydrogen evolution process.	22
1.7	Catalytic Pathways followed by Co ^{III} -corroles during Oxygen evolution process.	25
1.8	Vilsmeier reaction on cobalt corrole.	34
3.1	Synthetic route of A ₂ B cobalt corroles Co-(1 to 5) .	49
4.1	Schematic representation of transformation of Co-(1) and Co-(3-4) into bisX ⁻ -cobalt corrole adducts.	78
5.1	Synthesis scheme of (Co-6) .	100

LIST OF FIGURES

Figure No.	Title	Page No.
1.1	Schematic Presentation of cobalt incorporated (a) Co-corrin (b) Co-corrole and (c) Co-porphyrin and the aromatic pathway is highlighted in bold.	2
1.2	Sites of substitutions on Corrole macrocycle.	3
3.1	¹ H NMR spectrum of Co-1 in C ₆ D ₆ .	51
3.2	¹⁹ F NMR spectrum of Co-1 in C ₆ D ₆ .	51
3.3	HRMS spectra of Co-1 .	52
3.4	¹ H NMR spectrum of Co-2 in C ₆ D ₆ .	52
3.5	¹⁹ F NMR spectrum of Co-2 in C ₆ D ₆ .	53
3.6	HRMS spectra of Co-2 .	53
3.7	¹ H NMR spectrum of Co-3 in C ₆ D ₆ .	53
3.8	¹⁹ F NMR spectrum of Co-3 in C ₆ D ₆ .	54
3.9	HRMS spectra of Co-3	54
3.10	¹ H NMR spectrum of Co-4 in C ₆ D ₆ .	54
3.11	HRMS spectra of Co-4 .	55
3.12	¹ H NMR spectrum of Co-5 in CDCl ₃ .	55
3.13	HRMS spectra of Co-5 .	56
3.14	¹ H-NMR (room temperature, 400MHz) spectra of Co-(1 to 4) and Co-5 , recorded in C ₆ D ₆ and CDCl ₃ respectively.	60
3.15	¹⁹ F NMR (room temperature, 377 MHz) spectra of Co-(1 to 3) recorded in C ₆ D ₆ .	61
3.16	X-ray crystal structure of complex Co-2 (a) side view (b) top view.	61
3.17	Electronic absorption spectra of Co-(1 to 5) in (a) 10 ⁻⁶ M DCM (b) 10 ⁻⁴ M DCM (c) 10 ⁻⁵ pyridine solution.	64
3.18	UV-Vis spectra of Co-(1-5) in 10 ⁻⁵ M benzonitrile.	66
3.19	Titration of Co-(1 to 5) with pyridine. Hill plots for the binding constant analysis are shown in inset.	68

Figure No.	Title	Page No.
4.1	Tetrabutyl ammonium salts of anions (TBA ⁺ X ⁻) used for interaction.	75
4.2	UV-vis spectra of Co-(1-5) at 10 ⁻⁵ M in acetonitrile containing anions Cell path length = 10 dm.	82
4.3	The observed colour-change upon addition of 1.0 equivalent tetrabutylammonium salts of different anions into a solution of Co-(1-5) in acetonitrile. From left to right; A =Without anion, B =CN ⁻ , C = F ⁻ , D = CH ₃ COO ⁻ , E = Cl ⁻ , F = Br ⁻ , G = I ⁻ , H = NO ₃ ⁻ , I = H ₂ PO ₄ ⁻ , J = PF ₆ ⁻ , K = AsO ₃ ³⁻ , L = AsO ₄ ³⁻ , M = ClO ₄ ⁻ , N = S ²⁻ , O = HS ⁻ .	83
4.4	Left side: UV-Visible monitored titration of ~1×10 ⁻⁵ M Co-1 with CN ⁻ , F ⁻ and CH ₃ COO ⁻ in CH ₃ CN, Right side: Plot to determine the LOD value for Co-1 towards CN ⁻ , F ⁻ and CH ₃ COO ⁻ anions.	86
4.5	Left side: UV-Visible monitored titration of ~1×10 ⁻⁵ M Co-3 with CN ⁻ , F ⁻ and CH ₃ COO ⁻ in CH ₃ CN, Right side: Plot to determine the LOD value for Co-2 towards CN ⁻ , F ⁻ and CH ₃ COO ⁻ anions.	87
4.6	Left side: UV-Visible monitored titration of ~1×10 ⁻⁵ M Co-4 with CN ⁻ , F ⁻ and CH ₃ COO ⁻ in CH ₃ CN, Right side: Plot to determine the LOD value for Co-4 towards CN ⁻ , F ⁻ and CH ₃ COO ⁻ anions.	88
4.7	UV-Visible spectra at 10 ⁻⁵ M of the bis-X adducts in CH ₃ CN solvent of Co-(1-2) and Co-4 where X = CN ⁻ , F ⁻ , CH ₃ COO ⁻ ion at >10 equivalents.	91
5.1	¹ H NMR spectrum of Co-6 in CDCl ₃ .	100
5.2	¹⁹ F NMR spectrum of Co-6 in CDCl ₃ .	100
5.3	HRMS spectra of Co-6 .	101
5.4	X-ray single crystal structure of (Co-6), side (left) and top view (right).	101

Figure No.	Title	Page No.
5.5	HOMO-LUMO of Co-(1-5) .	103
5.6	Variation in HOMO-LUMO gap of Co-(1-5) .	104
5.7	Cyclic voltammograms of Co-(1-5) in DCM containing 0.1M TBAP and at scan rate of 100mV.	105
5.8	Reductive cyclic voltammetry of Co-3 in acetonitrile in the presence of 1.0–10.0 μ l of 10^{-3} M TFA with 0.1 M TBAP as the supporting electrolyte.	108
5.9	Titration of 10^{-3} M Co-3 at different conc. of trifluoroacetic acid.	108
5.10	(a) Reductive cyclic voltammetry of Co-3 in acetonitrile in the presence of 1.0–10.0 μ l of 10^{-3} M TFA with 0.1 M TBAP as the supporting electrolyte (b) Titration of 10^{-3} M Co-3 at different conc. of trifluoroacetic acid.	109

ABSTRACT

Corroles are synthetic and tetrapyrrolic systems that are frequently referred to as contracted porphyrins. In the past two decades, corroles have attracted a great deal of interest. These organic compounds have distinctive characteristics for undergoing metalation and, hence, co-ordinating to different metals. As a consequence, in the corrole cavity, several different metal ions across the periodic table covering the s, p, d, and f block elements have been introduced. Metallocorroles, because of their ease of synthesis as well as their fascinating spectral, electrochemical, and co-ordination properties, have gained significant attention since the very beginning. Their structure can be tuned by functionalization on β -pyrrole, *meso*- and axial positions, which affect their activity and, therefore, their characteristics towards different reaction processes, resulting in their suitability for a variety of applications. Cobalt corrole has been one of the earliest synthesized and extensively studied forms of metallocorrole. Apart from applications in the field of electrocatalysis such as HER, OER, ORR and CO₂ reduction reactions, the complexes of this family also perform well as sensors. The present thesis also encircles one such series of A₂B-cobalt corroles and has been divided into six chapters. Chapter 1 provides a comprehensive overview of the history and significance of corroles and metallocorroles. This overview assisted us in identifying the research gaps that required further investigation. In Chapter 3, the synthesis of a series of A₂B-type bispyridine-ligated cobalt corroles has been explained. Various techniques, such as ¹H NMR and ¹⁹F NMR spectroscopy, mass spectrometry, and Single Crystal XRD, have been used for characterization of those complexes. The complexes are characterized via UV–Visible spectroscopy also when present in their 10⁻⁴ M DCM,

10^{-6} M DCM and 10^{-5} M pyridine solutions. In Chapter 4, the potential of the synthesized cobalt corroles to sense anions has been investigated using colorimetric and spectroscopic approaches with 14 different tetrabutyl ammonium salts of F^- , CN^- , CH_3COO^- , NO_3^- , AsO_3^{3-} , AsO_4^{3-} , Cl^- , Br^- , I^- , ClO_4^- , $H_2PO_4^-$, S^{2-} , HS^- and PF_6^- . The three complexes are exclusively found to be binding F^- , CN^- and CH_3COO^- anions at their axial positions. Also, the limits of detection for the different anions have been calculated. In Chapter 5, the electrochemical properties of cobalt corroles in CH_3CN and DCM solvent using 0.1M TBAP as a supporting electrolyte are shown. The impact of substituting electron withdrawing or electron donating substituents on the overall oxidation/reduction potential is also examined by cyclic voltammetry. The catalytic efficiency of cobalt corroles has also been assessed.

CHAPTER 1

INTRODUCTION

1.1 GENERAL INTRODUCTION

Corroles are 18- π electron macrocyclic and tetra-pyrrolic systems, which are also fully conjugated just like porphyrins and hence aromatic.[1] Their skeletal structure resembles that of the corrin system, but the corrole moiety is fully conjugated, while corrin is a nonaromatic ring. Both corroles and corrins have one less methine (=CH-) bridge than porphyrins. Also, when fully deprotonated, corroles exist in trianionic form (corrole³⁻), whereas corrins and porphyrins are mono- and dianionic, respectively. In nature, porphyrins are found in the blood pigment haemoglobin, the cytochrome enzyme, and the plant pigment chlorophyll. On the other hand, corrin co-ordinated to Co-metal is found in vitamin B12 complex as cobalamin. Those essential biological applications of the macrocycles inspired researchers to synthesize the corrin and porphyrin moiety commercially. When researchers were attempting to synthesize the corrin macrocycle, they ended up synthesising a fully conjugated macrocycle called “corrole”. Hence, the corrole was for the first time synthesised and isolated in 1965 by Johnson and Kay serendipitously. Later in 1971, Nobel Laureate Dorothy C. Hodgkin resolved the first X-ray crystal structure of free base corroles.[2] Corroles, being trianionic in nature, have been shown to stabilize the metals in a higher oxidation state. They also show higher N-H acidity and high fluorescence levels when compared to porphyrins. Due to all these properties, a variety of elements from across the periodic table have been integrated with corroles and one of the most thoroughly studied of these is cobalt-corroles. **Figure 1.1** describes the schematic pathway of cobalt-incorporated,

Co-corrin, Co-corrole, and Co-porphyrin systems, where the movement of π -electrons is highlighted in bold.

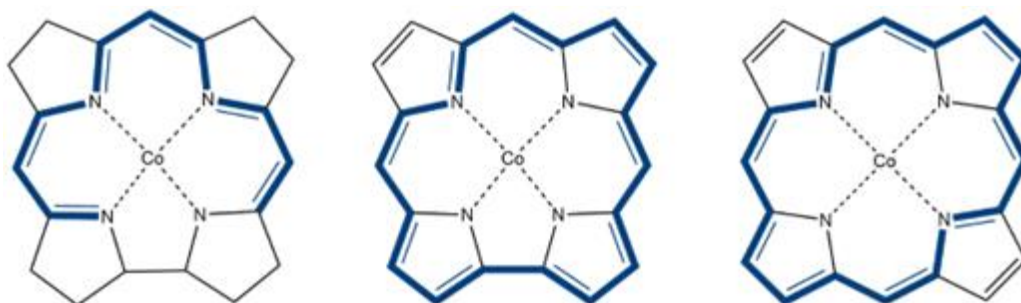


Figure 1.1 - Schematic Presentation of cobalt incorporated (a) Co-corrin (b) Co-corrole and (c) Co-porphyrin and the aromatic pathway is highlighted in bold.

1.2 SITES OF SUBSTITUTION:

In terms of corroles, the three sites of substitution are essentially feasible. (**Figure 1.2**) The peripheral functionalization can be performed at both the *meso*- or the β - pyrrolic positions of the corrole. The β -pyrrolic protons could be substituted by any halogen, aromatic or aliphatic group. The corrole macrocycle has three *meso*-positions that can be substituted with different acyclic or aromatic groups. The nomenclature of substituted corroles has more or less the same analogy as that of *meso*- substituted porphyrins. Depending upon the type of groups substituted, corrole are classified in three categories - A_3 , A_2B and ABC . The cavity of the macrocycle presents another possibility for the integration of any element from the periodic table. The three protons present in the cavity of the corrole macrocycle are highly acidic and hence can be easily deprotonated. The inner nitrogens are then free to co-ordinate with any element. Due to this unique ability, a large library of corroles featuring different arrangements has been compiled to date. The axial ligation capacity of the inner co-ordinated metal is another fascinating property of the corroles. The complexes display rich axial ligand chemistry,

and depending on the capacity of the element co-ordinated in the central cavity, they may be present in six, five, or four co-ordinated forms with two, one, or no axial ligands, respectively.

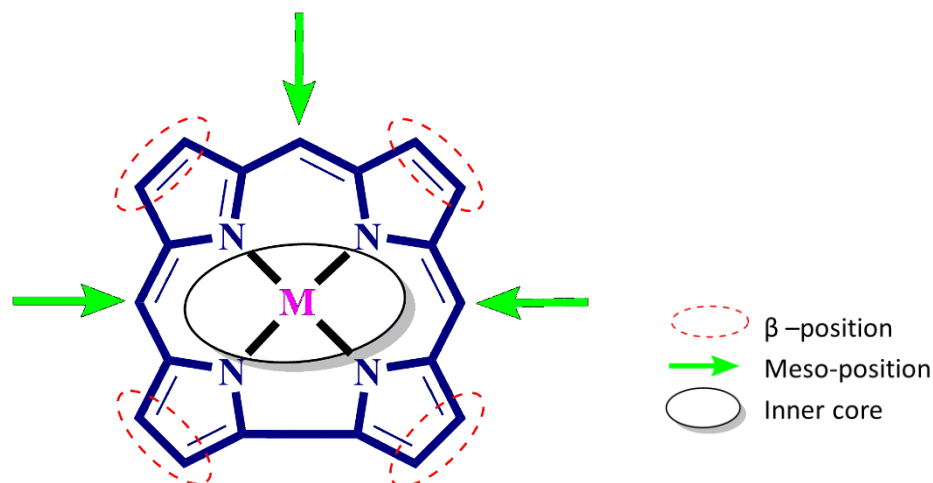
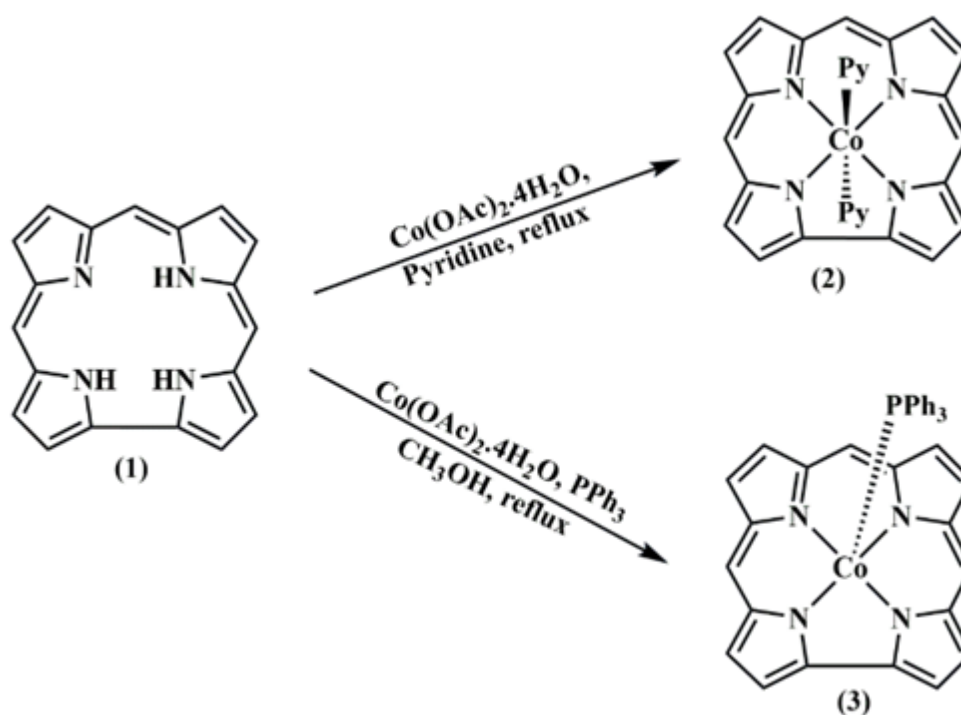


Figure 1.2 - Sites of substitutions on Corrole macrocycle.

1.3 COBALT CORROLES SYNTHESIS

Cobalt corrole has been an extensively studied form of metallocorrole.[3] Cobalt coordinated corrole macrocycles are thoroughly characterized and interpreted as five- or six-coordinate complexes, preferably as triphenylphosphine or dipyrindine ligated complexes.(**Scheme 1.1**) The most general method for the synthesis of cobalt corrole involves the reaction of free base corrole with cobalt metal salt. For the synthesis of cobalt dipyrindine corroles (**2**), the free base corrole (**1**) is dissolved in pyridine and refluxed for 15-20 minutes upon addition of $\text{Co}(\text{OAc})_2 \cdot 4\text{H}_2\text{O}$. Then the reaction mixture is dried and chromatographed using $\text{CH}_2\text{Cl}_2/\text{hexane}/1\text{-}2\%$ pyridine as an eluent. It is important to add pyridine since it functions as a labile axial ligand and can detach from the axial position easily. On the other side, when free-base corrole is dissolved in methanol containing cobalt acetate and refluxed for 1 hr, it gives penta- coordinated

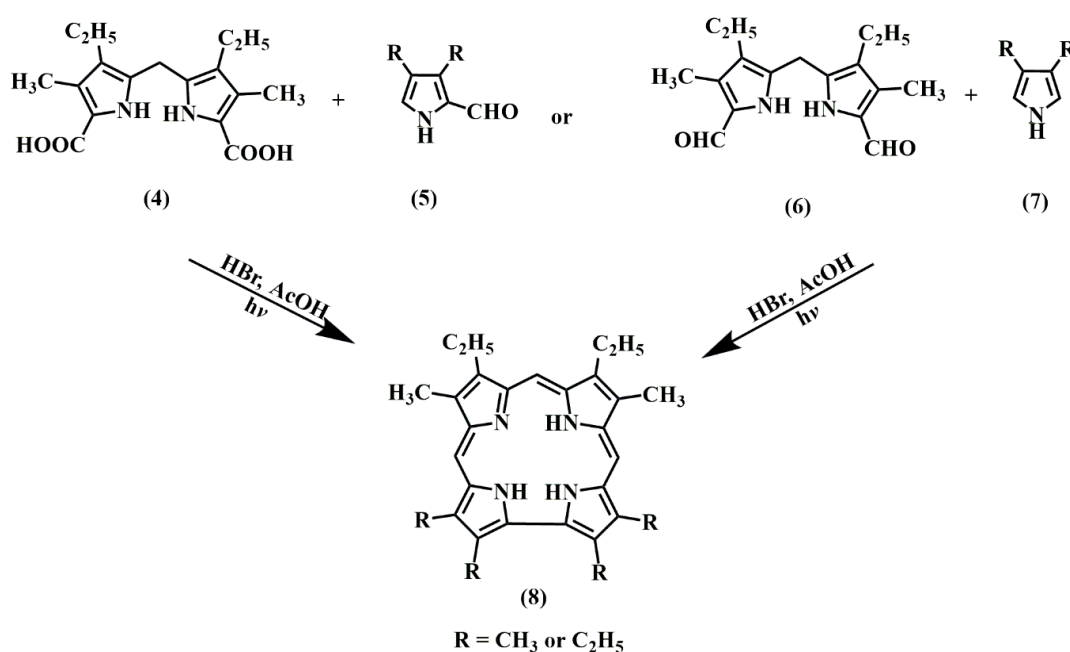
cobalt corrole (**3**) with triphenylphosphine supplied on the axial position.[4,5] Initially, in order to obtain the cobalt corroles, two main approaches were considered: the first involved the reaction of free base corrole with metal salt, while the second entails a [2+2] type route where cobalt metal is exercising the template action. Provided by Johnson and Key[6] in 1965, the very popular and



Scheme 1.1. Synthesis of cobalt-corrole from Free base corrole and Co^{II} salt

first synthetic method for β - substituted free base corrole preparation was through the biladiene-a,c route, which was then subsequently converted to cobalt corroles. The process comprises the condensation of either suitably substituted dipyrane dicarboxylic acid (**4**) with 2-formylpyrroles (**5**) or 5,5'-diformyldipyrane (**6**) with pyrroles (**7**). This gives a tetrapyrrolic precursor, 1,19-dideoxybiladiene-a,c dihydrobromide, which undergoes base assisted oxidative cyclisation upon UV-light irradiation and produce free base corrole in 58% yield as the final step.(**Scheme 1.2**) In

order to enhance the cyclisation phenomenon and compound yield, photo-irradiation has been replaced by oxidising agents such as alkaline potassium ferricyanide $K_3[Fe(CN)_6]$, ferric chloride ($FeCl_3$), hydrogen peroxide (H_2O_2), ceric sulphate ($CeSO_4$), di-*t*-butyl peroxide, and benzoyl peroxide (C_6H_5COO), producing 68-84% yield.[7] Later, Vogel et al. replaced it with the versatile

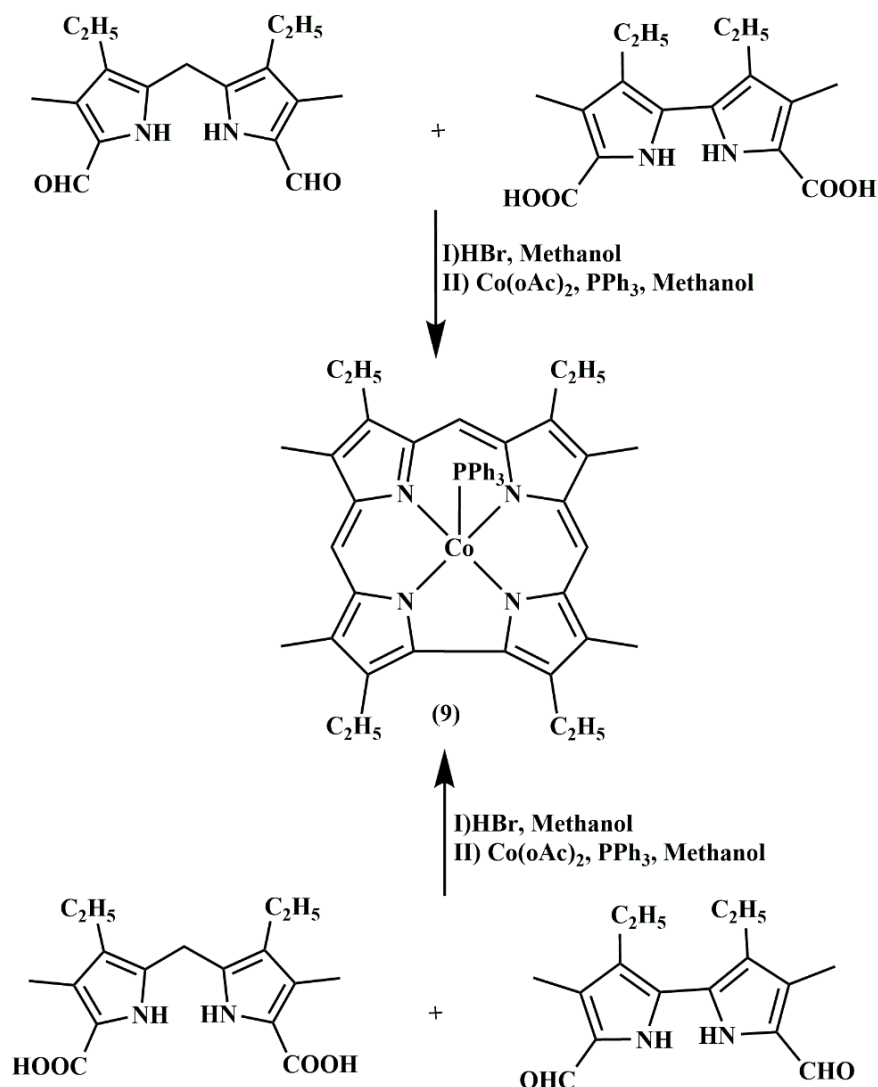


Scheme 1.2 - Synthesis of free base corroles via the biladiene-a,c route

oxidant chloranil.[8] The free base corrole, once formed, is then refluxed in the presence of pyridine and cobalt acetate to produce a cobaltic dipyridine complex, which then immediately transforms into a tetra co-ordinated form upon the addition of hot methanol.

In 1973, Conlon et al. proposed another synthetic idea, i.e., [2+2] route for the preparation of β -alkylcorroles as this did not involve direct bond formation in the last cyclisation step.[3] Reaction between suitably substituted dipyrane and 2,2'-bipyrrole in the presence of hydrobromic acid in methanol at 0 °C led to a red precipitate, which

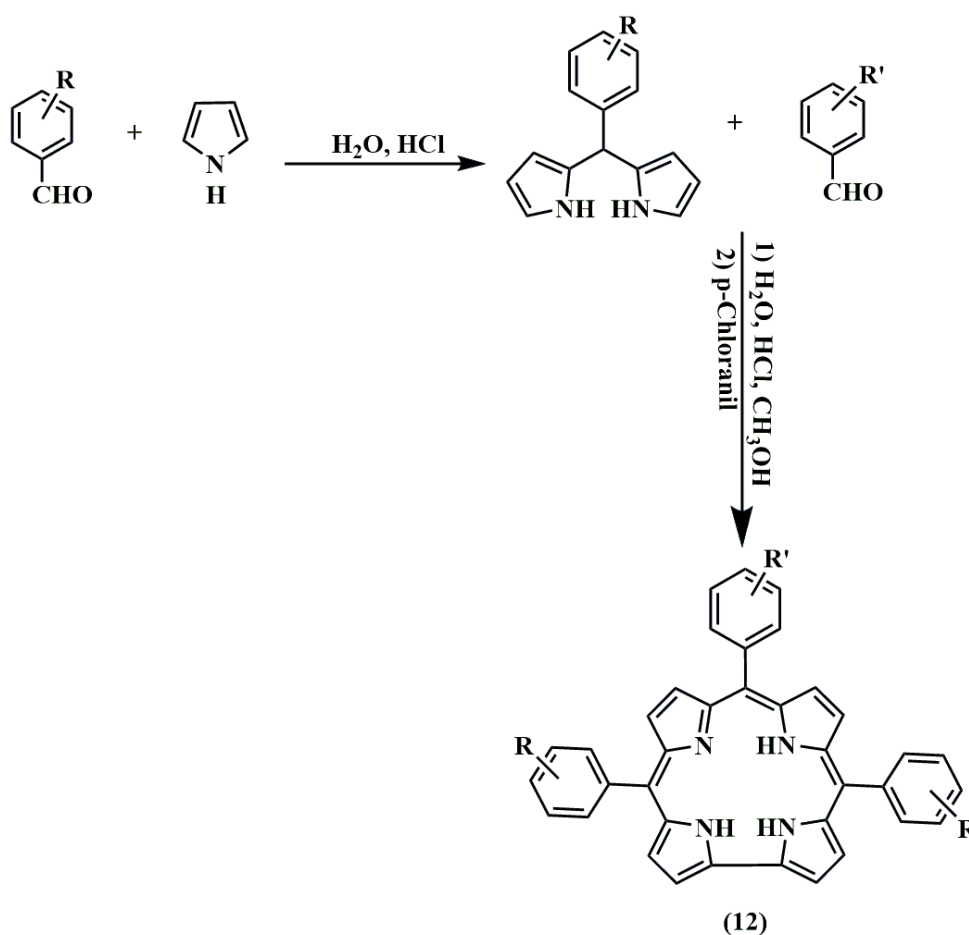
was then heated with cobalt(II) acetate in the presence of triphenylphosphine to convert into the corresponding five-coordinated corrole complex **(9)** (Scheme 1.3). The effective cyclisation occurs only in the presence of cobalt metal, which emphasizes the role of cobalt metal both in stabilizing the tetrapyrrolic intermediate and in



Scheme 1.3 - Synthesis of Triphenylphosphine ligated β -substituted cobalt corroles via [2+2] approach

exercising a template action, i.e., holding the reactive sites in close proximity. Prior to 1999, the corrole synthesis phenomenon was essentially restricted to aforementioned

strategies only, each of which required the extensive preparation of precursors. Also, the yield of the products was very low. Hence, the whole corrole field was largely dormant for around three decades since their discovery. Many attempts were made to develop a commercially viable synthetic route that was more facile and relied on the precursors commercially available. With the focus of improving yield, one pot synthesis method was developed to facilitate the generation of the free base *meso*-



Scheme 1.4 - Synthesis of A₂B corrole.

substituted macrocycle.[9–12] Gryko et al. synthesized A₃ and A₂B type *meso*-substituted free corroles using simple precursors. The procedure involved the reaction of suitably substituted aromatic aldehyde with prepared dipyrromethene, followed by

subsequent oxidation with p-chloranil.[12] This approach is widely regarded as the most efficient way to prepare the free base corrole macrocycle (**12**) to date (**Scheme 1.4**) Once formed, this free base corrole is then reacted with cobalt metal salt along with the coordinating ligands or solvent to prepare Co^{III} corroles.

1.4 STRUCTURE AND SPECTRAL CHARACTERIZATION OF COBALT CORROLES:

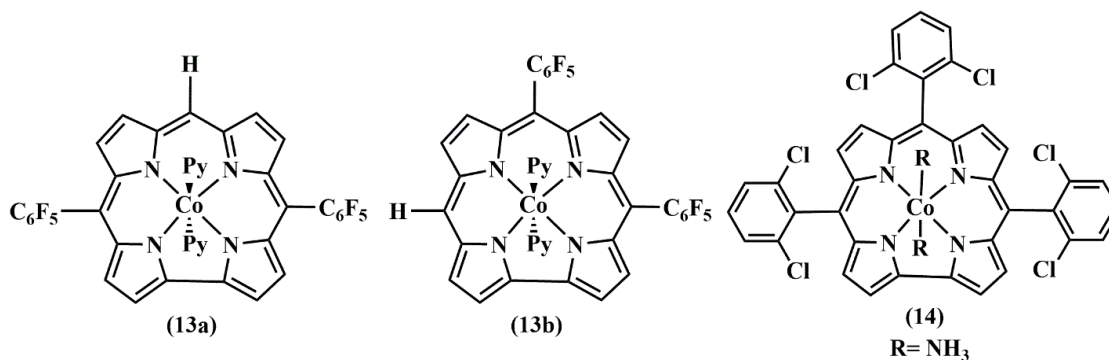
Cobalt corrole complexes have been among the earliest discovered metallocorroles, and hence their structural evaluation from spectroscopies has been widely observed to date. Spectroscopic methods such as X-ray crystallography, NMR, EPR, and cyclic voltammetry have yielded sufficient information regarding the behaviour of these compounds.

1.4.1 ¹H-NMR Spectroscopy:

¹H NMR spectroscopy plays an important role in the confirmation of the conjugated and aromatic nature of the corrole ring. The spectrum of free-base corroles discloses that the inner N-H protons may be seen resonating in the shielded region of δ -4 to -2 ppm. Both the *meso*- and β -pyrrolic protons resonate in the downfield region. *meso*-protons generally appear at δ 8-9 ppm, and the β -pyrrolic protons are found within the range δ 8-10 ppm.[13] The macrocyclic ring current effect is clearly the only possible reason for the extent of shifting in protons and hence points out the aromatic character of the corrole ring.

The cobalt corrole complexes are also usually characterized by the presence of four doublets due to δ - β -Hs, and are found in the range of 8-10 ppm. The protons of pyridine molecules in the bis-pyridine cobalt corroles are found to be up-field shifted due to the

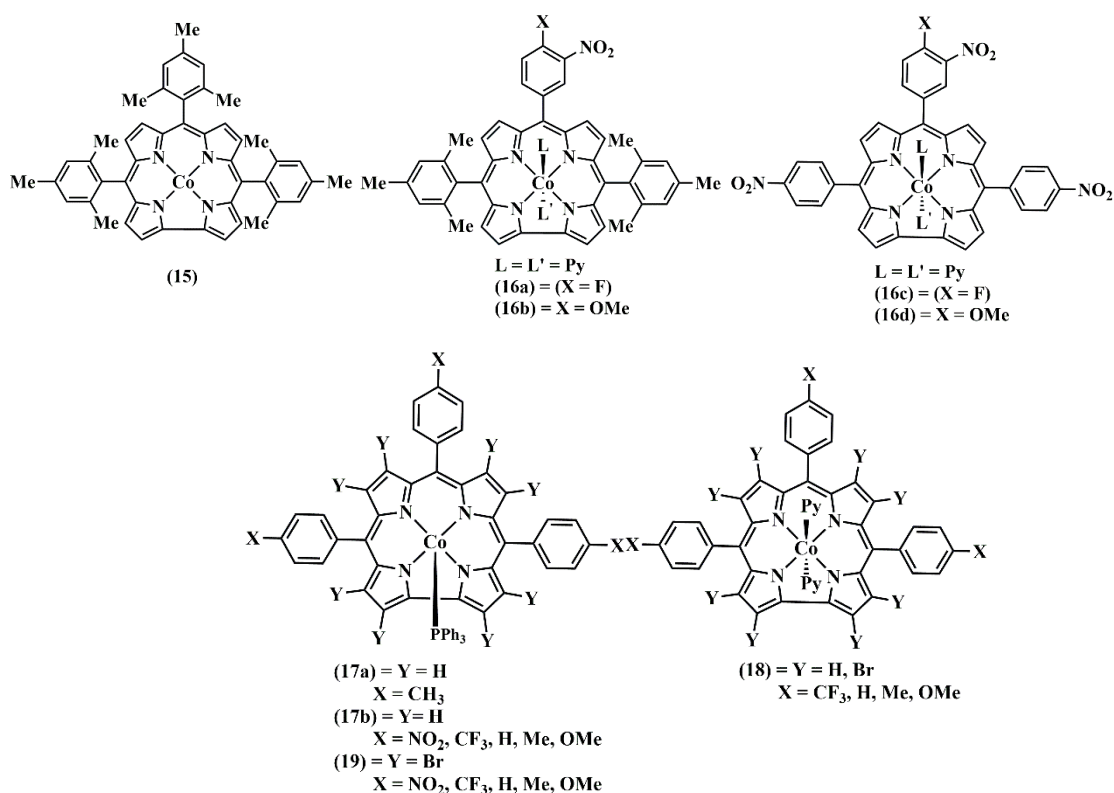
diamagnetic ring current effect of the corrole macrocycle.[14,15] The ^1H NMR spectrum of *meso*-free cobalt corrole **13(a)** similarly displayed eight signals due to the β -protons in the range of 8.76–9.40 ppm and a singlet signal of the *meso*-proton at 9.92 ppm, while **13(b)** exhibited four signals due to the pyrrolic β -protons at 9.32, 9.21, 9.04, and 8.85 ppm, and a singlet due to the *meso*-proton at 9.81 ppm in line with its higher molecular symmetry.[16] The diatropic ring-current effect causes an upfield shift of signals due to the ortho-positions of the axially coordinated pyridines and hence are found at 1.02 and 0.92 ppm for **13(a)** and **13(b)**, respectively. Hence, the molecules are rather easily distinguishable using ^1H -NMR spectroscopy. Complex **(14)** is obtained as a diamagnetic (low-spin d_6) cobalt(III) complex, which is clearly evident by its ^1H NMR spectrum, which discloses sharp and non-shifted resonances.[17]



1.4.2 UV-Visible Spectroscopy:

UV-Visible spectroscopy has been arguably one of the most convenient and practical methods of characterizing the corroles even at very low concentrations. Corroles are intensely coloured compounds. The extended π -conjugation of corrole macrocycles allows them to absorb in the visible part of the electromagnetic spectrum. The free base corrole formation is easily identified by the bands present at near 400-450 nm and at 550-650 nm.[18,19] Free base corroles are also fluorescent and show it in the 500-600

nm range.[13] Whereas in the case of metalated corroles, the bands are found in the blue shifted region. Cobalt corroles generally display the Soret band in 350-450 nm region and the Q-band from 550-750 nm, depending upon the configuration of groups present at the β -, *meso*- and axial positions. For e.g., the four-coordinated $(F_5PhMes_2Cor)Co$ exhibit the UV-Visible Soret band at 389 nm.[20] In 2018, Kadish and coworkers emphasized the concentration and solvent dependent sensitivity of the cobalt corroles. The formation of four coordinated Tri-mesityl substituted A_3 cobalt corrole (**15**) was confirmed by the Soret band at 388 nm and a very weak band at 543 nm in dilute conditions of DCM.[21]



In five coordinated complexes, a hump is emerged at near 570 nm in five coordinated forms of complexes. These are clearly distinguishable from the four coordinated complexes and may be identified as such. Kadish and coworkers found that (**15**) in

DMSO solvent at $\sim 10^{-3}$ M shows a broadened and blue shifted Soret band at 381 nm and a red-shifted Q-band at 563 nm which indicates its five-coordinate DMSO adduct formation.[22] In 10^{-5} M DCM solutions of **16(a)**, the bands are at 380, 424 and 550 nm, which confirms that the complex is present in its five coordinated form. The five coordinated tri-tolyl substituted cobalt corrole triphenylphosphine (**17a**) displayed its characteristic peaks at 394 and 566 nm.[23] Co[TpXPC](PPh₃) series of complexes, (**17(b)**) also displayed the characteristic peak close to 570 nm which confirmed its existence in five-coordinated form.[5]

The ligand non-innocence phenomenon has also been identified by UV-Visible spectroscopy. Sometimes the elements in centre cavity of corroles do not show their true high valent oxidation state and instead corrole macrocycle assumes an oxidized corrole^{•2-}-like state. This phenomenon is more common in 3d-transition elements. The corroles with 4d and 5d series and the main group elements are largely innocent metallocorrole systems. The complexes show variation in the Soret band with the nature of substituents in the phenyl group at *meso*-positions. It is evident from the observed Soret bands of Co[TpNO₂PC](PPh₃), which is found at 371 nm while 399 nm for more electron rich substituents at *meso*-positions i.e., for Co[TpOMePC](PPh₃). The [Co(OMC)PPh₃] [Co(OMMPC)PPh₃] and [Co(OMTPC)PPh₃] complexes displayed the Soret band at 366, 367 and 378 nm, respectively.[24] Thus, This phenomenon of red shifting in Soret band of the complexes as a result of insertion of more electron withdrawing group is simple yet reliable probe of realising the non-innocent character of the metallocorroles. A series of mono pyridine substituted cobalt corroles has shown same characteristic as well. Ghosh and coworkers reported a series of cobalt corroles (**18**) with pyridine substituted at axial position and they found that under neat DCM

conditions (when pyridine is not present) the complexes were preferably existing in their five-coordinated form while their Soret maxima is shifted to the right when phenyl group is substituted with a more electron donating group.[25] The electron withdrawing p-CF₃ phenyl group displayed the Soret band at 386 nm while at 402 nm, the *meso*- p-OMe phenyl substituted cobalt corrole was present, suggesting once again the noninnocent Co^{II}-corrole^{•2-} - like existence of these complexes.

Octa-brominated cobalt corroles of PPh₃ ligands shows the similar spectra and the peaks are located at comparable positions as found in their corresponding non-bromo substituted complexes.[25] These Octa-brominated complexes show invariant Soret maxima in their optical spectra. All the octa brominated Co[Br₈TpXPC](py)₂ complexes of series (**18**) shows the highest maxima at 391 nm only.[25] The possible reason of this muted substituent effect is the steric constraints imposed by β-Br groups which tend not to conjugate the *meso*-aryl groups with the corrole macrocycle. The behaviour of the same series, (**19**) with PPh₃ substituents at axial position likewise displayed the irregular variations in the Soret band irrespective to the type of substituent.[5] The corresponding cobalt corroles were compared with the rhodium corroles also, where the Soret maxima for Rh[TpXPC](PPh₃) complexes was observed invariant due to innocent Rh^{III}-corrole³⁻ character. In the case of six coordinated complexes, the Soret band is red shifted and broadens, while the Q-band is stronger in nature. The presence of Q-band close to 650 nm has been recognized as the marker band for the existence of six-coordinated cobalt corroles. In the bis-pyridine complexes **16(a-d)** the Q-band has been found to be emerging.[21,25–27] On contrary, the bis-cyano and bis-fluoro cobalt corrole complexes displays the Q-band in the red shifted region of 710-730 nm.[23,28,29]

The UV-Visible spectroscopy has made it feasible to report on five and six coordinated species that are in equilibrium when present in the solution form. The cobalt corrole complexes witnessed concentration and solvent dependency as their co-ordination number, electron charge density and the innocent-character are far changed with change in their concentration and type of solvent used. Kadish and co-workers[30] recently explored this important aspect and studied the mono-DMSO-cobalt-corroles with different tetrabutyl ammonium salts of anions. Kadish group found that out of 11 investigated anionic ligands (PF_6^- , BF_4^- , HSO_4^- , ClO_4^- , Br^- , I^- , Cl^- , OAc^- , F^- , OTs^- and CN^-) two molecules of CN^- anion in DCM solution were selectively ligated in stepwise addition at the axial position[29].

1.4.3 X-Ray Crystallography:

The X-ray crystallography is the fundamental technique to highlight the chemistry and structure of corrole complexes. The cobalt metallocorrole complexes are largely found planar where central cobalt atom lies almost in the 23-atom core of corrole mean plane.[11,27,31,32] These complexes show planarity even in the highly steric conditions of *meso*- or β - substituents.[15,33]

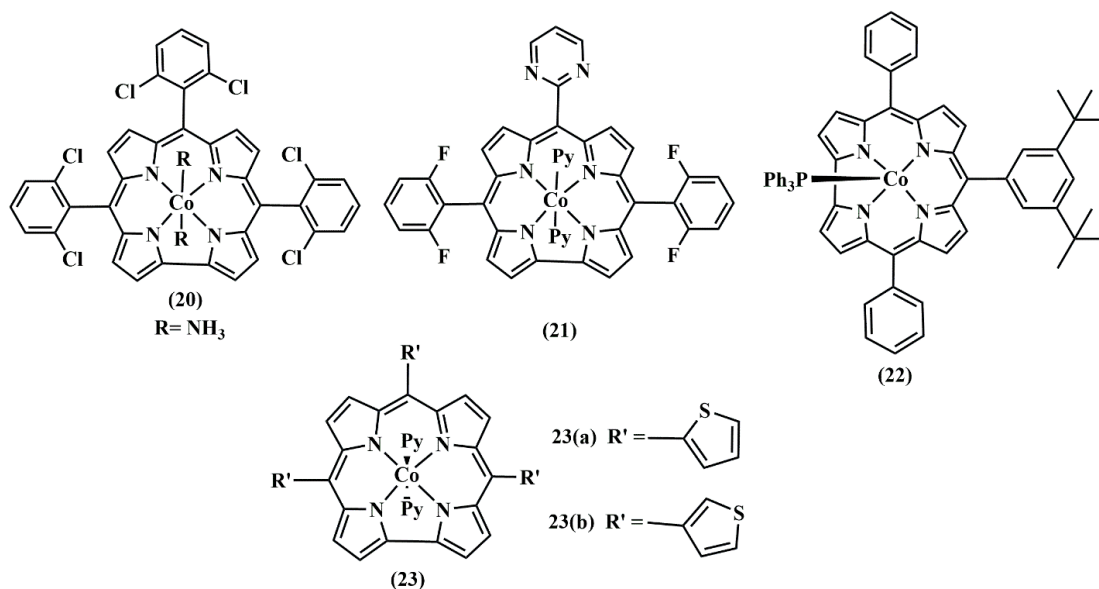
As early as 1976, Hitchcock and McLaughlin were able to disclose the first crystal structure of the five-coordinated (triphenylphosphine)cobalt corrole complex.[31] They demonstrated that the macrocyclic framework was nearly planar with the usual displacement of 0.38 Å of the cobalt atom above the plane as found in square planar complexes. The mean distance between the Co and N atoms of four pyrroles is 1.87 Å, which is similar in size to corrin (1.9 Å) but smaller than Co-porphyrins as expected. The Co-P bond distance was 2.210 Å which fulfilled the condition for the presence of

the complexes in their classic Co^{III} form. The *meso*-2,6-dichlorophenyl substituted complexes of cobalt corroles are also well defined, despite the significant disorder found for most of the dichlorophenyl substituted groups.[34] The triphenylphosphine ligand in those is tilted towards the unsubstituted phenyl positions, as evidenced by a smaller angle of 93.5° as compared to 103.5° formed with dichlorophenyl groups.

The average axial bond length ($\text{Co-N}_{\text{pyridine}}$) is observed to be longer than the average equatorial bond lengths ($\text{Co-N}_{\text{pyrrole}}$) in the bis-pyridine substituted metallocorroles as well, indicating that the complexes are present in the Co^{III} oxidation state.[14,27,35] For instance, the average $\text{Co-N}_{\text{pyrrole}}$ bond lengths of $(\text{Me}_4\text{Ph}_5\text{Cor})\text{Co}(\text{py})_2$ are 1.894 \AA whereas the average value of the two axial Co-N_{py} bond distances is found to be 1.991 \AA . Additionally, it is positioned at 0.021 \AA above the 4N_{p} -plane. The crystal structure of bis-ammonia substituted cobalt corrole (**20**) has also been evaluated, in which the $\text{Co-N}_{\text{pyrrole}}$ bond distances range from 1.868 to 1.908 \AA while the axial Co-NH_3 bond lengths were 1.964 and $1.974(6) \text{ \AA}$. [30] The complex is found to be essentially planar, with the C_{36} atom having the greatest deviation from the mean plane of 0.13 . However, the axial bond values are found to be shorter than the cobalt–pyridine distances for the same type of compound, i.e., 1.981 – 1.990 \AA . The NH_3 and Cl groups of the substituents produce intermolecular hydrogen bonding that controls the crystalline stacking, resulting in the formation of a molecular wire connected by hydrogen bonds.

Gross and co-workers came up with the X-ray structure of $\text{Co}(\text{tpfc})(\text{py})_2$ and its dimeric form, which is formed by a bond of length 1.48 \AA between two $\text{C}_3(\beta)$ – $\text{C}_3(\beta)$ atoms of the two corrole rings.[35] The twist angle between the two corrole rings is 45° , and the noticeable thing is that the bond lengths were found quite comparable with their

monomeric units. Substituent with 2,6-pyrimidyl cobalt corroles (**21**) are also evaluated through crystallography, which indicated that the complex is essentially planar.[17] The two 2,6-difluorophenyl aryl groups have dihedral angles of 70.3° and 86.7° with regard to the $N_{(\text{pyrrole})4}$ -plane of the corrole ring, respectively, whereas a smaller angle of 53.2° with respect to the N_4 -plane is found for the 2,2'-pyrimidyl group. The obvious reason of this is the absence of protons at two -o positions in the pyrimidyl ring, which causes it to have a more flattened orientation with respect to the corrole macrocycle. This results in shorter distances for the pyrimidyl nitrogens from the corrole-inserted ions than is observed for the 2,6-difluorophenyl aryls, i.e., within 5.49–5.54 Å.



In order to observe the host-guest interactions, the co-crystals of (**22**) with fullerenes (C₆₀) were also grown by Zheng et al. The crystallographic data shows that each C₆₀ is surrounded by two (**22**) molecule hosts, and the unit cell is made up of two 2:1s of (**22**) and C₆₀. To reduce steric strain, the 3,5-di-tert-butyl phenyl groups are packed in the crystal in a zigzag pattern with virtually opposite directions. The Co-Co distance between two corrole units is 10.27, and the two corrole planes subtend a 75° angle. Due

to the coordination effect of the PPh_3 , the Co atom is slightly out of the plane on the opposite side of the corrole from the fullerene. It's interesting to note that the bond length of 2.20 Å for Co-P is the same as that found for other reported PPh_3 -substituted complexes, which indicated negligible interaction between cobalt metal and the C_{60} unit. Therefore, the main factor influencing the formation of the complex may be the π - π interaction between the planar cobalt corrole macrocycle and the C_{60} convex surface.

The cobalt corroles substituted with 2-thienyl (**23a**) or 3-thienyl (**23b**) groups at *meso*-positions were also characterized by Churchill and co-workers.[15] A wide range of $\text{C}_{\text{pyrrolyl}}\text{-C}_{\text{meso}}\text{-C}_{\text{ipso}}\text{-C}_{\text{thienyl}}$ dihedral values for **23(a)** were 52°, 86° and 87° and for **23(b)** were 55°, 60° and 80°, indicating the partial contribution of the thienyl group to the corrole core conjugation. Bis-pyridine complexes of Free *meso*-positions (**13a**) and (**13b**) have also shown the similar octahedron X-ray structural relationship.[16] The Co-Npy bond distances are found in the range of 1.992–1.994 Å in (**13a**) and 1.994–1.995 Å in (**13b**), which are as usually longer than the Co-N_{pyrrole} bonds (1.877–1.96 Å in 43a and 1.775–1.93 Å in (**13b**)).

1.5 APPLICATIONS OF COBALT CORROLES:

Cobalt Corrole is significantly inexpensive and is abundant in nature. Also, those complexes have ability to attain variable oxidation states (Co^+ , Co^{2+} , Co^{3+} , Co^{4+} and

Hydrogen Evolution Reactions

Oxygen Evolution Reactions

Oxygen Reduction Reactions

Anion Sensors

Co⁵⁺). Also, due to the structural diversity, ease in synthesis and peculiar properties, with the time, those complexes have attracted great attention of researchers. Numerous applications of those complexes have been explored by various research groups in different fields such as catalysis, anion and gaseous sensor and the organic catalysis applications. Hence the cobalt corrole complexes have been considered as a versatile catalyst. In this section, a few of those applications listed below have been discussed in brief.

Electrocatalytic Applications:

Cobalt corroles have been extensively studied as electrocatalysts for O₂ reduction, H₂ Reduction and O₂ evolution processes. Those complexes have shown superiority and have been found good substituents of Pt and Pd based complexes. Actually, in general, expensive and rare noble atom-based systems are used for such catalytic reactions and therefore their substitution with certain other compounds that are less volatile, easily accessible and have comparable catalytic efficiency against these reactions was a required goal.

The ability of cobalt metal to stabilize and acquire +V oxidation state, is the significant feature of cobalt corrole which led the O₂ reduction and O₂ evolution process feasible. These applications have been frequently reviewed by Nocera and co-workers.[36] When using the cobalt corroles as catalyst, those can either be dissolved in electrolyte solution or used as an electrode material to pursue such reactions. In this section, we summarize developments of cobalt corroles for the catalytic activities accomplished by tuning the structural modification and reaction conditions.

1.5.1 Oxygen Reduction Reaction:

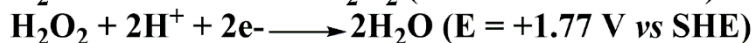
The general reduction scheme of oxygen reduction in water is depicted below. (**Scheme 1.5**) Beginning with Oxygen, the complete reduction pathway utilises $4e^-$, $4H^+$ yields two equivalents of H_2O , whereas partial reduction of oxygen following the $2e^-$, $2H^+$ pathway gives H_2O_2 and the further reduction convert it to H_2O molecule. Both the two- and four-electron reductions of O_2 are found energetically downhill, however approximately 0.5 V of extra energy is needed in 2-electron pathway.

Four e- pathway

At Cathode: Oxygen reduction reaction (ORR)



2 e- pathway



Scheme 1.5 - The two and four-electron pathway of oxygen reduction reaction.

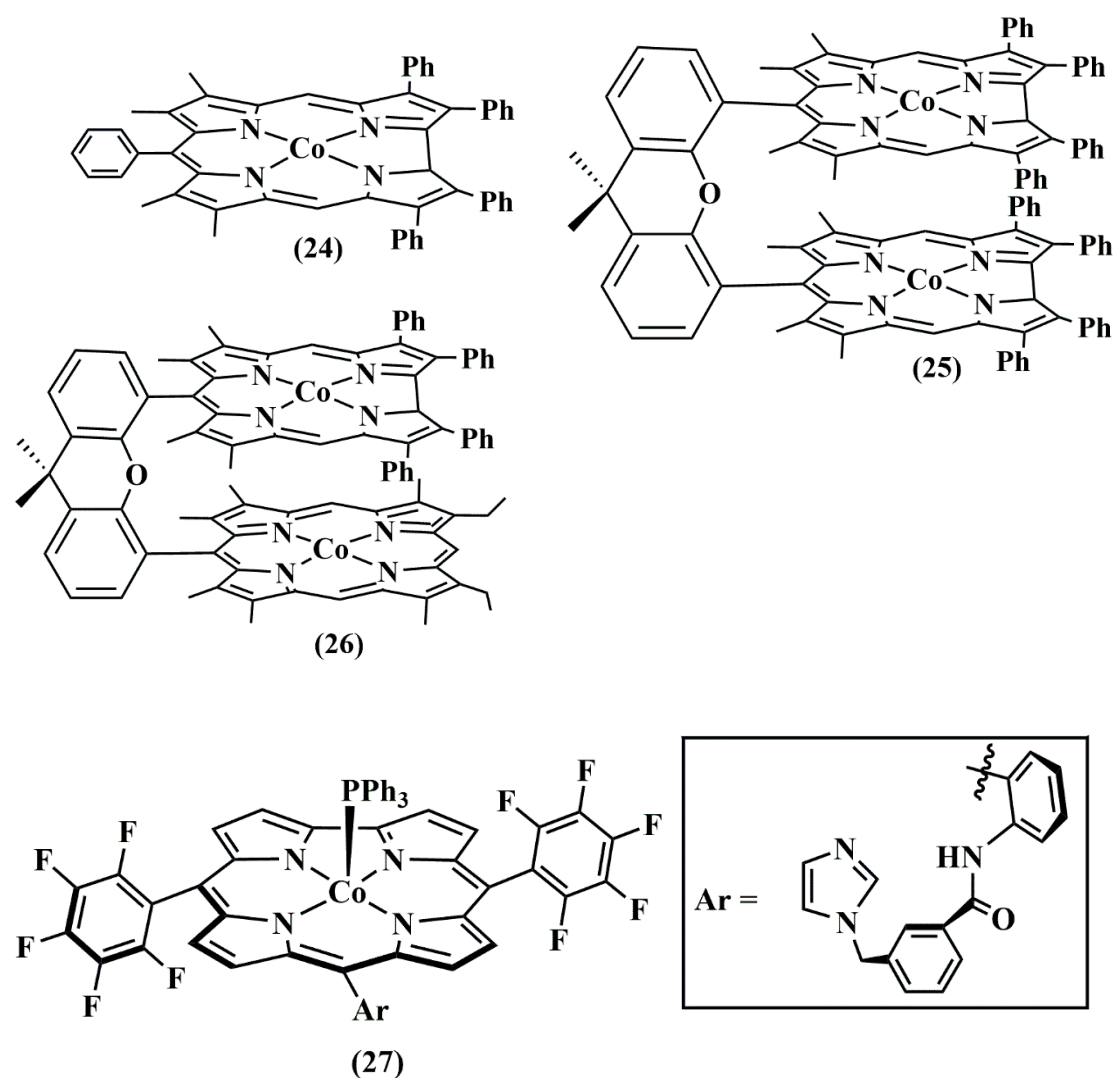
The potential chain of chemical reactions that might result in the production of water includes the attachment of an oxygen molecule to the cobalt-metal centre as the first step in the process. Simultaneously, the cobalt metal at core gets an electron, which results in the formation of the hydro-peroxyl species. After that, the species might go through one of the following processes: (i) The proton-coupled electron gain mechanism, which forms an oxo-complex at the cobalt metal centre and simultaneously release the first water molecule. The second proton-coupled electron gain mechanism create hydroxyl adducts which leads to the production of water molecules as well as species of Co^{IV} . (ii) However, there is yet another process that includes the receiving of a proton and the formation of the H_2O_2 molecule.

The very first metallocorroles activity concerning O₂ reduction was investigated by Kadish and coworkers in 2005. They examined the activity of metallocorroles dyads (Co^{III}) corrole monomer (**24**), Co^{III} bis-corrole (**25**) and Co^{II} porphyrin-Co^{III} corrole (**26**) which were adsorbed on surface of an electrode[37]. When compared to dyads, the monomeric cobalt corroles in this study exhibited the 4 e- route with significantly lower selectivity and competence. In spite of this, the results of the research demonstrated that monomeric cobalt corroles have the potential to catalyse the direct 4-electron reduction of H₂O, and hence eliminates the requirement for two redox active centres.

The effect of tuning the metal has significant effect on the catalytic activity of corroles. The electrocatalytic O₂ reduction behaviour of highly electron withdrawing **27**–Co(PPh₃) corrole with its Fe and Mn counterpart was compared by Collman and coworkers[38] in 2006. It was found that the Co and Mn–substituted corroles were able to catalyse only 2–electron reduction affording H₂O₂ from O₂ whereas the Fe–substituted–corroles catalysed both two and four–electron reduction but four-electron reduction is favored predominantly.

The tuning of the ligand framework i.e., β- and *meso*–substituent on the electrochemical (CV) and spectral properties of metal corroles has been also well observed by the researchers time to time.[20,40,41] The Koutecky-Levich plot method is generally adopted for to exactly determine the number of electrons transferred and hence the type of pathway followed. The cobalt corrole *meso*-substituted complexes have been found to produce a mixture of both H₂O and H₂O₂ (n > 2). On introduction of electron–donating groups are present at *meso*- positions, the complexes led primarily to a 2–electron reduction of O₂ and concomitant H₂O₂ formation. While number of electrons

transferred frequently enhance on introduction of EWG. Kadish and co-workers frequently justified the fact by comparing a series of cobalt corrole species involving 0,1, 2 and 3 para–nitrophenyl substituents where the number of electrons transferred during the O₂ reduction process measured through RRDE were found to be 2.6, 2.7, 2.9 and 3.0 for 0,1,2 and 3 para–nitrophenyl substituted corrole complexes.[41]



Later examination of 5,10,15-tri(2,4-dichlorophenylcobaltcorrole) adsorbed on an EPG electrode (1.0 M HClO₄) revealed the number of electrons transferred for O₂ reduction exactly two and hence the O₂ was reduced to H₂O₂ solely.[34] This presence

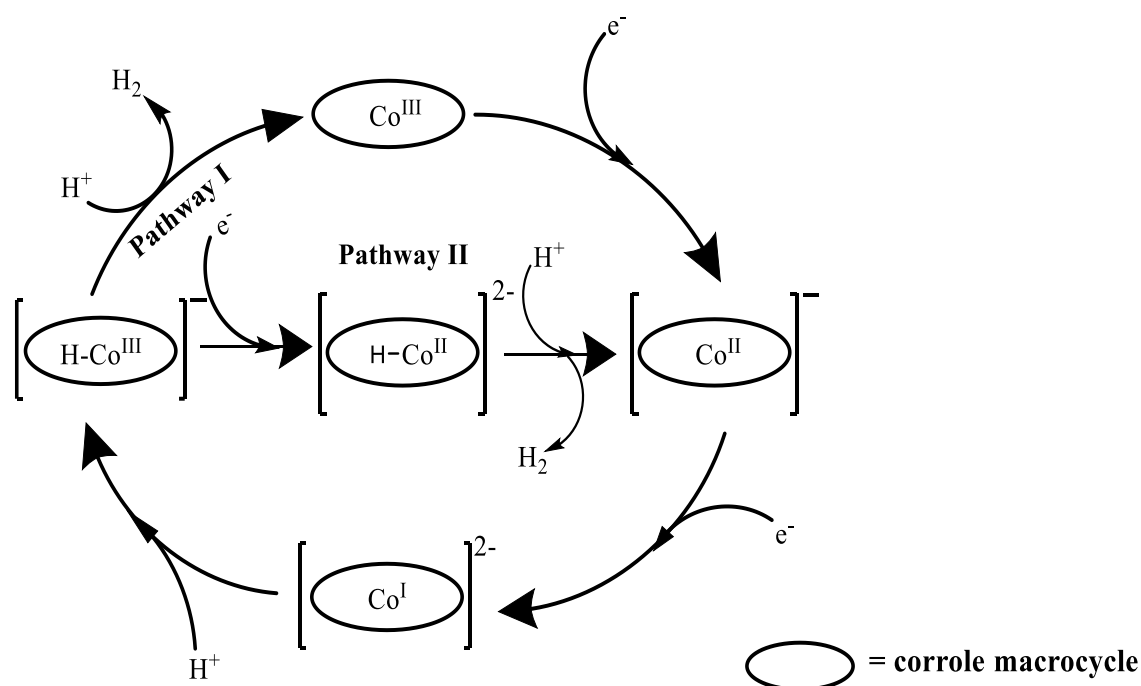
of -Cl group at ortho position causes steric hindrance, which in turn impedes the normally predicted π - π interactions between the two macrocycles. As a result, the creation of corrole dimers is inhibited by this bulkiness, which is believed to be essential for the 4-electron reduction. Hence, the production of H_2O_2 is the only product. Rana et al. examined the catalytic activity of $\text{Co}(\text{tpfc})\text{Py}_2$ and found that the complex was highly efficient as had a large TON (50,000) and a high turnover frequency (275 s^{-1}) toward H_2O_2 production. There was 100% selectivity in the 2-electron pathway followed. In the presence of ferrocene, acting as a one electron reductant in the presence of HClO_4 , the O_2 turns into H_2O_2 at an overpotential of 317mV.[42]

The introduction of electron withdrawing groups at the β -pyrrolic positions, also helps in converting the two-electron channel for O_2 reduction to a four-electron pathway, and hence favoring the H_2O generation only. For *meso*-tris-pentafluorophenyl-Co-corroles ($\text{Co}(\text{tpfc})\text{-Br}_8$ substituted with eight β -pyrrole bromide at the pH range of 3–4, the number of electrons transferred during ORR was close to four, which indicated that the O_2 was entirely reduced to H_2O . [39] While the comparison of $\text{Co}(\text{tpfc})\text{-Br}_8$ with its Fe, Ni, Mn and Cu analogue displayed the superior activity of Co-substituted corrole over other metals. The order of activity followed is $\text{Co} > \text{Fe} > \text{Ni} > \text{Mn} > \text{Cu}$.

1.5.2 Hydrogen Evolution Reaction:

Utilisation of non-precious metal electrocatalysts for hydrogen evolution has been the focus of researchers nowadays.[43,44] Hydrogen production is currently evaluated using either aqueous or organic solutions. The most frequent approach for detection of evolution is to record the cyclic voltammetry (CV) of the complex under observation, in the presence of increasing amounts of a proton source, typically a weak acid or water.

An irreversible wave, which keep on rising with increasing acid concentrations, is the proof of catalytic hydrogen evolution. Various parameters such as overpotential, turn over frequency (TOF), catalytic current-enhancement parameter (i_c/i_p), Faradaic yield and turnover number (TON) are frequently calculated in order to exactly determine the catalytic efficacy of a catalyst.[45–51]The possible reaction pathways for the HER catalyzed by cobalt corroles are depicted in **Scheme 1.6**. The mechanism suggests that the di-reduced intermediate Co^{I} is the catalytically active species for the proton reduction process.[52,53] The electrophilic attack of a proton source on this species gives Co^{III} -hydride intermediate. The species thus formed can combine with the proton supplied to it to generate the H_2 molecule as suggested in pathway I, also called the EECC pathway. This might undergo the evolution of hydrogen by adhering to pathway II, which is called the EECEC pathway.



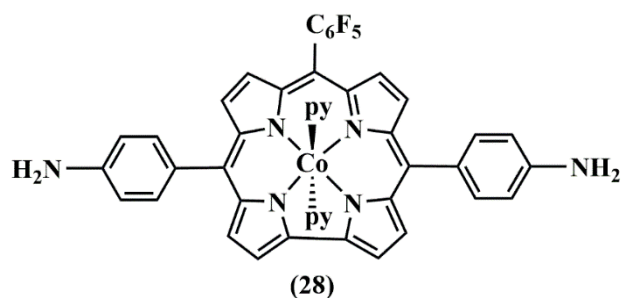
Scheme 1.6 - Catalytic Pathways followed by Co^{III} -corroles during hydrogen evolution process .[53]

Gross and coworkers reported the hydrogen evolution activity of Co(tpfc)Py₂ using the aqueous sulfuric acid and natural sources such as water from a nearby pond, Ganges River, Bay of Bengal, Dead Sea and Sea of Galilee as proton sources. The TOF for the HER at room temperature and under anaerobic conditions was 600 and 1140 s⁻¹ at -0.7 and -0.8 V (vs Ag/AgCl), respectively. While the Faradaic yield in a 0.5 M H₂SO₄ using aerobic conditions was 52% at -0.8 V (vs Ag/AgCl). The comparison of different halide substituents on the β-carbons of Co-corroles was also done in a subsequent study by Gross and coworkers. The authors examined and demonstrated it to have a noticeable effect on the reduction potentials and the hydrogen evolution process.[54] The onset potentials for catalytic hydrogen evolution recorded were -0.4, -0.55, and -0.6 V (vs Ag/AgCl) for Co(tpfc)-Br₈, Co(tpfc)-Cl₈ and Co(tpfc)-F₈, respectively, in homogeneous acetonitrile solutions and in the presence of 2–4 mM TFA. The onset potential was found to be earliest for Co(tpfc)-Br₈ whereas Co(tpfc)-F₈ was found to be the most active catalyst in terms of the kinetic reactivity. Simply coating the Co(tpfc)Py₂ on the ITO electrode without the β-pyrrolic substitution for the heterogeneous catalysis is although found more preferable from the standpoint of cost and ease of synthesis.[55] The turnover frequency for electrocatalytic proton reduction from this system was determined to be 1010 s⁻¹ at -1.0 V (vs. Ag/AgCl, pH = 0.5), whereas at -1.1 V the TOF was found to be 6150 s⁻¹.

Structural modification and grafting onto different surfaces are also done to enhance the catalytic activity of corroles.[4,46,49,56] Cao and colleagues reported one such corrole with structurally modifications. They reported *meso*-pyrene substituted cobalt corroles and displayed that there was enhancement in the catalytic activity.[57] They also emphasized on the significance of the axially present group as better results were

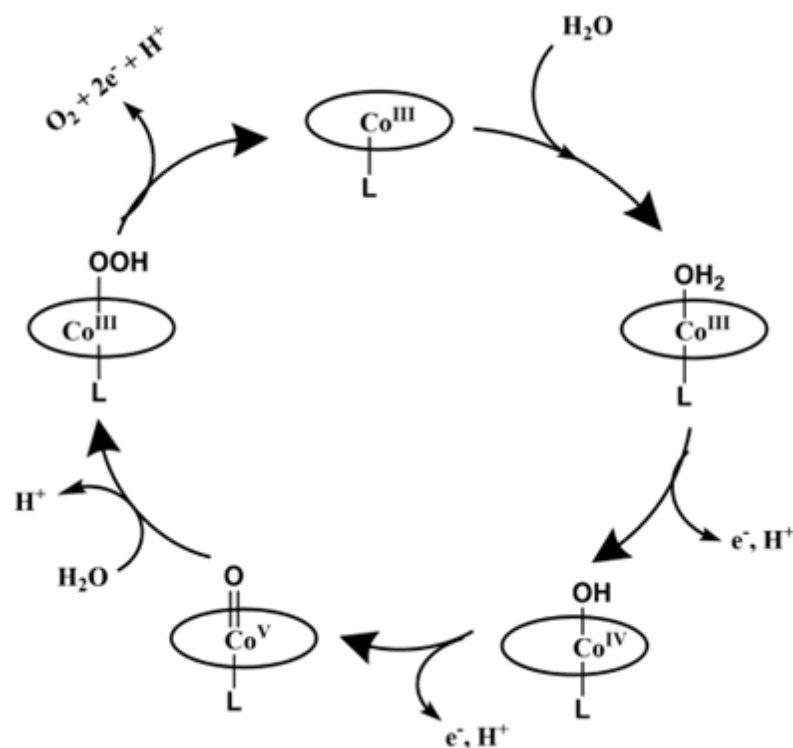
shown by PPh_3 substituted corroles over Pyridine substituted corroles. They explained it by claiming that the PPh_3 ligand causes a “push effect” and facilitates the attack of the proton at its trans position. Zhang and coworkers also examined the influence of *meso*-substitution on the HER activity of cobalt corroles.[4] The i_{cat}/i_p ratio, and hence efficiency of HER catalysts was found to be increasing with the introduction of electron-withdrawing groups onto the corrole moiety. In order to improve the HER efficacy of the complexes, Cao and his colleagues developed two distinct techniques of amidation for attaching the amine group carrying Co-corroles onto oxidised CNTs that had multiple surface carboxyl groups.[58] Liang and co-workers provided a series of six *meso*-expanded Co^{III} triarylcorroles. Those modulated *meso*-substituents provided effective electron transfer routes and hence were discovered to be good electrocatalyst for HER process as well.[59]

Sankar and coworkers synthesized and characterised **28**, a complex possessing bifunctional electrocatalytic activity towards the HER and OER under both homogeneous and heterogeneous conditions.[60] The significant enhancement of the cathodic current for the second reduction wave with the notably lower onset potential of 0.26 V upon the addition of TFA (10.0 mmol) with **28**



indicates that the Co^{I} intermediates in the solution are crucial for the catalytic performance. The first-order rate constant k_{cat} towards the hydrogen evolution process was found to be 952.0 s^{-1} . Moreover, excellent activity was observed in heterogeneous media, with a lower onset potential for the OER (0.95 V) and the HER (-0.25 V) in basic and acidic solutions, respectively. In heterogeneous medium where **28** is drop-

casted on an GC-electrode, the HER activity was examined both in acidic and basic medium. The turnover number and turn-over frequency by the **28** were estimated to be 3606 and 0.12 s^{-1} , respectively, at the potential of 0.95 V versus NHE in a 1.0 M KOH electrolyte solution.



Scheme 1.7 - Catalytic Pathways followed by Co^{III}-corroles during Oxygen evolution process.[61]

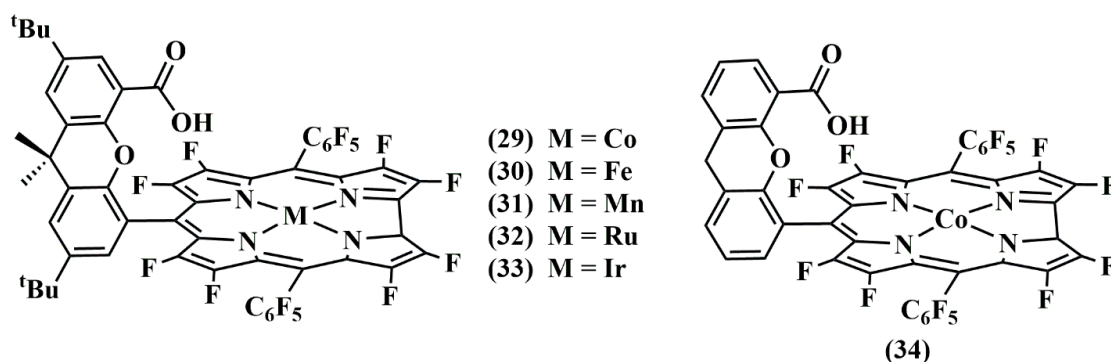
1.5.3 Oxygen Evolution Reaction:

The oxygen evolution process is one of the essential processes for meeting the current energy needs of world. Consequently, it has been the focus of recent research. Various processes such as Photocatalytic, electrocatalytic, or photoelectro-catalytic may be utilised to split water into its component H₂ and O₂. This process involves the formation of O-O bonds, which is a thermodynamically challenging uphill process. The water

oxidation process overall requires $4e^-/4H^+$ during its transformation process. A number of cobalt corrole catalysts with the ability to function homogeneously and heterogeneously have been discovered for this process.

The general mechanism followed by cobalt corroles is shown in **Scheme 1.7**. The scheme explains that the process begins with the water molecule attacking the cobalt active centre. After a series of distinct oxidation steps one oxygen molecule is formed out of the two water molecules employed during reaction. The corrole moiety Co^V -oxo species formed in between the process has been identified as the catalytically active species for the process.[14,61,62]

Nocera et al. studied the activity of O_2 evolution of the Co^{III} -hangman corrole complexes **29** substituted with β -octafluoro groups. They used FTO glass electrodes and reported that the catalytic performance of these complexes was excellent. The TOF of the corrole as catalyst is found to be 0.81^{-1} at an overpotential of 780 mV. The catalytic current was evidenced higher due to the presence of $-COOH$ group present in hangman group.



Using DFT calculations, the mechanism of O_2 evolution for various hangman metallocorroles, was attempted to understand by Lai and coworkers[63] and Ertem and

coworkers.[64] (29-34) It was concluded that the inclusion of fluoro groups at β -pyrrolic positions also contributed to the stability of the oxidized corrole macrocycle. The fluoro groups enhance the electrophilicity of the system. With regard to the O-O bond formation, the Co-metal with a formal oxidation number of (V) is found more reactive than its counterpart with a formal oxidation number of (IV) and the other metals that were taken into consideration. The Co(V) species is rather present as $\text{Co}^{\text{IV}}\text{-corrole}^{\bullet+}$ with cation radical character in the corrole ring. This is due to the ease of the $\text{M}^{\text{V}}=\text{O}$ center to undergo a two-electron reduction. As a result, theoretical calculations indicated the sequence as: $\text{Co}^{\text{V}} > \text{Fe}^{\text{V}} > \text{Mn}^{\text{V}}$.

Four Co-corroles with different pendants of acidic and basic nature were synthesised[50]. It was observed that Co metal seems to be susceptible enough to act as an intramolecular base to facilitate H_2O to attack on the Co-oxo unit to form the O-O bond. Not only does hangman boost the catalytic activity for OER, but C_6F_5 , present at two other *meso*-positions, does so as well by decreasing the electron density on Co-metal and shifting the electrode potential to the anodic direction. Two oxidation and reduction waves are seen in the CV of these corroles in an acetonitrile solvent, which also corresponds to the redox features of non-hangman corroles. All four Co corroles were found to have Faradaic efficiencies for O_2 evolution more than 90% and throughout the 5-hour CPE experiments, the currents exhibited a notable degree of stability.

Lei et. al. examined the OER activity of $[\text{Co}(\text{tpfc})(\text{py})_2]$ in 0.5 M H_2SO_4 under nitrogen atmosphere.[14] The complexes had sufficient oxidizing power for water oxidation, and thus they are potential WOCs. The electrocatalytic study of ITO coated Co-corrole

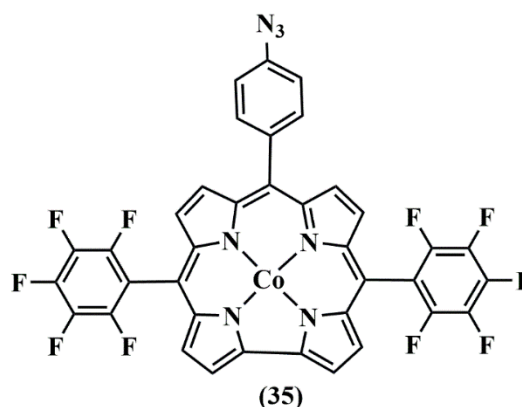
showed that the catalyst is stable during catalytic cycles, The electrolysis study displayed greater than 95% of Faradaic efficiency. Density functional theory (DFT) calculations indicated that there were two sequential $1e^-/1H^+$ oxidation steps. The first result in the formation of $[Co^{*+}-Co^{III}-OH]$ having doublet ground state, followed by the formation of $[Co^{*+}-Co^{III}-O^*]$ having triplet ground state. The calculated energy barrier of $18.1 \text{ kcal mol}^{-1}$ which was in good agreement with that experimental activation barrier for water oxidation.

Co^{III} corrole complex with a pyrene moiety, immobilised on MWCNTs shows potent activity and durability toward the OER process and hence oxidises H_2O to O_2 in neutral aqueous solution with $V_{onset} = 1.15 \text{ V vs. NHE}$. The GC electrode coated with **Co-corrole**/MWCNT was immersed in a 0.1 M pH buffer, and its electrocatalytic OER properties were examined[65]. A significant catalytic current was found with $V_{onset} = 1.15 \text{ V}$ corresponding to an onset overpotential of 330 mV and is smaller compared to other OER catalysts. The faradaic efficiency of the system was found to be better than 95% and the surface stability is improved due to $\pi-\pi$ interactions between the pyrene moiety and the carbon surface.

In 2017, Xu and coworkers[66] conducted a study on six cobalt corroles having different axial ligands to investigate their potential for OER. The authors also predicted the reaction mechanism of the process and determined that the cobalt corrole centre was activated by two PCET steps. Interestingly, from a possible ligand displacement point of view, the formation of the O–O bond is contingent upon the axial ligand attached to cobalt corroles. The study employed catalyst-coated fluorine-doped tin oxide (FTO) working electrodes, to investigate the catalytic waves exhibited by water oxidation in

0.1 M pH 7.0 phosphate buffer solutions. The Faradaic efficiency for all the Co-corroles under consideration was >90% and onset overpotentials fall within the range of 510 to 580 mV. The complexes possessing strong electron-donating axial ligands are more efficient in catalyzing water oxidation than those having electron-withdrawing axial ligands.

Cao et al. (2018) gave the first example of a bifunctional catalyst for H₂ and O₂ reduction by immobilising Co-corrole on CNTs by covalent bonds and studied the effects of various immobilization techniques on OER.[56] In pH 0-14, these hybrids loaded on



GC electrodes show remarkable stability and efficiency for OER. The hybrid of **35** grafted onto CNTs covalently by short conjugated linkers shows high electrocatalytic performance for OER across all pH ranges. Its observed onset potential is 450 mV relative to the hybrid of **35** with elongated alkane chains. At pH 0 and pH 14, the measured catalytic currents for the OER process are 25.4 mA μg⁻¹ and 324 mA μg⁻¹, respectively, at η = 770 mV. The estimated TOFs for OER at pH 0, 7, and 14 in aqueous solutions were 14176, 4345, and 36863 h⁻¹, respectively. This phenomenon can be justified by virtue of its significant capacity for electron transfer between catalyst and CNTs via short conjugated linkers.

In 2018, Gross and co-workers investigated Co(tpfc) to have a clear understanding of the mechanism of action, which was necessary to design the systems of optimal performance for WOR.[67] The steps involved identification of redox states and the

effect of axial ligands on the activity of doubly oxidised complexes. CV experiments were conducted in the presence and absence of Co(tpfc) under similar experimental conditions, albeit with varying concentrations of base. The catalyst caused an earlier shift of the V_{onset} for electrochemical water oxidation by 200–400 mV. Even at neutral conditions, the WOR proceeds very effectively at an earlier voltage. For selected hydroxide concentrations, it is found that although with increase in amount of base, the onset potential shifted to lower value in both presence and absence of catalyst but the absolute number were much positive in absence of catalyst.

Sankar and coworkers found **28** as an efficient catalyst for the oxygen evolution process.[60] The aminophenyl groups present at the *meso*-position increase the basicity of the catalyst, resulting in excellent activity with a first-order rate constant of 0.2 s^{-1} , obtained by plotting the graph between $i_{\text{cat}}/i_{\text{p}}$ vs. $[\text{H}_2\text{O}]^{1/2}$. The CV data recorded in the presence of 3% water results in a significant increase in the anodic current ($\Delta I = 7.6 \text{ }\mu\text{A}$) for only the second oxidation wave at 1.37 V, whereas the first oxidation wave was unaffected throughout the experiment. OER is thought to be responsible for the strong electrocatalytic current observed with a significant decrease in the onset potential (1.10 V), which again implies that the Co^{V} -corrole intermediate is the catalytically active species for the process.

1.5.4 Cobalt Corroles as Sensors:

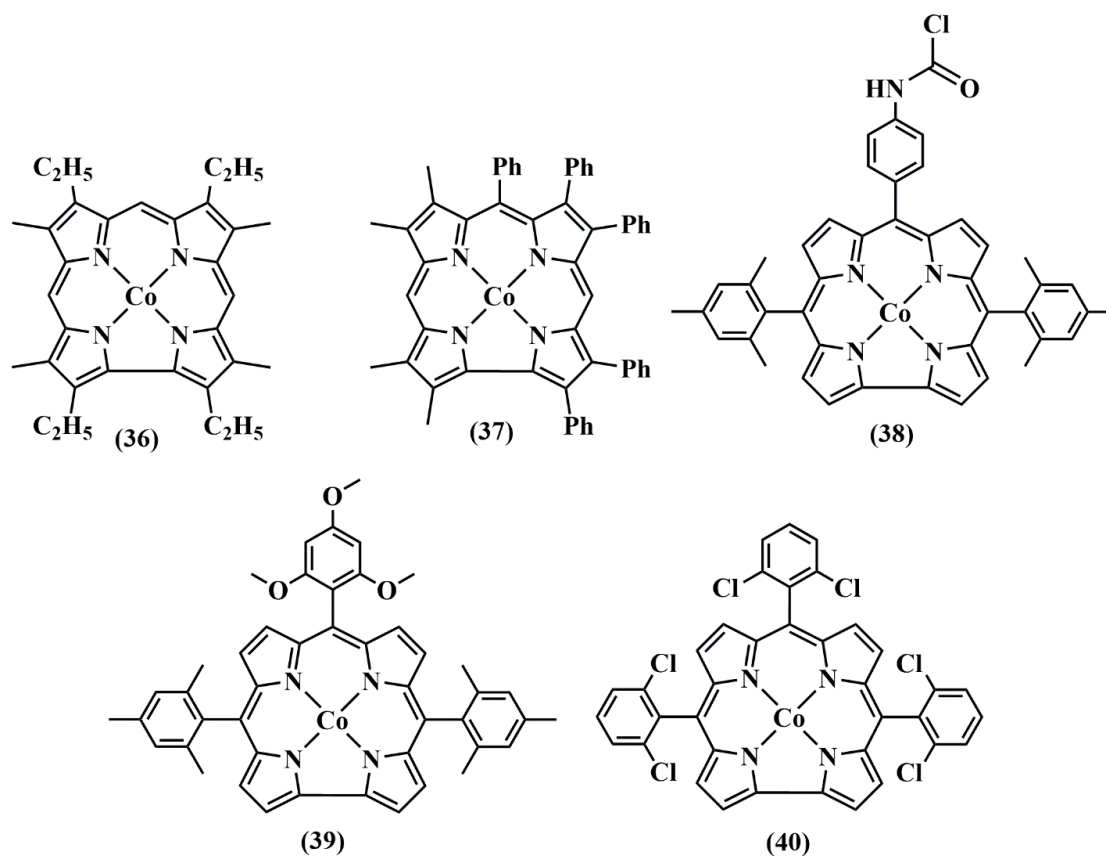
Besides its usage in the aforementioned HER, OER, and ORR processes, cobalt corroles also has a variety of additional uses. These compounds are widely utilized in the detection of ligands and gaseous molecules. The central Co^{III} metal coordinated in the corrole core has the ability to connect any ligand to it. These complexes have shown

promise for use as sensors depending on the replacement of *meso*-, β - or axial positions. Cobalt corroles display catalytic activity in various chemical reactions, such as the catalytic oxidation of alkenes or nitrene transfer reactions.

Cobalt complexes are known to have a high affinity to bind small gaseous molecules. These have shown the potential to bind one CO molecule at the axial position, which was confirmed through the Hill equation, which gives the slope ~ 1 indicating the binding of one CO ligand at the axial position.[27,68] Theoretical studies of cobalt corroles with different atmospheric diatomic ligands such as CO, N₂ and O₂ have been studied. This prompted Guilard and colleagues to investigate the detection of CO molecules using **Co(tpfc)** and **36-40**. [69] They found that cobalt corrole complexes show strong affinity and 100% selectivity for carbon monoxide gas, with no interference from N₂ and O₂ present in the air. These compounds were demonstrated by adsorption isotherms and were found to be reversible, which was the prerequisite condition for sensing. Their detection properties are also seen to be influenced by the Lewis acidic character of the Co^{III} metal ion, as the detection ability was enhanced when the more electron withdrawing substituents were located at the macrocycle ring.

Later, the inorganic-organic composites of cobalt corrole complexes were prepared by grafting these into silica matrices [70,71]. The co-polycondensation of corroles, activated through linking the hydrolysable -Si(OEt)₃ terminal groups with Tetraethoxysilane (TEOS) and methyltriethoxysilane (MTEOS). The detection affinities were demonstrated through the adsorption phenomenon, and the compounds adsorbed CO with greater selectivity in contrast to O₂ and N₂. Similar outcomes were obtained when the mesoporous hybrid materials were prepared by grafting cobalt

corrole complexes onto mesostructured silica of the SBA-15 type, except that these complexes were stable over a period of several months, whereas the capacities of xerogel materials declined steadily.[71]

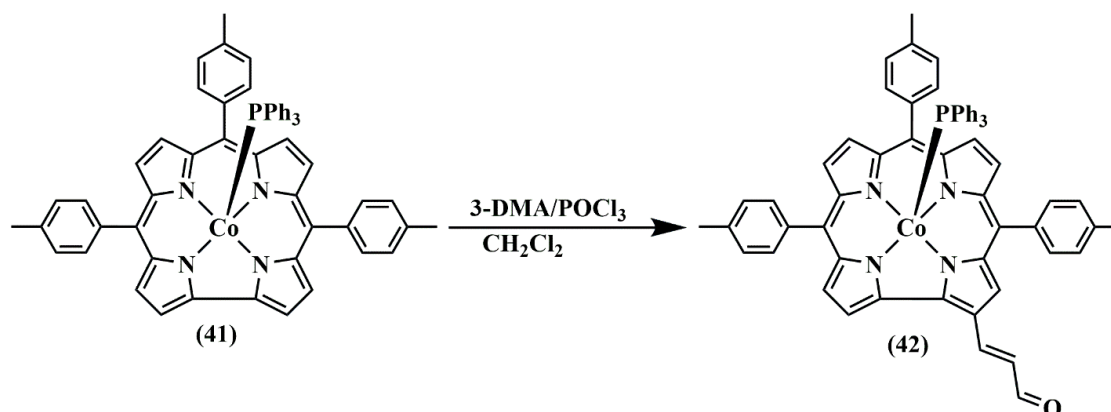


In order to further monitor and enhance the CO detection limit using cobalt corrole complexes, sensors based on surface acoustic wave (SAW) were prepared[72,73]. The love waves monitored the phase variations in delay lines built on the cut of quartz surface versus various CO concentrations. So, a time response of a few seconds is observed upon changing from normal air to CO-polluted conditions. Through experimental studies, the detection limit in this scientific work approached ppm levels. These sensors were prepared by depositing the thin films of **40** onto the surface of the delay lines by spray coating.[72] Later, using the same corrole Field

effect devices were also prepared by directly employing it to the gap window of a MOS capacitor.[74] This device worked because the chemisorption of CO resulted in a negatively charged complex. The variation in surface charge versus CO concentration gave linear proportionality ($6.46[\text{ppm}\cdot\text{m}^2\cdot\mu\text{C}^{-1}]$) corresponding to the doping level ($N_A^{2/3}$) $23.5 \mu\text{C}/\text{m}^2$. The high affinity of **40** for CO corresponds to sluggish desorption, which was compensated by photo illumination at 395nm.

Nanogravimetry based transducers such as Thickness Shear Mode Resonators (TSMRs) are also functionalized with different cobalt corroles in order to make the chemical sensors.[75] The authors have emphasized the effect of peripheral substitution, i.e., -OH groups at the corrole and corresponding porphyrin macrocycle. In accordance with this, the adsorption isotherm proposes better sensitivity for -OH substituted porphyrinoids as they form a porous supramolecular layer by exerting the hydrogen-bond network to entrap the gaseous molecules. Since these were mass transducers, they were therefore sensitive to any interference between receptor and analyte resulting in variation of mass, which did not limit them to NO and CO detection only, so giving exposure to sense different other gases also. Later, the nanogravimetric transducers activities are said to enhanced using the composite material made up through exploiting the functionalised corrole with polymeric nanostructures.[76] The 3-acrolein-substituted corrole was prepared for this reason by the reaction of **41** with dimethylaminoacrolein following the Vilsmeier reaction conditions.(**Scheme 1.8**) This modified corrole complex **42** was then copolymerized with acrolein to achieve corrole-functionalized microparticles.

The resulting sensing material, due to the combined effect of different properties of corrole and PA provided an amplified response with good sensitivity.



Scheme 1.8 - Vilsmeier reaction on cobalt corrole.[76]

The complex **41** with TDACl as an anion exchanger optimized in a 1:3 molar ratio and deposited on paper support was also used to prepare an optical sensor for CN⁻ in aqueous solution.[23] A smartphone coupled to the sensing device records the colorimetric response immediately after the sample has been deposited, which is interpreted by a home-written colour intensity software. The sensing device displays selectivity over other anion species such as Br⁻, NO₂⁻, Cl⁻, F⁻, OAc⁻, ClO₄⁻, SCN⁻, NO₃⁻, HCO₃⁻ and H₂PO₄⁻ ions as only the presence of CN⁻ ion triggers the shift in colour of the sensing spot from yellow to red. The prepared sensor determines the target analyte with a LOD of 0.053 mg/L and shows recovery rates of 96-110%, which render the sensor promising for practical applications.

References-

- [1] A. Kumar, D. Kim, S. Kumar, A. Mahammed, D.G. Churchill, Z. Gross, Milestones in corrole chemistry: historical ligand syntheses and post-functionalization, *Chem. Soc. Rev.* 52 (2022) 573–600. <https://doi.org/10.1039/d1cs01137e>.
- [2] M.M. Kruk, D. V. Klenitsky, W. Maes, Molecular structure and conformation of free base corroles, *Macroheterocycles*. 12 (2019) 58–67. <https://doi.org/10.6060/mhc190229k>.
- [3] M. Conlon, A.W. Johnson, W.R. Overend, D. Rajapaksa, C.M. Elson, Structure and reactions of cobalt corroles, *J. Chem. Soc. Perkin Trans. 1.* (1973) 2281. <https://doi.org/10.1039/p19730002281>.
- [4] Y. Niu, M. Li, Q. Zhang, W. Zhu, J. Mack, G. Fomo, T. Nyokong, X. Liang, Halogen substituted A₂B type Co(III)triarylcorroles: Synthesis, electronic structure and two step modulation of electrocatalyzed hydrogen evolution reactions, *Dye. Pigment.* 142 (2017) 416–428. <https://doi.org/10.1016/j.dyepig.2017.02.049>.
- [5] S. Ganguly, D. Renz, L.J. Giles, K.J. Gagnon, L.J. McCormick, J. Conradie, R. Sarangi, A. Ghosh, Cobalt- and Rhodium-Corrole-Triphenylphosphine Complexes Revisited: The Question of a Noninnocent Corrole, *Inorg. Chem.* 56 (2017) 14788–14800. <https://doi.org/10.1021/acs.inorgchem.7b01828>.
- [6] A.W. Johnson, I.T. Kay, 306. Corroles. Part I. Synthesis, *J. Chem. Soc.* (1965) 1620. <https://doi.org/10.1039/jr9650001620>.
- [7] B.D. Dolphin, A.W. Johnson, J. Leng, p. van den broek, The Base-catalysed Cyclisations of 1,19-Dideoxybiladienes-ac, *J. Chem. Soc.* (1966) 880–884. <https://doi.org/10.1039/j39660000880>.
- [8] E. Vogel, S. Will, A.S. Tilling, L. Neumann, J. Lex, E. Bill, A.X. Trautwein, K. Wieghardt, Metallocorroles with Formally Tetravalent Iron, *Angew. Chemie Int. Ed. English.* 33 (1994) 731–735. <https://doi.org/10.1002/anie.199407311>.
- [9] Z. Gross, N. Galili, I. Saltsman, The first direct synthesis of corroles from pyrrole, *Angew. Chemie - Int. Ed.* 38 (1999) 1427–1429. [https://doi.org/10.1002/\(SICI\)1521-3773\(19990517\)38:10<1427](https://doi.org/10.1002/(SICI)1521-3773(19990517)38:10<1427).

- [10] R. Paolesse, L. Jaquinod, D.J. Nurco, S. Mini, F. Sagone, T. Boschi, K.M. Smith, 5,10,15-Triphenylcorrole: A product from a modified Rothemund reaction, *Chem. Commun.* 2 (1999) 1307–1308. <https://doi.org/10.1039/a903247i>.
- [11] L. Simkhovich, I. Goldberg, Z. Gross, Easy preparation of cobalt corrole and hexaphyrin and isolation of new oligopyrroles in the solvent-free condensation of pyrrole with pentafluorobenzaldehyde, *Org. Lett.* 5 (2003) 1241–1244. <https://doi.org/10.1021/ol0341142>.
- [12] B. Koszarna, D.T. Gryko, Efficient synthesis of meso-substituted corroles in a H₂O-MeOH mixture, *J. Org. Chem.* 71 (2006) 3707–3717. <https://doi.org/10.1021/jo060007k>.
- [13] R. Paolesse, F. Sagone, A. Macagnano, T. Boschi, L. Prodi, M. Montalti, N. Zaccheroni, F. Bolletta, K.M. Smith, Photophysical Behaviour of Corrole and its Symmetrical and Unsymmetrical Dyads, *J. Porphyr. Phthalocyanines.* 3 (1999) 364–370. [https://doi.org/10.1002/\(SICI\)1099-1409\(199906\)3:5<364::AID-JPP141>3.0.CO;2-4](https://doi.org/10.1002/(SICI)1099-1409(199906)3:5<364::AID-JPP141>3.0.CO;2-4).
- [14] H. Lei, A. Han, F. Li, M. Zhang, Y. Han, P. Du, W. Lai, R. Cao, Electrochemical, spectroscopic and theoretical studies of a simple bifunctional cobalt corrole catalyst for oxygen evolution and hydrogen production, *Phys. Chem. Chem. Phys.* 16 (2014) 1883–1893. <https://doi.org/10.1039/c3cp54361g>.
- [15] N. Maiti, J. Lee, S.J. Kwon, J. Kwak, Y. Do, D.G. Churchill, Synthetic, crystallographic and electrochemical studies of thienyl-substituted corrole complexes of copper and cobalt, *Polyhedron.* 25 (2006) 1519–1530. <https://doi.org/10.1016/j.poly.2005.10.016>.
- [16] S. Ooi, T. Tanaka, A. Osuka, Cobalt(III) and gallium(III) complexes of meso-free corroles with distinct position-dependent substituent effects, *J. Porphyr. Phthalocyanines.* 20 (2016) 274–281. <https://doi.org/10.1142/S1088424616500061>.
- [17] I. Saltsman, I. Goldberg, Z. Gross, Porphyrins and Corroles with 2,6-Pyrimidyl Substituents, *Org. Lett.* 17 (2015) 3214–3217. <https://doi.org/10.1021/acs.orglett.5b01297>.
- [18] O. Yadav, A. Varshney, A. Kumar, R.K. Ratnesh, M.S. Mehata, A₂B corroles: Fluorescence signaling systems for sensing fluoride ions, *Spectrochim. Acta - Part A Mol. Biomol. Spectrosc.* 202 (2018) 207–213. <https://doi.org/10.1016/j.saa.2018.05.051>.

- [19] A. Varshney, A. Kumar, S. Yadav, Catalytic activity of bis p-nitro A₂B (oxo)Mn(V) corroles towards oxygen transfer reaction to sulphides, *Inorganica Chim. Acta.* 514 (2021) 120013. <https://doi.org/10.1016/j.ica.2020.120013>.
- [20] K.M. Kadish, J. Shen, L. Frémond, P. Chen, M. El Ojaimi, M. Chkounda, C.P. Gros, J.M. Barbe, K. Ohkubo, S. Fukuzumi, R. Guilard, Clarification of the oxidation state of cobalt corroles in heterogeneous and homogeneous catalytic reduction of dioxygen, *Inorg. Chem.* 47 (2008) 6726–6737. <https://doi.org/10.1021/ic800458s>.
- [21] X. Jiang, M.L. Naitana, N. Desbois, V. Quesneau, S. Brandès, Y. Rousselin, W. Shan, W.R. Osterloh, V. Blondeau-Patissier, C.P. Gros, K.M. Kadish, Electrochemistry of Bis(pyridine)cobalt (Nitrophenyl)corroles in Nonaqueous Media, *Inorg. Chem.* 57 (2018) 1226–1241. <https://doi.org/10.1021/acs.inorgchem.7b02655>.
- [22] X. Jiang, W. Shan, N. Desbois, V. Quesneau, S. Brandès, E. Van Caemelbecke, W.R. Osterloh, V. Blondeau-Patissier, C.P. Gros, K.M. Kadish, Mono-DMSO ligated cobalt nitrophenylcorroles: Electrochemical and spectral characterization, *New J. Chem.* 42 (2018) 8220–8229. <https://doi.org/10.1039/c8nj00300a>.
- [23] L. Lvova, G. Pomarico, F. Mandoj, F. Caroleo, C. Di Natale, K.M. Kadish, S. Nardis, Smartphone coupled with a paper-based optode: Towards a selective cyanide detection, *J. Porphyr. Phthalocyanines.* 1088424620 (2020). <https://doi.org/10.1142/S1088424620500091>.
- [24] R. Paolesse, S. Licoccia, M. Fanciullo, E. Morgante, T. Boschi, Synthesis and characterization of cobalt(III) complexes of meso-phenyl-substituted corroles, *Inorganica Chim. Acta.* 203 (1993) 107–114. [https://doi.org/10.1016/S0020-1693\(00\)82913-8](https://doi.org/10.1016/S0020-1693(00)82913-8).
- [25] S. Ganguly, J. Conradie, J. Bendix, K.J. Gagnon, L.J. McCormick, A. Ghosh, Electronic Structure of Cobalt–Corrole–Pyridine Complexes: Noninnocent Five-Coordinate Co(II) Corrole–Radical States, *J. Phys. Chem. A.* 121 (2017) 9589–9598. <https://doi.org/10.1021/acs.jpca.7b09440>.
- [26] Jyoti, N. Fridman, A. Kumar, S.G. Warkar, Synthesis, structural characterization and binding ability of A₂B cobalt(III) corroles with pyridine, *Inorganica Chim. Acta.* 527 (2021) 120580. <https://doi.org/10.1016/j.ica.2021.120580>.

- [27] R. Guillard, C.P. Gros, J. Shao, J. Fischer, R. Weiss, K.M. Kadish, S. Gabriel, D. Bourgogne, B. Gabriel, I. Le Bel, L. Pasteur, R.B. Pascal, Alkyl and Aryl Substituted Corroles . 1 . Synthesis and Characterization of Free Base and Cobalt Containing Derivatives . X-ray Structure of (Me 4 Ph 5 Cor) Co (py) 2, *Chart.* (2001) 4845–4855.
- [28] W.R. Osterloh, N. Desbois, V. Quesneau, S. Brandès, P. Fleurat-Lessard, Y. Fang, V. Blondeau-Patissier, R. Paolesse, C.P. Gros, K.M. Kadish, Old Dog, New Tricks: Innocent, Five-coordinate Cyanocobalt Corroles, *Inorg. Chem.* 59 (2020) 8562–8579. <https://doi.org/10.1021/acs.inorgchem.0c01037>.
- [29] W.R. Osterloh, V. Quesneau, N. Desbois, S. Brandès, W. Shan, V. Blondeau-Patissier, R. Paolesse, C.P. Gros, K.M. Kadish, Synthesis and the Effect of Anions on the Spectroscopy and Electrochemistry of Mono(dimethyl sulfoxide)-Ligated Cobalt Corroles, *Inorg. Chem.* 59 (2020) 595–611. <https://doi.org/10.1021/acs.inorgchem.9b02855>.
- [30] V. Quesneau, W. Shan, N. Desbois, S. Brandès, Y. Rousselin, M. Vanotti, V. Blondeau-Patissier, M. Naitana, P. Fleurat-Lessard, E. Van Caemelbecke, K.M. Kadish, C.P. Gros, Cobalt Corroles with Bis-Ammonia or Mono-DMSO Axial Ligands. Electrochemical, Spectroscopic Characterizations and Ligand Binding Properties, *Eur. J. Inorg. Chem.* 2018 (2018) 4265–4277. <https://doi.org/10.1002/ejic.201800897>.
- [31] P.B. Hitchcock, G.M. McLaughlin, Five-co-ordinate cobalt(III): Crystal and molecular structure of corrole(triphenylphosphine)cobalt(III), *J. Chem. Soc. Dalt. Trans.* (1976) 1927–1930. <https://doi.org/10.1039/DT9760001927>.
- [32] R. Paolesse, S. Licoccia, G. Bandoli, A. Dolmeua, T. Boschi, T. Chimiche, R. Tor, V. Ricerca, S. Farmaceutiche, U. Padova, First Direct Synthesis of a Corrole Ring from a Monopyrrolic Precursor , Crystal and Molecular, *Inorg. Chem.* (1994) 1171–1176. [https://doi.org/0020-166919411333-1171\\$04.50/0](https://doi.org/0020-166919411333-1171$04.50/0).
- [33] A. Kumar, I. Goldberg, M. Botoshansky, Y. Buchman, Z. Gross, Oxygen atom transfer reactions from isolated (Oxo)manganese(V) corroles to sulfides, *J. Am. Chem. Soc.* 132 (2010) 15233–15245. <https://doi.org/10.1021/ja1050296>.

- [34] J. Tang, Z. Ou, L. Ye, M. Yuan, Y. Fang, Z. Xue, K.M. Kadish, Meso-dichlorophenyl substituted Co(III) corrole: A selective electrocatalyst for the two-electron reduction of dioxygen in acid media, X-ray crystal structure analysis and electrochemistry, *J. Porphyr. Phthalocyanines*. 18 (2014) 891–898. <https://doi.org/10.1142/S1088424614500734>.
- [35] I.G. and Z.G. Atif Mahammed Ilona Giladi, Synthesis and Structural Characterization of a novel Covalently-Bound Corrole Dimer, *Chem. Eur. J.* 2001., 723 (2001) 4259–4265. <https://doi.org/0947-6539/01/0719-4259> \$ 17.50+.50/0.
- [36] C.M. Lemon, D.K. Dogutan, D.G. Nocera, Porphyrin and Corrole Platforms for Water Oxidation, Oxygen Reduction, and Peroxide Dismutation, in: *Handb. Porphyr. Sci.*, 2012: pp. 1–143. https://doi.org/10.1142/9789814397605_0001.
- [37] K.M. Kadish, J. Shao, Z. Ou, R. Zhan, F. Burdet, J.M. Barbe, C.P. Gros, R. Guillard, Electrochemistry and spectroelectrochemistry of heterobimetallic porphyrin-corrole dyads. Influence of the spacer, metal ion, and oxidation state on the pyridine binding ability, *Inorg. Chem.* 44 (2005) 9023–9038. <https://doi.org/10.1021/ic051073s>.
- [38] J.P. Collman, M. Kaplun, R.A. Decréau, Metal corroles as electrocatalysts for oxygen reduction, *Dalt. Trans.* (2006) 554–559. <https://doi.org/10.1039/b512982f>.
- [39] A. Schechter, M. Stanevsky, A. Mahammed, Z. Gross, Four-Electron Oxygen Reduction by Brominated Cobalt Corrole, *Inorg. Chem.* 51 (2012) 22-24. <https://doi.org/10.1021/ic202139f>.
- [40] D.K. Dogutan, S.A. Stoian, R. McGuire, M. Schwalbe, T.S. Teets, D.G. Nocera, Hangman Corroles: Efficient Synthesis and Oxygen Reaction Chemistry, *J. Am. Chem. Soc.* 133 (2011) 131–140. <https://doi.org/10.1021/ja108904s>.
- [41] B. Li, Z. Ou, D. Meng, J. Tang, Y. Fang, R. Liu, K.M. Kadish, Cobalt triarylcorroles containing one, two or three nitro groups. Effect of NO₂ substitution on electrochemical properties and catalytic activity for reduction of molecular oxygen in acid media, *J. Inorg. Biochem.* 136 (2014) 130–139. <https://doi.org/10.1016/j.jinorgbio.2013.12.014>.
- [42] A. Rana, Y.M. Lee, X. Li, R. Cao, S. Fukuzumi, W. Nam, Highly Efficient Catalytic Two-Electron Two-Proton Reduction of Dioxygen to Hydrogen Peroxide with a Cobalt Corrole Complex, *ACS Catal.* 11 (2021) 3073–3083. <https://doi.org/10.1021/acscatal.0c05003>.

- [43] P. Trogadas, M.O. Coppens, Nature-inspired electrocatalysts and devices for energy conversion, *Chem. Soc. Rev.* 49 (2020) 3107–3141. <https://doi.org/10.1039/C8CS00797G>.
- [44] V.A. Vaillard, P.D. Nieres, S.E. Vaillard, F. Doctorovich, B. Sarkar, N.I. Neuman, Cobalt, Iron, and Manganese Metalloporphyrins in Catalytic Oxidation of Water. An Overview of the Synthesis, Selected Redox and Electronic Properties, and Catalytic Activities, *Eur. J. Inorg. Chem.* 2022 (2022). <https://doi.org/10.1002/ejic.202100767>.
- [45] V. Artero, M. Chavarot-Kerlidou, M. Fontecave, Splitting water with cobalt, *Angew. Chemie - Int. Ed.* 50 (2011) 7238–7266. <https://doi.org/10.1002/anie.201007987>.
- [46] Y. Chen, Q.H. Fan, M.S. Hossain, S.Z. Zhan, H.Y. Liu, L.P. Si, Electrocatalytic Hydrogen Evolution of Cobalt and Free-base Triaryl Corrole Bearing Hydroxyethyl Amino Groups, *Eur. J. Inorg. Chem.* 2020 (2020) 491–498. <https://doi.org/10.1002/ejic.201900996>.
- [47] H. Lin, M.S. Hossain, S.Z. Zhan, H.Y. Liu, L.P. Si, Electrocatalytic hydrogen evolution using triaryl corrole cobalt complex, *Appl. Organomet. Chem.* (2020) 1–10. <https://doi.org/10.1002/aoc.5583>.
- [48] H. Chen, D.L. Huang, M.S. Hossain, G.T. Luo, H.Y. Liu, Electrocatalytic activity of cobalt tris(4-nitrophenyl)corrole for hydrogen evolution from water, *J. Coord. Chem.* 72 (2019) 2791–2803. <https://doi.org/10.1080/00958972.2019.1671588>.
- [49] M.A. Morales Vásquez, M. Hamer, N.I. Neuman, A.Y. Tesio, A. Hunt, H. Bogo, E.J. Calvo, F. Doctorovich, Iron and cobalt corroles in solution and on carbon nanotubes as molecular photocatalysts for hydrogen production by water reduction, *ChemCatChem.* 9 (2017) 3259–3268. <https://doi.org/10.1002/cctc.201700349>.
- [50] H. Sun, Y. Han, H. Lei, M. Chen, R. Cao, Cobalt corroles with phosphonic acid pendants as catalysts for oxygen and hydrogen evolution from neutral aqueous solution, *Chem. Commun.* 53 (2017) 6195–6198. <https://doi.org/10.1039/c7cc02400b>.
- [51] K. Sudhakar, A. Mahammed, N. Fridman, Z. Gross, Trifluoromethylation for affecting the structural, electronic and redox properties of cobalt corroles, *Dalt. Trans.* 48 (2019) 4798–4810. <https://doi.org/10.1039/c9dt00675c>.

- [52] W. Zhang, W. Lai, R. Cao, Energy-Related Small Molecule Activation Reactions: Oxygen Reduction and Hydrogen and Oxygen Evolution Reactions Catalyzed by Porphyrin- and Corrole-Based Systems, *Chem. Rev.* 117 (2017) 3717–3797. <https://doi.org/10.1021/acs.chemrev.6b00299>.
- [53] B. Mondal, K. Sengupta, A. Rana, A. Mahammed, M. Botoshansky, S.G. Dey, Z. Gross, A. Dey, Cobalt Corrole Catalyst for Efficient Hydrogen Evolution Reaction from H₂O under Ambient Conditions: Reactivity, Spectroscopy, and Density Functional Theory Calculations, *Inorg. Chem.* 52 (2013) 3381–3387. <https://doi.org/10.1021/ic4000473>.
- [54] A. Mahammed, B. Mondal, A. Rana, A. Dey, Z. Gross, The cobalt corrole catalyzed hydrogen evolution reaction: surprising electronic effects and characterization of key reaction intermediates, *Chem. Commun.* 50 (2014) 2725–2727. <https://doi.org/10.1039/C3CC48462A>.
- [55] H. Sun, Y. Han, H. Lei, M. Chen, R. Cao, Cobalt corroles with phosphonic acid pendants as catalysts for oxygen and hydrogen evolution from neutral aqueous solution, *Chem. Commun.* 53 (2017) 6195–6198. <https://doi.org/10.1039/c7cc02400b>.
- [56] X. Li, H. Lei, J. Liu, X. Zhao, S. Ding, Z. Zhang, X. Tao, W. Zhang, W. Wang, X. Zheng, R. Cao, Carbon Nanotubes with Cobalt Corroles for Hydrogen and Oxygen Evolution in pH 0–14 Solutions, *Angew. Chemie - Int. Ed.* 57 (2018) 15070–15075. <https://doi.org/10.1002/anie.201807996>.
- [57] X. Li, H. Lei, X. Guo, X. Zhao, S. Ding, X. Gao, W. Zhang, R. Cao, Graphene-Supported Pyrene-Modified Cobalt Corrole with Axial Triphenylphosphine for Enhanced Hydrogen Evolution in pH 0–14 Aqueous Solutions, *ChemSusChem.* 10 (2017) 4632–4641. <https://doi.org/10.1002/cssc.201701196>.
- [58] H. Li, X. Li, H. Lei, G. Zhou, W. Zhang, R. Cao, Convenient Immobilization of Cobalt Corroles on Carbon Nanotubes through Covalent Bonds for Electrocatalytic Hydrogen and Oxygen Evolution Reactions, *ChemSusChem.* 12 (2019) 801–806. <https://doi.org/10.1002/cssc.201802765>.
- [59] X. Liang, Y. Qiu, X. Zhang, W. Zhu, The post-functionalization of Co(III)PPh₃ triarylcorroles through Suzuki-Miyaura couplings and their tunable electrochemically-catalyzed hydrogen evolution and oxygen reduction, *Dalt. Trans.* 49 (2020) 3326–3332. <https://doi.org/10.1039/c9dt04917g>.

- [60] A. Kumar, S. Sujesh, P. Varshney, A. Paul, S. Jeyaraman, Aminophenyl-substituted cobalt(III) corrole: A bifunctional electrocatalyst for the oxygen and hydrogen evolution reactions, *Dalt. Trans.* 48 (2019) 11345–11351. <https://doi.org/10.1039/c9dt02339a>.
- [61] L. Xu, H. Lei, Z. Zhang, Z. Yao, J. Li, Z. Yu, R. Cao, The effect of the: Trans axial ligand of cobalt corroles on water oxidation activity in neutral aqueous solutions, *Phys. Chem. Chem. Phys.* 19 (2017) 9755–9761. <https://doi.org/10.1039/c6cp08495h>.
- [62] D.K. Dogutan, R. McGuire, D.G. Nocera, Electrocatalytic water oxidation by cobalt(III) hangerman β -octafluoro corroles, *J. Am. Chem. Soc.* 133 (2011) 9178–9180. <https://doi.org/10.1021/ja202138m>.
- [63] W. Lai, R. Cao, G. Dong, S. Shaik, J. Yao, H. Chen, Why is cobalt the best transition metal in transition-metal hangerman corroles for O-O bond formation during water oxidation?, *J. Phys. Chem. Lett.* 3 (2012) 2315–2319. <https://doi.org/10.1021/jz3008535>.
- [64] M.Z. Ertem, C.J. Cramer, Quantum chemical characterization of the mechanism of a supported cobalt-based water oxidation catalyst, *Dalt. Trans.* 41 (2012) 12213. <https://doi.org/10.1039/c2dt31871g>.
- [65] H. Lei, C. Liu, Z. Wang, Z. Zhang, M. Zhang, X. Chang, W. Zhang, R. Cao, Noncovalent Immobilization of a Pyrene-Modified Cobalt Corrole on Carbon Supports for Enhanced Electrocatalytic Oxygen Reduction and Oxygen Evolution in Aqueous Solutions, *ACS Catal.* 6 (2016) 6429–6437. <https://doi.org/10.1021/acscatal.6b01579>.
- [66] L. Xu, H. Lei, Z. Zhang, Z. Yao, J. Li, Z. Yu, R. Cao, The effect of the: Trans axial ligand of cobalt corroles on water oxidation activity in neutral aqueous solutions, *Phys. Chem. Chem. Phys.* 19 (2017) 9755–9761. <https://doi.org/10.1039/c6cp08495h>.
- [67] W. Sinha, A. Mizrahi, A. Mahammed, B. Tumanskii, Z. Gross, Reactive Intermediates Involved in Cobalt Corrole Catalyzed Water Oxidation (and Oxygen Reduction), *Inorg. Chem.* 57 (2018) 478–485. <https://doi.org/10.1021/acs.inorgchem.7b02696>.
- [68] H. Vazquez-Lima, J. Conradie, A. Ghosh, Metalloporrole Interactions with Carbon Monoxide, Nitric Oxide, and Nitroxyl - A DFT Study of Low-Energy Bound States, *Inorg. Chem.* 55 (2016) 8248–8250. <https://doi.org/10.1021/acs.inorgchem.6b01189>.

- [69] J.M. Barbe, G. Canard, S. Brandès, G. Dubois, R. Guillard, Metalloporphyrins as sensing components for gas sensors: Remarkable affinity and selectivity of cobalt(III) porphyrins for CO vs. O₂ and N₂, *Dalt. Trans.* 4 (2004) 1208–1214. <https://doi.org/10.1039/b316706b>.
- [70] J.M. Barbe, G. Canard, S. Brandès, R. Guillard, Organic-inorganic hybrid sol-gel materials incorporating functionalized cobalt(III) porphyrins for the selective detection of CO, *Angew. Chemie - Int. Ed.* 44 (2005) 3103–3106. <https://doi.org/10.1002/anie.200463009>.
- [71] J.M. Barbe, G. Canard, S. Brandès, R. Guillard, Selective chemisorption of carbon monoxide by organic-inorganic hybrid materials incorporating cobalt(III) porphyrins as sensing components, *Chem. - A Eur. J.* 13 (2007) 2118–2129. <https://doi.org/10.1002/chem.200601143>.
- [72] M. Vanotti, V. Blondeau-Patissier, D. Rabus, J.Y. Rauch, J.M. Barbe, S. Ballandras, Development of acoustic devices functionalized with cobalt porphyrins or metalloporphyrins for the detection of carbon monoxide at low concentration, *Sensors and Transducers.* 14 (2012) 197–211.
- [73] V. Blondeau-Patissier, M. Vanotti, T. Prêtre, D. Rabus, L. Tortora, J.M. Barbe, S. Ballandras, Detection and monitoring of carbon monoxide using cobalt porphyrin film on love wave devices with delay line configuration, *Procedia Eng.* 25 (2011) 1085–1088. <https://doi.org/10.1016/j.proeng.2011.12.267>.
- [74] R. Aragón, R. Lombardi, Field Effect Devices Sensitive to CO at Room Temperature, *Sensors & Transducers.* 180 (2014) 80–84.
- [75] L. Tortora, G. Pomarico, S. Nardis, E. Martinelli, A. Catini, A. D'Amico, C. Di Natale, R. Paolesse, Supramolecular sensing mechanism of porphyrin thin films, *Sensors Actuators, B Chem.* 187 (2013) 72–77. <https://doi.org/10.1016/j.snb.2012.09.055>.
- [76] A. Savoldelli, G. Magna, C. Di Natale, A. Catini, S. Nardis, F.R. Fronczek, K.M. Smith, R. Paolesse, β -Acrolein-Substituted Porphyrins: A Route to the Preparation of Functionalized Polyacrolein Microspheres for Chemical Sensor Applications, *Chem. - A Eur. J.* 23 (2017) 14819–14826. <https://doi.org/10.1002/chem.201702380>.

CHAPTER 2

SCOPE OF THE WORK

Corroles and metallocorroles, due to their ease of synthesis as well as their fascinating spectral, electrochemical, and coordination properties, have gained significant attention since the very beginning. Their structure can be tuned by functionalization at β -pyrrolic, *meso*-, and axial positions, which affect their activity and, therefore, their characteristics towards different reaction processes, resulting in their suitability for a variety of applications. Catalysis, sensing, and fluorescence emission are some of the noteworthy features of corroles and metallocorroles. Cobalt corroles are among the first metallocorroles described by Johnson in the early 1960s. These are of tremendous interest due to their structural similarity to cobalt corrins and cobalt porphyrins, but they have superior properties in a variety of ways. These complexes offer both, metal- and ring-centred reactions depending on the reaction parameters, such as type and number of substituents in *meso*-, β - and axial positions. This critical feature has been assessed using a number of techniques, including UV–Visible, NMR, DFT, cyclic voltammetry, and controlled-potential electrolysis. These are frequently found in the form of triphenylphosphine or dipyridine-ligated complexes. The bis-pyridine ligated cobalt corroles display variation in co-ordination numbers in different media. Therefore, a greater insight into the Bis-pyridine ligated series of A_2B cobalt corroles was needed. The pyridine ligation exhibits a peculiar axial ligation behaviour that need to be described more and calls for further explanations. Additionally, the UV-Visible Spectroscopic properties of ABA/A_2B cobalt corroles may be thoroughly investigated. In-depth research on the characteristics and behaviour of those complexes when placed

in a variety of non-aqueous mediums may be further studied. Also, there was insufficient investigation of the activity of cobalt corroles when exposed to a variety of anions. It is also possible that the catalytic activity of such complexes may be investigated further as well.

- The **objectives** of the present dissertation are as follows:
- Synthesis of a series of A₂B type free base and their bis pyridine and triphenylphosphine ligated cobalt corroles.
 - Characterization of synthesized cobalt corroles using different spectral techniques: ¹H NMR, UV-Visible Spectroscopy, mass spectrometry and Single Crystal XRD.
 - Study the anion interaction with the synthesised cobalt corroles using colorimetric and spectroscopic approaches.
 - Study the Electrochemical properties of cobalt corroles using Cyclic voltammetry technique.

CHAPTER 3

SYNTHESIS, STRUCTURAL CHARACTERIZATION AND BINDING ABILITY OF A₂B COBALT(III) CORROLES WITH PYRIDINE

3.1 INTRODUCTION

The axially co-ordinating ligands which exert a huge effect on the electrochemical and redox properties of these metallocorroles have lately been focused on.[1–8] The cobalt corroles with axially ligating pyridine, DMSO, NH₃ or CO have evidenced this impact as these co-ordinating ligands cause not only changes in electron density at the metal ion, but also, in certain instances, a change in the oxidation state of both metal and ligand.[1–3] The ligand co-ordination with the central cobalt incorporated into the macrocyclic ligand is largely found solvent and concentration dependent. The anion interaction of a series of different cobalt A₃-triarylcorroles was also recently reported, where among 11 different anions, namely CN⁻, PF₆⁻, BF₄⁻, HSO₄⁻, ClO₄⁻, Br⁻, I⁻, Cl⁻, OAc⁻, F⁻, and OTs⁻, the only exception was CN⁻ that interacted with the neutral form of Co-corroles.[9] This led to the formation of mono- and bis-cyanocobalt complexes in DCM solution, the first example of air stable Co-corroles with anionic axial ligands. Later, their chemical properties were discussed in comparison to mono-DMSO precursors, bis-pyridine analogues and the transient mixed-ligand adducts comprising one CN⁻ and one pyridine axial ligand.[10] For CO₂ conversion to CO, a comparative investigation of Cobalt chelated superstructured corroles with PPh₃ and bis-pyridine present axially was also conducted where these complexes performed efficiently towards CO₂ reduction.[7] To further insight into the spectroscopic properties of cobalt

corroles, we have synthesized a new series of A₂B type, bis-pyridine ligated complexes where two *meso*- positions, C₅ and C₁₅, are p-NO₂ phenyl substituted whereas substituents present at C₁₀ position are either electron withdrawing or releasing group. (**Scheme 3.1**) In present study, we investigated the impact of electron withdrawing or electron donating substituents on the binding constant of these cobalt complexes with pyridine in detail.[11] NMR spectroscopy for these complexes was also studied which revealed a strong shift in pyridine protons as the electron density increased on the corrole macrocycle, indicating that different substituents had a distinct effect on the overall structure of the complex. The X-ray crystallographic parameters and the chemical shift of β-protons inferred that cobalt is coordinated to a corrole macrocycle and present in low spin Co^{III} complex.

3.2 EXPERIMENTAL SECTION

3.2.1 Instrumentation:

Nuclear magnetic resonance spectroscopy: ¹H and ¹⁹F NMR spectra were recorded on a Bruker Avance spectrometer operating at 400 MHz for ¹H and 377 MHz for ¹⁹F NMR. Chemical shifts are reported in ppm relative to residual solvent peaks of chloroform ($\delta = 7.26$ ppm) or benzene ($\delta = 7.16$ ppm) in the ¹H NMR spectra. The obtained spectra were evaluated by using MesteRenova software.

Mass spectroscopy: High-resolution mass spectra (HRMS) of complexes were recorded by Maxis Impact HD Mass Spectrometer and APCI (atmospheric pressure chemical ionization) was used as a direct probe in either positive or negative mode.

UV-Visible spectroscopy: Spectral measurements were carried out with the UV-1800 Shimadzu Spectrophotometer. Cuvettes made up of Quartz with optical path lengths of 1 cm were used.

3.2.2 Binding Constant Determination:

Binding constant for pyridine was experimentally determined by UV-Visible spectroscopic method for all the complexes. In this method, the titration of cobalt complexes solution with pyridine was monitored using UV-Visible spectroscopy. Later the data was fitted in Hill equation (eq (3.1)) and the graph between concentration of pyridine vs absorbance was plotted.[12,13]

$$\log \left[\frac{(A_i - A_0)}{(A_f - A_i)} \right] = \log K + n \log [L] \quad \text{eq (3.1)}$$

Where A_0 is the initial absorbance when concentration of ligand [L] is zero, A_i is absorbance at a specific concentration of L and A_f signifies final absorbance value when only a fully ligated species of corrole complex remains in solution. $\log K$ values were obtained from intercept of the graph plotted between $\log((A_i - A_0)/(A_f - A_i))$ vs $\log [L]$ and is the binding constant for 'n' number of ligands coordinated axially.

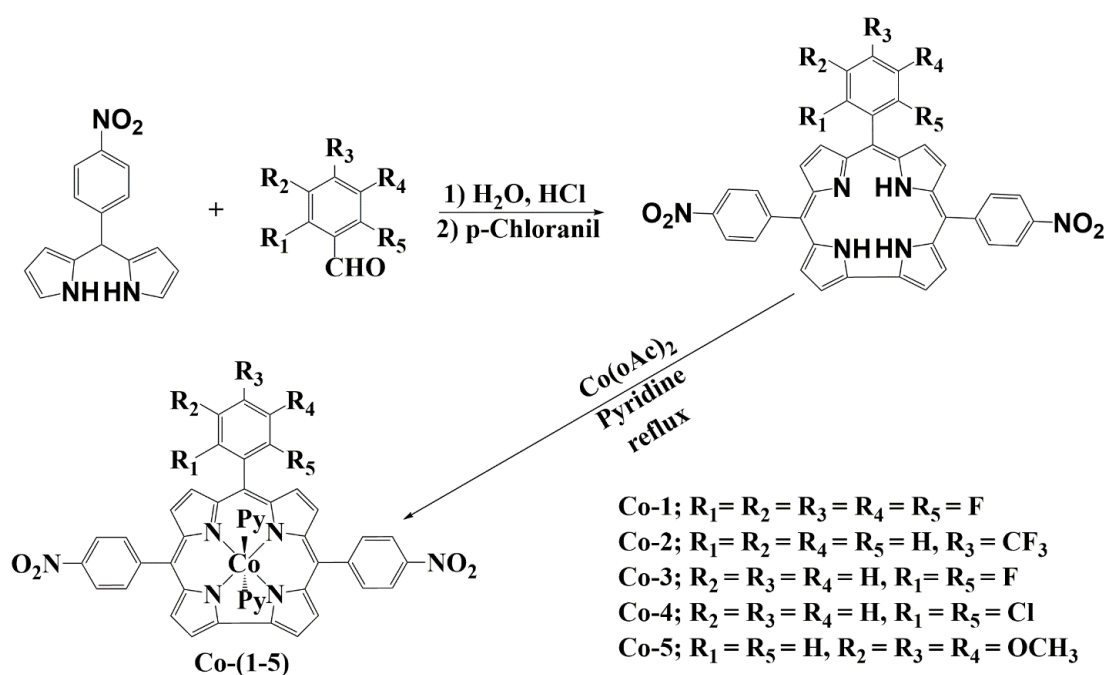
3.2.3 Chemicals

All chemicals and solvents were used as purchased without further purification else otherwise noted. Silica gel (230-440 mesh) and neutral alumina were used for column chromatography. Benzonitrile (PhCN) purchased from Sigma-Aldrich chemical Co. was used. Pyridine (99%) and p-chloranil (98%), were obtained from Avra chemicals and dichloromethane (CH_2Cl_2) from Merck and used without further purification.

3.2.4 Synthesis

A similar procedure for the preparation of all the desired five cobalt corroles (Co-1 to 5) was followed. To prepare the free base corroles, the pathway provided by Gryko *et*

al.[14] was utilized and then insertion of cobalt metal was performed using Co(OAc)₂·4H₂O in pyridine (acting as solvent as well as coordinating ligand) to obtain the corresponding metallocorroles derivatives (Scheme 3.1).[15] The free base synthesis involved dipyrromethane (1 mmol) and aromatic aldehyde (0.5 mmol) dissolved in 150 mL of CH₃OH in a round-bottom flask. Then 2.5 mL of HCl (36%) in 50 mL water was added to it and stirred at room temperature for 2 h. The mixture was extracted with CHCl₃, washed twice with water, and dried over Na₂SO₄. The organic layer was then filtered and diluted to a volume of 250 ml using CHCl₃. The mixture was then stirred overnight at room temperature after adding p-chloranil (1.5 mmol) as an oxidising agent to it. This reaction mixture was then chromatographed on a silica gel column using the DCM/Hexane as eluent. The green coloured free base corrole was obtained which further underwent metal insertion reaction and resulted in the desired cobalt corrole Co-(1-5) formation. For the metalation of free



Scheme 3.1. Synthetic route of A₂B cobalt corroles Co-(1 to 5).

base corroles, in a 100 mL round-bottom flask the synthesised free base corrole (19 mg) and Co(OAc)₂·4H₂O (33.61 mg) was dissolved in pyridine (15 mL) and the resulting solution was refluxed with stirring in an oil bath at 100°C for 20-30 min. The completion of the reaction was monitored through TLC. Afterwards, the reaction mixture was cooled to room temperature and pyridine was evaporated on a rotary evaporator. The residue was dissolved in a minimum amount of DCM and passed over the silica gel column. The mixture containing DCM, hexane as well as pyridine under different concentrations (described below for each corrole) was used as eluent.

3.2.4.1 Bis-pyridine[10-(2,3,4,5,6-pentafluorophenyl)-5,15-bis(4-nitrophenyl)corrolato] Cobalt(III) (Co-1) was obtained through silica gel chromatography with DCM:Hexane:Pyridine (2:8:0.1) as eluent in 79% yield (19.51 mg, 0.0198 mmol). UV-Visible [DCM + pyridine (0.1%); λ , nm]: 376 (50.4), 426 (49.3), 652 (0.305). ¹H NMR (400 MHz, C₆D₆) δ 9.21 (d, ³J_{H,H} = 4.3 Hz, 2H, β -pyrrolic), 8.92 (d, ³J_{H,H} = 4.8 Hz, 2H, β -pyrrolic), 8.74 (d, ³J_{H,H} = 4.3 Hz, 2H, β -pyrrolic), 8.61 (d, ³J_{H,H} = 4.7 Hz, 2H, β -pyrrolic), 8.04 (d, ³J_{H,H} = 8.7 Hz, 4H, *o/m*-Ph), 7.85 (d, ³J_{H,H} = 8.7 Hz, 4H, *o/m*-Ph), 4.58 (br s, 2H, *p*-H of pyridine), 3.95 (br s, 4H, *m*-H of pyridine), 1.33 (br s, 4H, *o*-H of pyridine overlapped with a solvent signal). **(Figure 3.1)** ¹⁹F NMR (377 MHz, C₆D₆) δ -139.37 (dd, ³J_{F,F} = 26.2, 9.1 Hz, 2F, *o*-F of Ph), -153.77 (t, ³J_{F,F} = 20.3 Hz, 1F, *p*-F of Ph), -162.86 (ddd, ³J_{F,F} = 26.1, 22.3, 8.9 Hz, 2F, *m*-F of Ph). **(Figure 3.2)** HRMS: Calcd for C₃₇H₁₆CoF₅N₆O₄ ([M-2py]⁺) m/z 762.0485, m/z found 762.0504 ([M-2py]⁺). **(Figure 3.3)**

3.2.4.2 Bis-pyridine[10-(4-trifluoromethylphenyl)-5,15-bis(4-nitrophenyl)corrolato] Cobalt (III) (Co-2) was obtained through silica gel chromatography with DCM:Hexane:Pyridine (4:8:0.1) as eluent in 82% yield (20.42 mg, 0.0227 mmol). UV-Visible [DCM + pyridine (0.1%); λ , nm ($\epsilon \times 10^{-3}$, L mol⁻¹ cm⁻¹)]: 370 (54.3), 421 (47.1), 562 (9.1), 644 (22.3). ¹H NMR (400 MHz, C₆D₆)

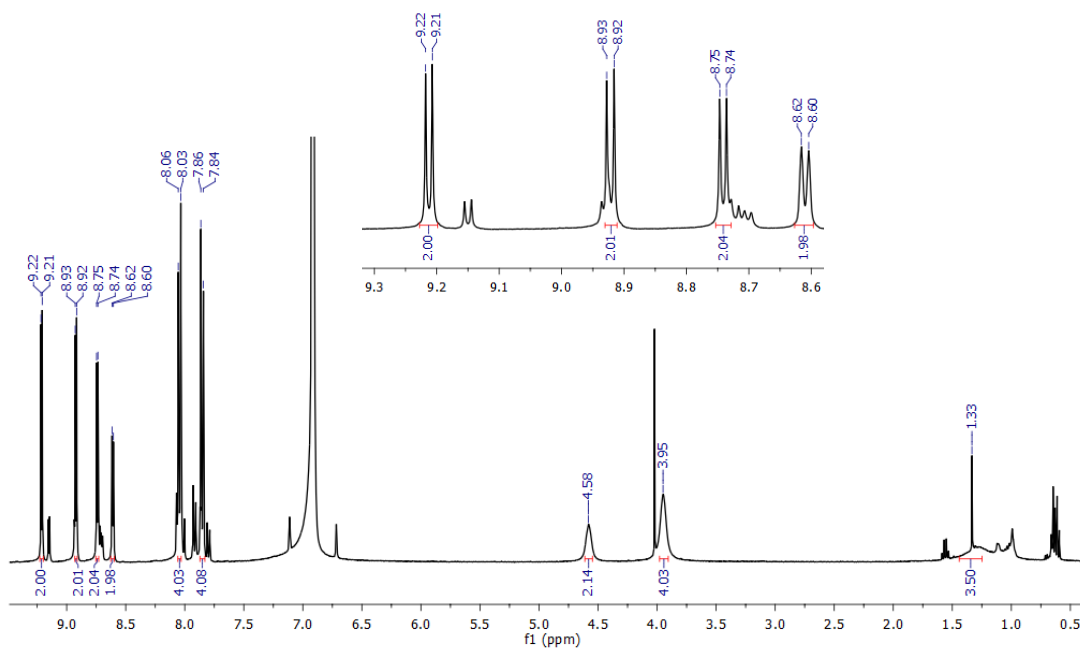


Figure 3.1. ¹H NMR spectrum of Co-1 in C₆D₆.

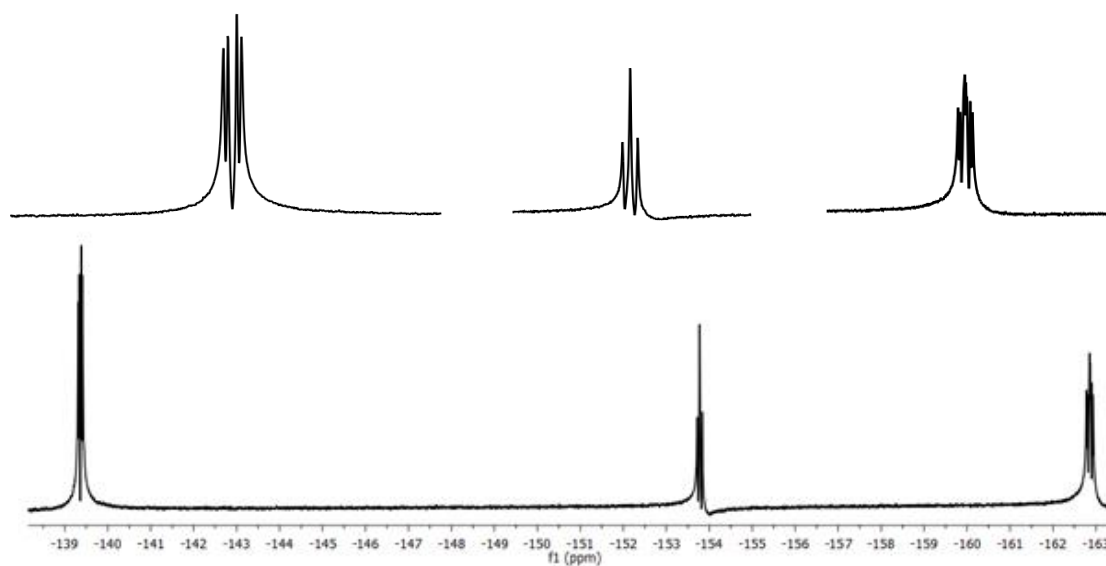
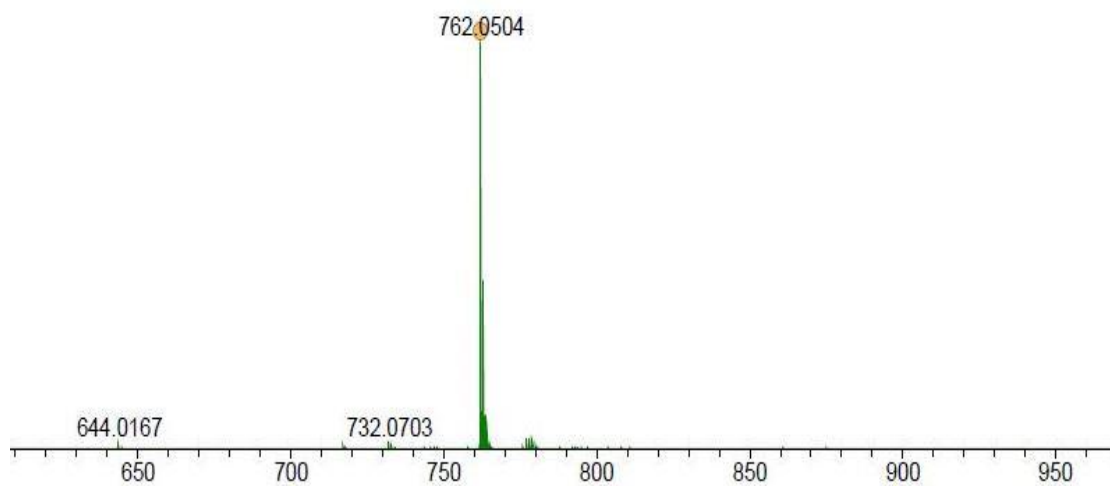
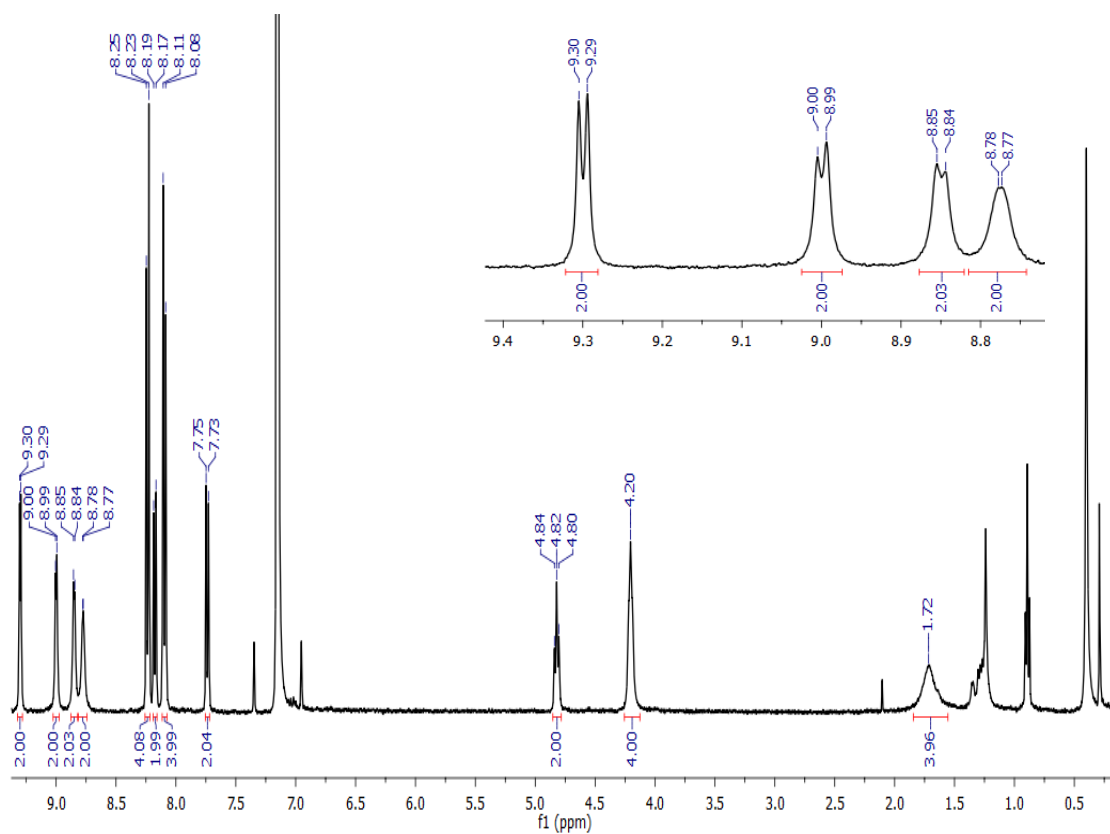


Figure 3.2. ¹⁹F NMR spectrum of Co-1 in C₆D₆.

**Figure 3.3.** HRMS spectra of Co-1.**Figure 3.4.** ^1H NMR spectrum of Co-2 in C_6D_6 .

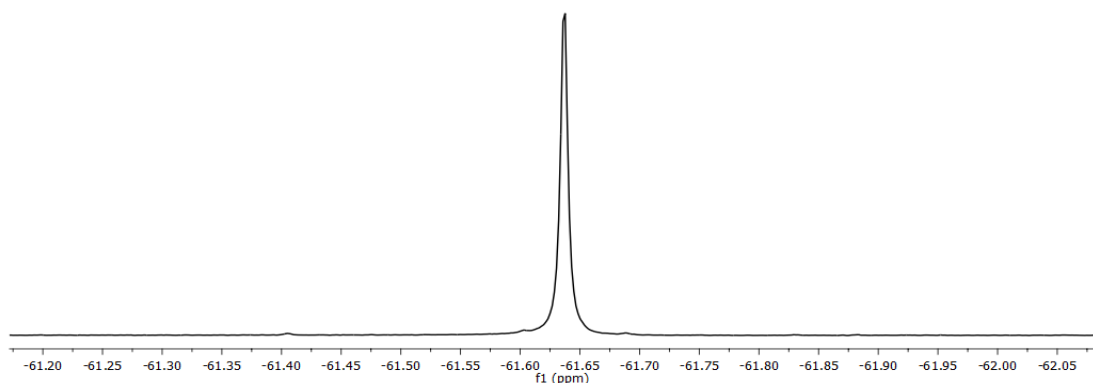


Figure 3.5. ¹⁹F NMR spectrum of Co-2 in C₆D₆.

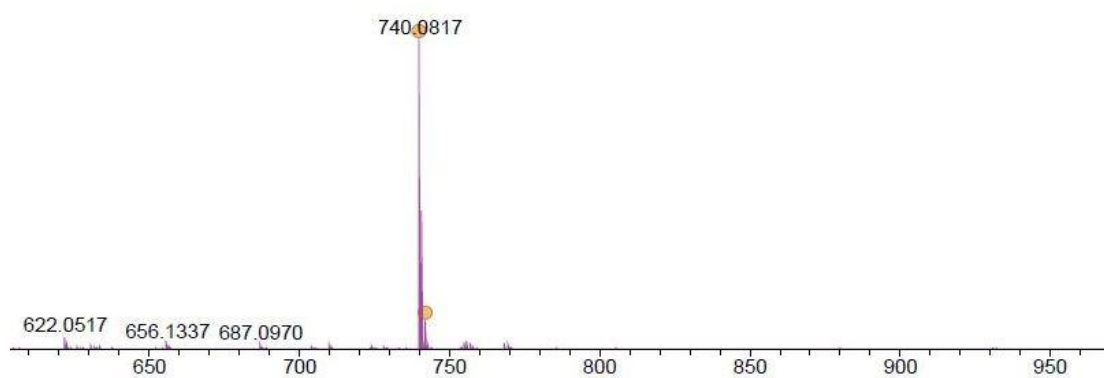


Figure 3.6. HRMS spectra of Co-2.

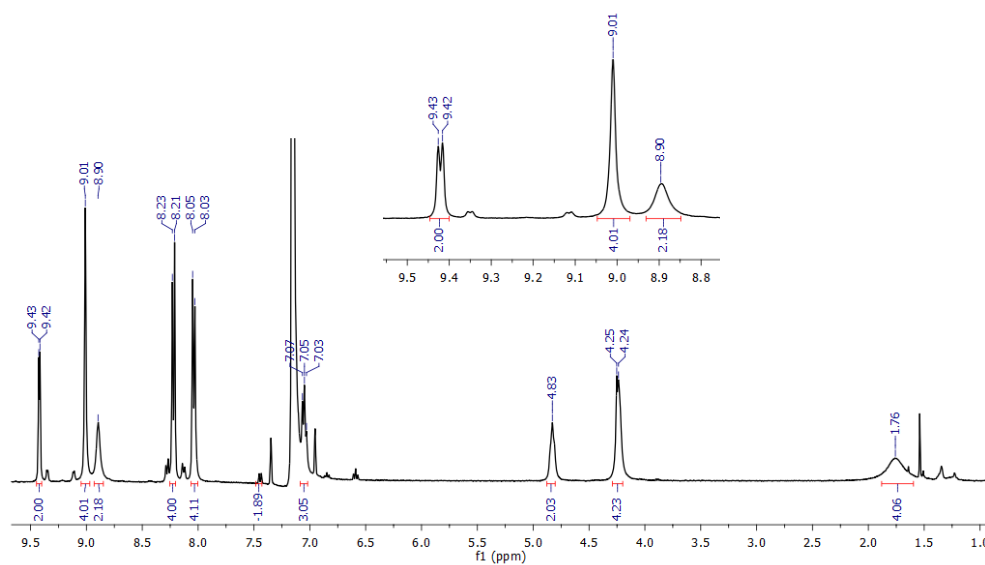
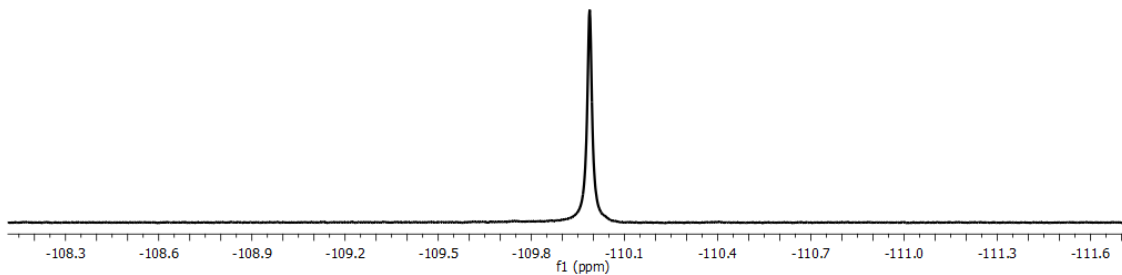
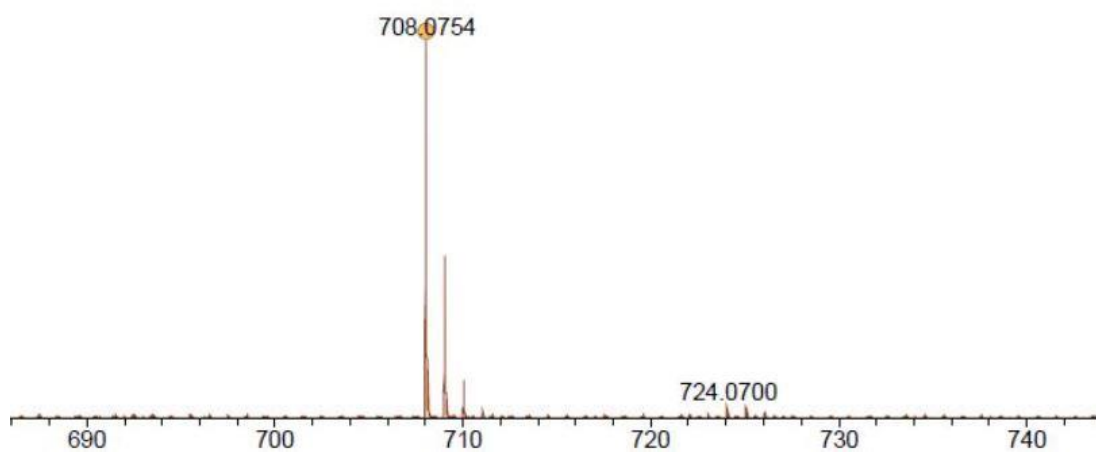
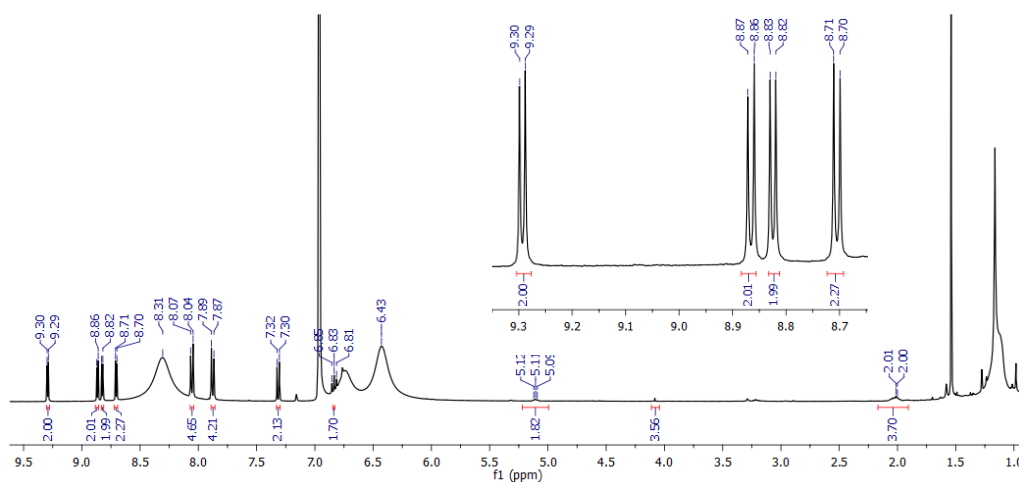
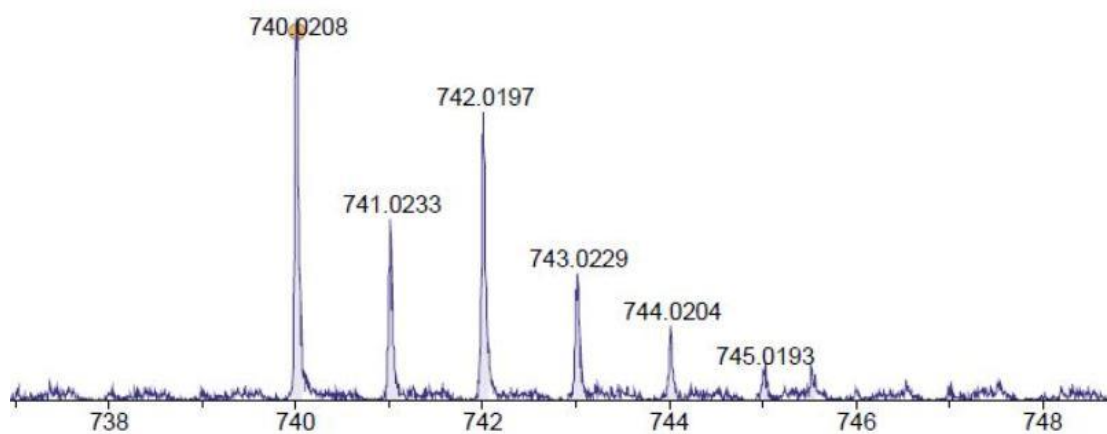
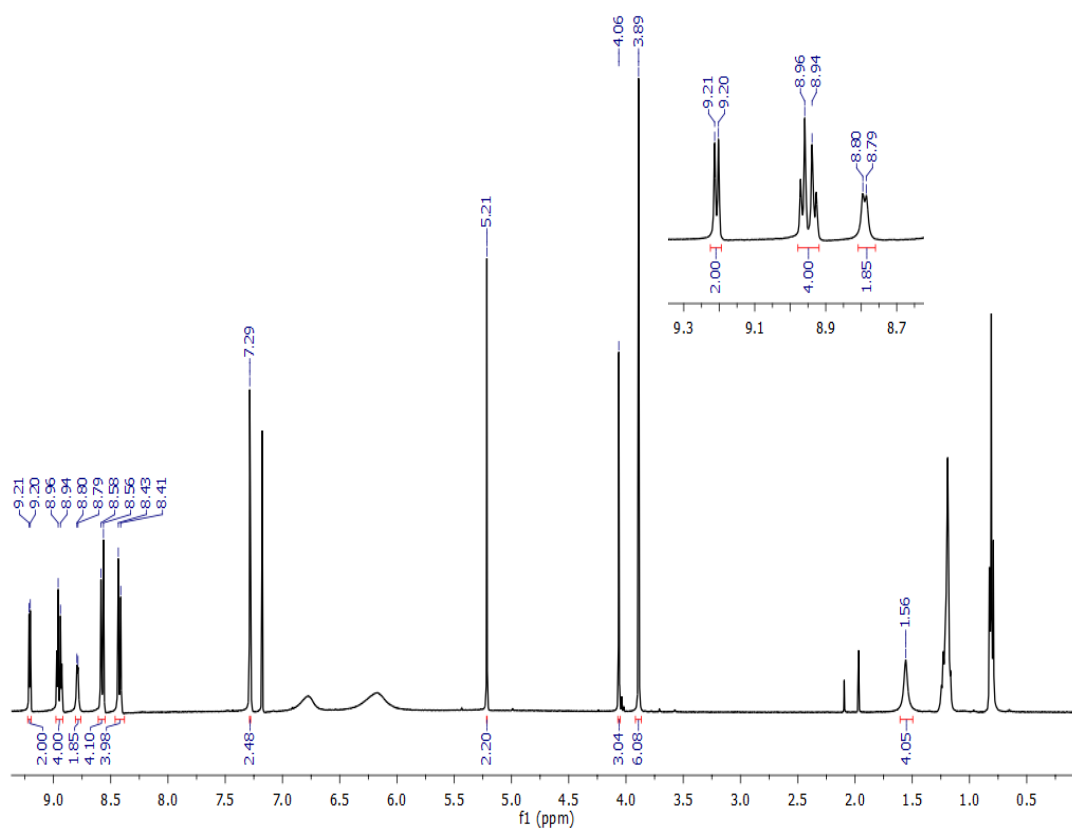


Figure 3.7. ¹H NMR spectrum of Co-3 in C₆D₆.

**Figure 3.8.** ¹⁹F NMR spectrum of Co-3 in C₆D₆.**Figure 3.9.** HRMS spectra of Co-3.**Figure 3.10.** ¹H NMR spectrum of Co-4 in C₆D₆.

**Figure 3.11.** HRMS spectra of Co-4.**Figure 3.12.** ¹H NMR spectrum of Co-5 in CDCl₃.

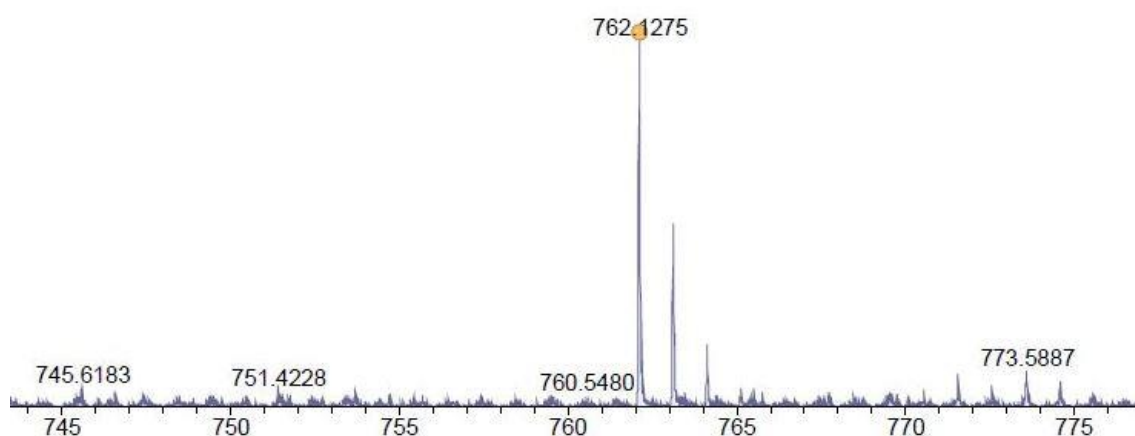


Figure 3.13. HRMS spectra of **Co-5**.

δ 9.30 (d, $^3J_{\text{H,H}} = 3.8$ Hz, 2H, β -pyrrolic), 9.00 (d, $^3J_{\text{H,H}} = 3.4$ Hz, 2H, β -pyrrolic), 8.85 (d, $^3J_{\text{H,H}} = 2.7$ Hz, 2H, β -pyrrolic), 8.78 (br s, 2H, β -pyrrolic), 8.24 (d, $^3J_{\text{H,H}} = 8.6$ Hz, 4H, *o/m*-Ph), 8.18 (d, $^3J_{\text{H,H}} = 7.9$ Hz, 2H, *o/m*-Ph), 8.10 (d, $^3J_{\text{H,H}} = 8.6$ Hz, 4H, *o/m*-Ph), 7.74 (d, $^3J_{\text{H,H}} = 8.0$ Hz, 2H, *o/m*-Ph), 4.82 (t, $^3J_{\text{H,H}} = 7.3$ Hz, 2H, *p*-H of pyridine), 4.20 (br s, 4H, *m*-H of pyridine), 1.72 (br d, 4H, *o*-H of pyridine). **(Figure 3.4)** ^{19}F NMR (377 MHz, C_6D_6) δ -61.64 (s, 3F, *p*- CF_3 of Ph). **(Figure 3.5)** HRMS: Calcd for $\text{C}_{38}\text{H}_{20}\text{CoF}_3\text{N}_6\text{O}_4$ ($[\text{M}-2\text{py}]^+$) m/z 740.0830, m/z found 740.0817 ($[\text{M}-2\text{py}]^+$). **(Figure 3.6)**

3.2.4.3 Bis-pyridine[10-(2,6-difluorophenyl)-5,15-bis(4-nitrophenyl)corrolato]

Cobalt(III) (**Co-3**) was obtained through silica gel chromatography with DCM:Hexane:Pyridine (5:8:0.1) as eluent in 78% yield (19.63 mg, 0.0227 mmol). UV-Visible [DCM + pyridine (0.1%); λ , nm ($\epsilon \times 10^{-3}$, $\text{L mol}^{-1} \text{cm}^{-1}$)]: 377 (88.1), 446 (68.3), 560 (19.0), 650 (54.1). ^1H NMR (400 MHz, C_6D_6) δ 9.42 (d, $^3J_{\text{H,H}} = 4.1$ Hz, 2H, β -pyrrolic), 9.01 (br s, 4H, β -pyrrolic), 8.90 (br s, 2H *m*-Ph), 8.22 (d, $^3J_{\text{H,H}} = 8.1$ Hz, 4H, *o/m*-Ph), 8.04 (d, $^3J_{\text{H,H}} = 8.1$ Hz, 4H, *o/m*-Ph), 7.09–7.02 (m, 3H *p*-Ph overlapped with a deuterated solvent residual signal), 4.83 (br s, 2H, *p*-H of pyridine), 4.24 (d, $^3J_{\text{H,H}} = 6.4$ Hz, 4H, *m*-H of pyridine),

1.76 (br s, 4H, *o*-H of pyridine). **(Figure 3.7)** ¹⁹F NMR (377 MHz, C₆D₆) δ -109.99 (s, 2F, *o*-F of Ph). **(Figure 3.8)** HRMS: Calcd for C₃₇H₁₉CoF₂N₆O₄ ([M-2py]⁺) m/z 708.0768, m/z found 708.0754 ([M-2py]⁺). **(Figure 3.9)**

3.2.4.4 Bis-pyridine[10-(2,6-dichlorophenyl)-5,15-bis(4-nitrophenyl)corrolato]Cobalt(III)

(Co-4) was obtained through silica gel chromatography with DCM:Hexane:Pyridine (5:8:0.1) as eluent in 81% yield (20.15 mg, 0.022 mmol). UV-Visible [DCM + pyridine (0.1%); λ, nm (ε × 10⁻³, L mol⁻¹ cm⁻¹): 378 (67.4), 419 (63.1), 649 (47.3). ¹H NMR (400 MHz, C₆D₆) δ 9.29 (d, ³J_{H,H} = 4.3 Hz, 2H), 8.87 (d, ³J_{H,H} = 4.8 Hz, 2H), 8.82 (d, ³J_{H,H} = 4.3 Hz, 2H), 8.70 (d, ³J_{H,H} = 4.8 Hz, 2H), 8.06 (d, ³J_{H,H} = 8.7 Hz, 4H), 7.88 (d, ³J_{H,H} = 8.7 Hz, 4H), 7.31 (d, ³J_{H,H} = 8.2 Hz, 2H), 6.83 (t, 1H *p*-Ph, Ph overlapped with a deuterated solvent residual signal), 5.22 – 4.99 (m, 2H, *p*-H of pyridine), 4.08 (br s, 4H, *o*-H of pyridine), 2.01 (br, 4H, *m*-H of pyridine). **(Figure 3.10)** HRMS: calculated for C₃₇H₁₉Cl₂CoN₆O₄ ([M-2py]⁺) m/z 740.0177, m/z found 740.0208 ([M-2py]⁺). **(Figure 3.11)**

3.2.4.5 Bis-pyridine[10-(3,4,5-trimethoxyphenyl)-5,15-bis(4-nitrophenyl)corrolato]Cobalt

(III) (Co-5) was obtained through silica gel chromatography with DCM:Hexane:Pyridine (3:8:0.1) as eluent in 79% yield (22.47 mg, 0.0244 mmol). UV-Visible [DCM + pyridine (0.1%); λ, nm (ε × 10⁻³, L mol⁻¹ cm⁻¹): 376 (70.8), 426 (69.9), 570 (17.1), 652 (32.6). ¹H NMR (400 MHz, CDCl₃) δ 9.21 (d, ³J_{H,H} = 4.3 Hz, 2H, β-pyrrolic), 8.95 (br m, 4H, β-pyrrolic), 8.79 (d, ³J_{H,H} = 3.9 Hz, 2H, β-pyrrolic), 8.57 (d, ³J_{H,H} = 8.6 Hz, 4H, *o/m*-Ph), 8.42 (d, ³J_{H,H} = 8.6 Hz, 4H, *o/m*-Ph), 7.18 (s, 2H, *o*-Ph), 5.21 (s, 2H, *p*-H of pyridine), 4.06 (s, 3H, -OCH₃), 3.89 (s, 6H, -OCH₃), 1.56 (br s, overlapped with a H₂O solvent signal, 4H, *o*-H of pyridine). **(Figure 3.12)** HRMS: Calcd for C₄₀H₂₇CoN₆O₇ ([M-2py]⁺) m/z 762.1273, m/z found 762.1275 ([M-2py]⁺). **(Figure 3.13)**

3.2.5 Single crystal X-ray structure determination

Single crystals of C₄₈H₃₀CoF₃N₈O₄ (**Co-2**) were grown by slow evaporation of DCM solution of compound in heptane. A suitable crystal was selected and mounted on a diffractometer. The crystal was kept at 200.15 K during data collection. Using Olex2[16], the structure was solved with the olex2.solve[17] structure solution program using Charge Flipping and refined with the SHELXL[18] refinement package using Least Squares minimization.

Crystal data. C₄₈H₃₀CoF₃N₈O₄ (*M* = 898.73 g/mol): monoclinic, space group C2/c (no. 15), *a* = 18.5859(15) Å, *b* = 16.8267(13) Å, *c* = 13.3423(11) Å, *β* = 109.583(2)°, *V* = 3931.3(5) Å³, *Z* = 4, *T* = 200.15 K, *μ*(MoK α) = 0.511 mm⁻¹, *D*_{calc} = 1.518 g/cm³, 15364 reflections measured (3.356° ≤ 2 θ ≤ 50.278°), 3494 unique (*R*_{int} = 0.0768, *R*_{sigma} = 0.0627) which were used in all calculations. The final *R*₁ was 0.0512 (*I* > 2 σ (*I*)) and *wR*₂ was 0.1488 (all data). **CCDC No. 2081897.**

3.3. RESULTS AND DISCUSSION

3.3.1 Synthesis. A series of cobalt corroles (**Co-1 to 5**) was synthesized in good yield following the procedure described in literature.[14,15] The reaction involved the corresponding free base corroles refluxed at 100 °C in the presence of Co^{II} acetate in pyridine for 20-30 min (**Scheme 3.1**). The reaction was monitored through UV-Visible spectroscopy as well as with TLC and the appearance of strong Q-band confirmed the association of cobalt metal in the corrole macrocycle affording the six-coordinated bispyridine-cobalt-corroles. Once the reaction was completed, the reaction mixture was cooled to room temperature, evaporated the solvent and the pure compound was extracted using column chromatography. For elution, ~1-5% pyridine was added with DCM/Hexane during the chromatographic separation. In the absence of it, impure compound with a variety of side products were produced. This phenomenon was noticed and shown to lead to C-C bond dimers. TLC, ¹H-

NMR spectra and HRMS were used to validate the purity of the green compounds produced. The X-ray crystals of bispyridine[10-(4-trifluorophenyl)-5,15-bis(4-nitrophenyl)corrolato]Cobalt(III) (**Co-2**) were also obtained in good quality which further confirmed the proof of composition and insertion of cobalt metal as well as ligated pyridine.

3.3.2 NMR Spectroscopy. The ¹H-NMR spectra for all the five compounds displayed sharp signals for β-pyrrolic protons in the 8.0-9.5 ppm range.(**Figure 3.14**) The signal due to pyridine protons, on the other hand, showed 4:4:2 of integrated peaks and were found strongly downfield shifted. For example, the pyridine protons of **Co-1** resonate at 4.58, 3.95 and 1.33 ppm for *p*-, *m*- and *o*-Hs respectively.(**Figure 3.1**) Similarly, the chemical shifts for **Co-2** were found at 4.64, 4.04 and 1.57 for *p*-, *m*- and *o*-Hs of pyridine respectively.(**Figure 3.4**) The diamagnetic ring current effect of corrole macrocycle has been proposed as the responsible factor for this extent of lower δ values.[19–21] ¹⁹F-NMR spectra of **Co-(1 to 3)** was also examined in C₆D₆. The *o*-, *m*- and *p*-F in **Co-1** showed signals at -139.37, -162.86, -153.77 ppm respectively integrated in 2:2:1 (*p*: *m*: *o* respectively), while **Co-2** and **Co-3** exhibited singlet peaks, respectively at -61.64 and -109.99 ppm.(**Figure 3.15**) The well resolved spectra obtained for all the three complexes reflects that the pyridine ligands are coordinated symmetrically at axial positions, consistent with the octahedral geometry of complexes. The spectral range and nature of spectra of both the ¹H-NMR and ¹⁹F-NMR is indicative of the existence of the diamagnetic Co^{III} oxidation state of complexes.[3,20] Another conclusion is that the complexes are 6-coordinate with two pyridines in the axial positions, at the concentrations used for the NMR examinations which are about 4.0 × 10⁻³ M.

3.3.3. Single-crystal X-ray structure of Co-2. The **Co-2** complex was crystallized in the presence of a mixture of benzene/n-heptane/pyridine. The crystal was solved, and a well-defined bis(pyridine) cobalt core as shown in **Figure 3.16** was obtained, exhibiting a tetragonally distorted octahedron coordination due to four practically identical nitrogen atoms

of the corrole macrocycle and two nitrogen atoms of axially bounded pyridine molecules with longer metal-nitrogen bonds.

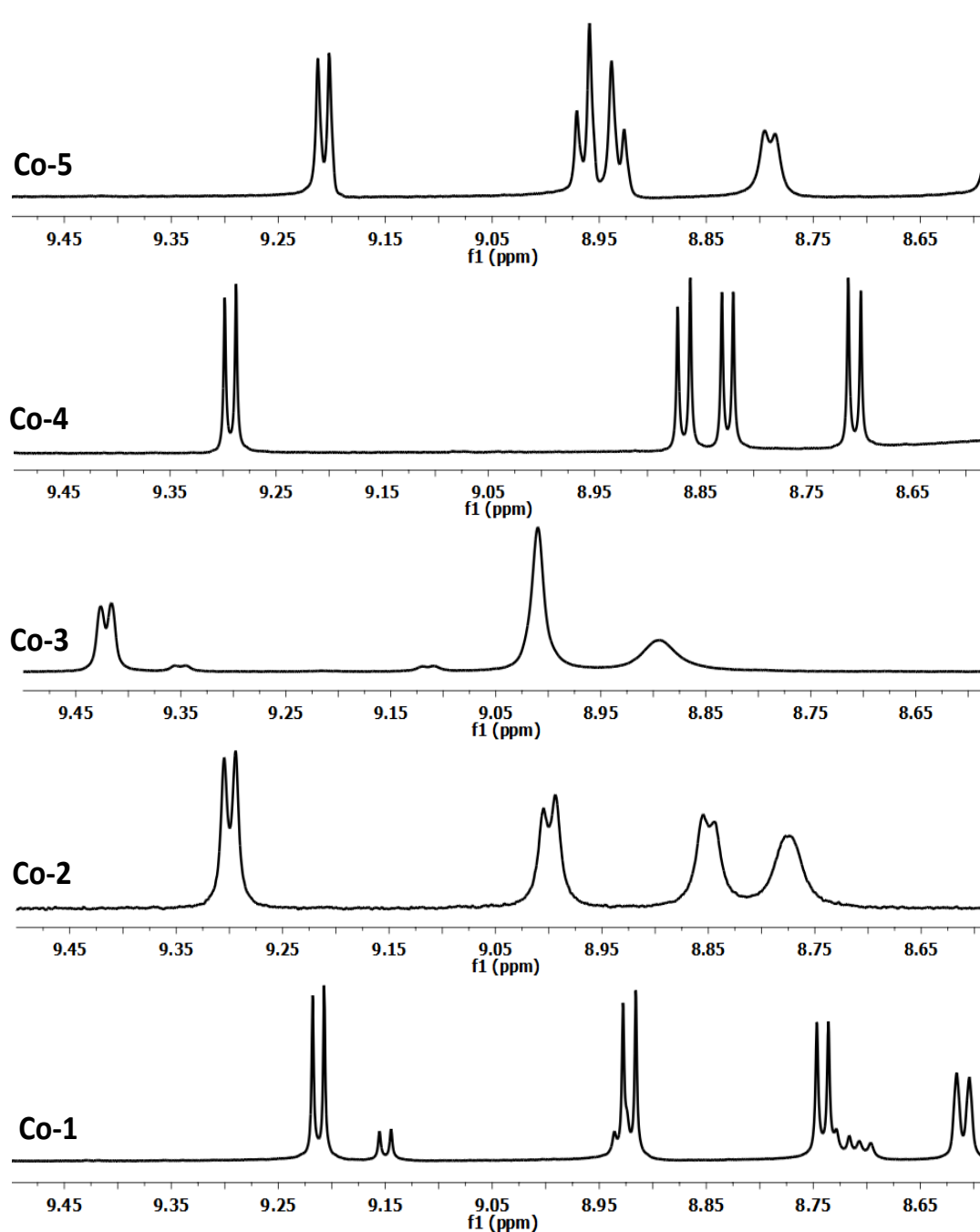


Figure 3.14. ¹H-NMR (room temperature, 400MHz) spectra of Co-(1 to 4) and Co-5, recorded in C₆D₆ and CDCl₃ respectively.

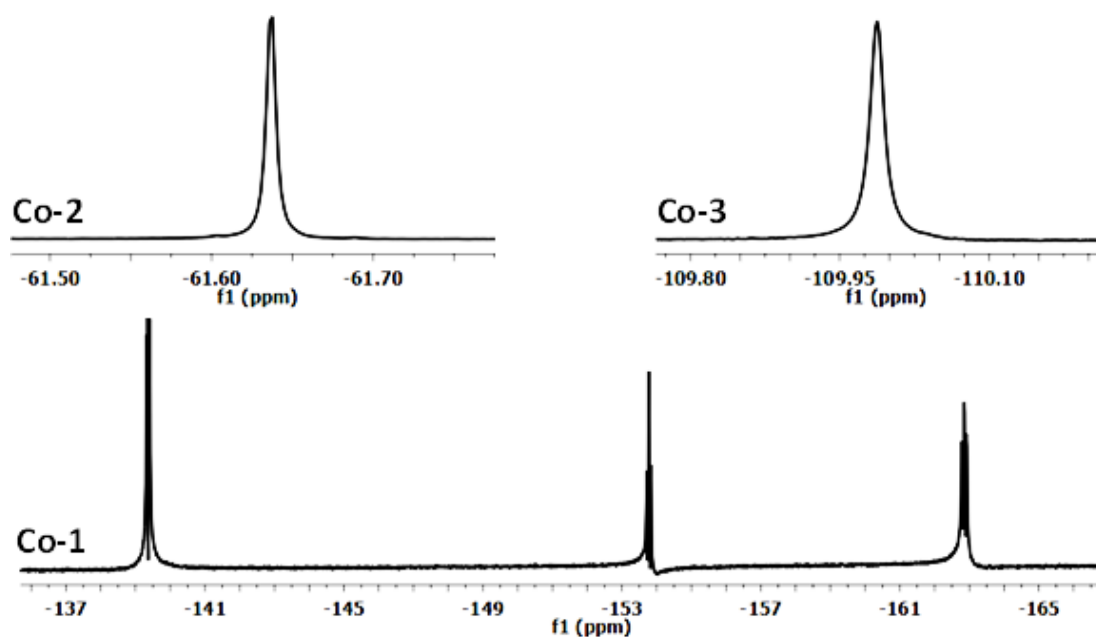


Figure 3.15. ¹⁹F NMR (room temperature, 377 MHz) spectra of Co-(1 to 3) recorded in C₆D₆.

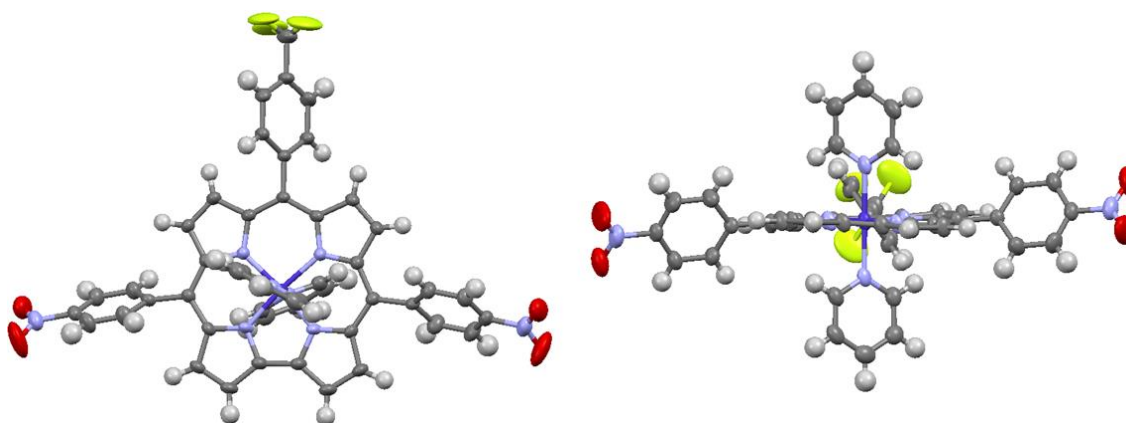


Figure 3.16. X-ray crystal structure of complex Co-2 (a) side view (b) top view

The Co–N_{pyrrolic} bond lengths of the identified molecule are 1.8845(3) Å (on average) and the Co–N_{pyridine} bond distances are 2.013(3) Å which are in strong agreement with the literature value.[3,12,19,22,23] The axial bond lengths are found greater than equatorial bond distances i.e., Co–N_{pyridine} > Co–N_{pyrrolic} which also indicates the low spin Co^{III} complex. Also, these respective bond distance values are found slightly

longer than the previously reported [tpFCor]Co(py)₂ (1.995 Å, 1.879 Å respectively)[24] and [10-(4-F-3-NO₂)Ph-5,15-di-MesitylCor]Co(py)₂ (1.9897 Å, 1.713825 Å respectively).[3] **Table 3.1** compares the bond length distances of **Co-2** to those stated in literature previously.[3,24]

Table 3.1. Comparison of Selected bond distances (Å) of **Co-2** with previously reported dipyridine-cobalt corrole complexes

Crystallographic Data	[(p-CF ₃ Ph)(p-NO ₂ Ph) ₂ Cor]Co(py) ₂ (Co-2)	[tpFCor]Co(py) ₂	[10-(4-F-3-NO ₂)Ph-5,15-di-MesitylCor]Co(py) ₂
Crystal System	monoclinic	Triclinic	monoclinic
Co-N₁(pyrrolic) (Å)	1.874(3)	1.897(7)	1.8718(17)
Co-N₂(pyrrolic) (Å)	1.874(3)	1.899(7)	1.8679(17)
Co-N₃(pyrrolic) (Å)	1.895(3)	1.866(8)	1.8996(17)
Co-N₄(pyrrolic) (Å)	1.895(3)	1.854(7)	1.216(3)
Co-N₅(pyridine) (Å)	2.013(3)	1.998(8)	1.9822(17)
Co-N₆(pyridine) (Å)	2.013(3)	1.992(7)	1.9972(17)

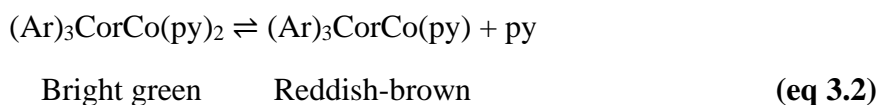
The cobalt ion is located at the center of a tetragonally elongated octahedron with a typical D_{4h} symmetry. The dihedral angle between the two pyridine molecules is 86.66°. The central cobalt atom **Co-2** lies in the corrole 23-atom core mean plane as well in 4-pyrrolic nitrogen atoms mean plane.

3.3.4. UV–Visible spectroscopy of Co–(1 to 5). In a 10⁻⁴ M DCM solution, the **Co-1** displayed major bands at 377, 450, 566, 637 nm (**Figure 3.17(b)**) while in the 10⁻⁶ M DCM solution, the bands appeared at 376, 442, 566.(**Figure 3.17(a)**) The existence of a band at around 640 nm in the more concentrated solution indicates that the complexes

were somewhat present in a 6-coordinated form where the pyridine ligands occupied the axial position. While in highly diluted environments, the complex has mono-pyridine as the major form. As shown in **Figure 3.17**, all the complexes behaved similarly. This confirms that the dilution effect has a significant impact on the coordination number of cobalt corrole complexes.

On the other hand, when the solution of these complexes was prepared in neat pyridine conditions, the coordinating solvent immediately transformed the complex into 6-coordinated form, as seen by the variations in UV-Vis spectral bands (**Figure 3.17(c)**) and accompanied by an immediate color change from reddish-brown to green. The strong Q-band at 647 nm is the marker band for pyridine in metallocorrole that is bounded axially to cobalt metal.[1,25] A similar band was also observed for all the **Co-(1 to 5)** complexes in 10⁻⁴ M DCM solution but was absent for 10⁻⁶ M DCM solutions. All the absorption bands and spectral variations for **Co-(1 to 5)** for DCM and pyridine solution are depicted in **Figure 3.17** and **Table 3.2**.

The bands associated with the UV-visible spectra of the five- and six- coordinate species of **Co-(1 to 5)** are close to the spectra of the mono- and bis(pyridine) adducts of other (Ar)₃CorCo and DPPCo derivatives previously mentioned in the literature.[12,26,27] It can therefore be inferred that the complexes are present majorly in 5-coordinated form in 10⁻⁶ M DCM solution, hexa-coordinated in neat pyridine while present in an equilibrium condition between the pent- and hexa-coordinated form at conc. 10⁻⁴ M DCM solution, which can be represented by (**eq 3.2**).



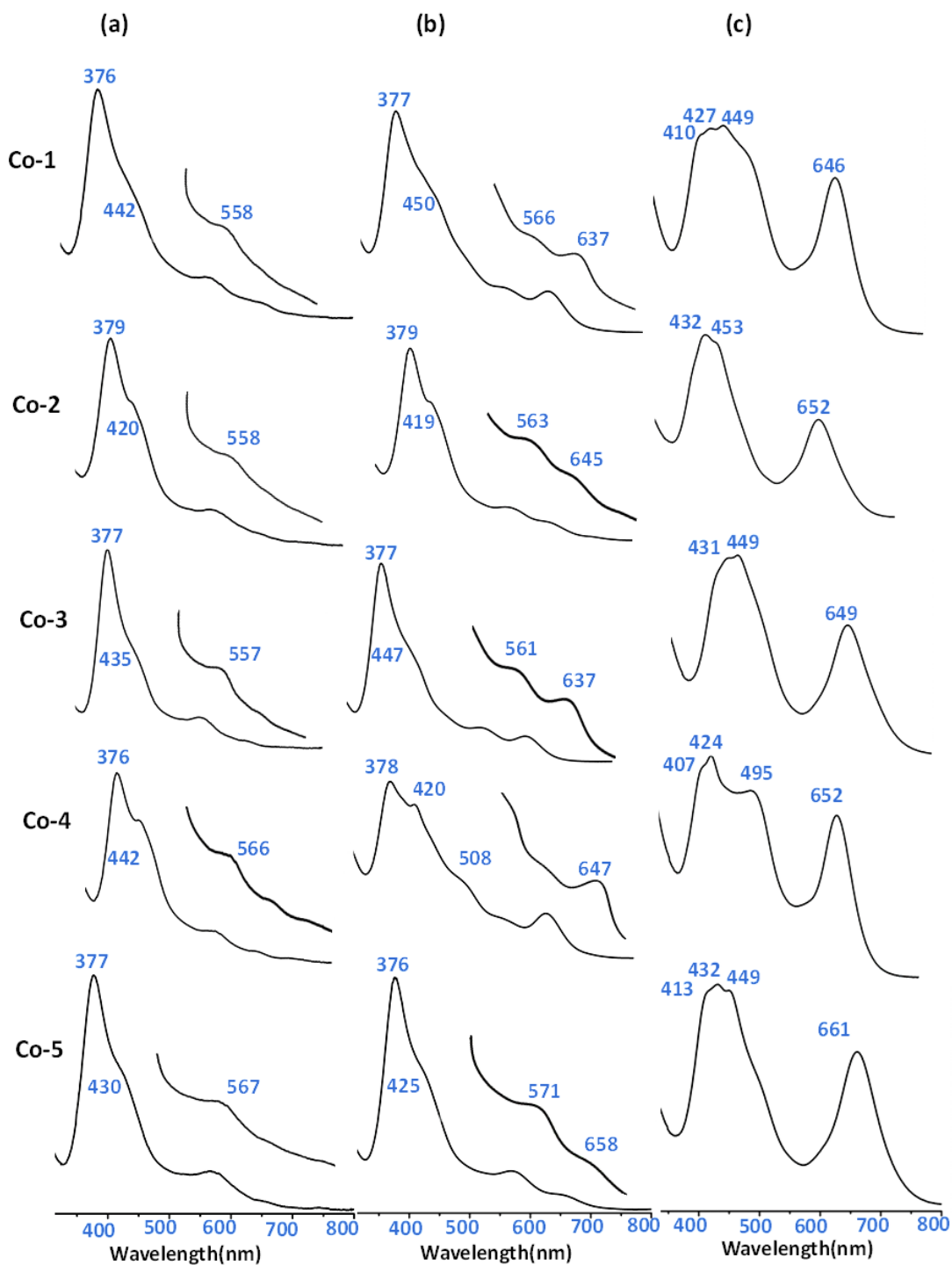


Figure 3.17 - Electronic absorption spectra of **Co-(1 to 5)** in (a) 10⁻⁶ M DCM (b) 10⁻⁴ M DCM (c) 10⁻⁵ pyridine solution.

Table 3.2. UV-Vis spectral bands of **Co-(1-5)** in (a) 10⁻⁶ M DCM (b) 10⁻⁵ pyridine (c) 10⁻⁵ benzonitrile solution.

Solvent	Compound	λ nm ($\epsilon \times 10^{-4}$ L mol ⁻¹ cm ⁻¹)			
		Soret region bands		Visible region bands	
Dichloromethane	Co-1	376 (21.9)	442 (11.3)		558 (4.2)
	Co-2	379 (26.0)	420 (18.3)		558 (3.4)
	Co-3	377 (20.9)	435 (9.9)		557 (3.8)
	Co-4	376 (23.4)	442 (17.6)		566 (4.1)
	Co-5	377 (19.1)	430 (10.6)		567 (5.5)
Pyridine	Co-1	410 (5.0)	427 (5.2)	449 (5.3)	646 (4.0)
	Co-2	432 (5.4)	453 (5.2)		652 (3.4)
	Co-3	431 (5.2)	449 (5.3)		649 (2.9)
	Co-4	407 (4.8)	424 (5.12)	495 (4.3)	652 (3.7)
	Co-5	413 (5.12)	432 (5.3)	449 (5.1)	661 (3.7)
Benzonitrile	Co-1	426 (6.4)	444 (6.2)		646 (4.1)
	Co-2	430 (6.1)	453 (5.5)		651 (2.7)
	Co-3	427 (7.0)	443 (6.8)		646 (4.5)
	Co-4	407 (6.1)	424 (6.4)	502 (5.0)	653 (4.1)
	Co-5	415 (6.6)	448 (5.7)	598 (1.8)	661 (3.2)

The donor number is often linked to the solvent's coordination ability at axial position with cobalt-corroles.[28] As the Gutmann solvent donor number for pyridine is highest among the four below mentioned solvents (**eq 3.3**), the coordinating abilities are also found higher for pyridine. Acetonitrile (PhCN) has a donor number of 11.0 as well. Hence, it could also have the capacity to bind axially with cobalt corroles.



$$0.0 < 11.9 < 20.0 < 33.1$$

(eq 3.3)

In order to analyse the benzonitrile interaction with synthesized cobalt corroles, the complexes were examined by UV-Vis spectroscopy in 10^{-5} M benzonitrile solution. **(Figure 3.18)** Similar bands for the **Co-(1 to 5)** complexes were observed as appearing in pyridine. For **Co-1** the bands detected were at 426, 444, and 646 nm. At 646 nm, the strong Q-band emergence, indicated that the benzonitrile solvent is functioning as a coordinating solvent in this case.

Nevertheless, these effects have never been seen before in cobalt corroles. The band at 646 nm is a strong indication of the presence of a 6-coordinated form of the complexes. As our major focus was on pyridine, the rest of the study on benzonitrile behavior with cobalt corroles is beyond the scope.

To further study the coordination number of cobalt corrole complexes and to exactly determine the number of pyridine ligands binding axially, the binding constant of all the complexes was calculated which involved the titration of cobalt

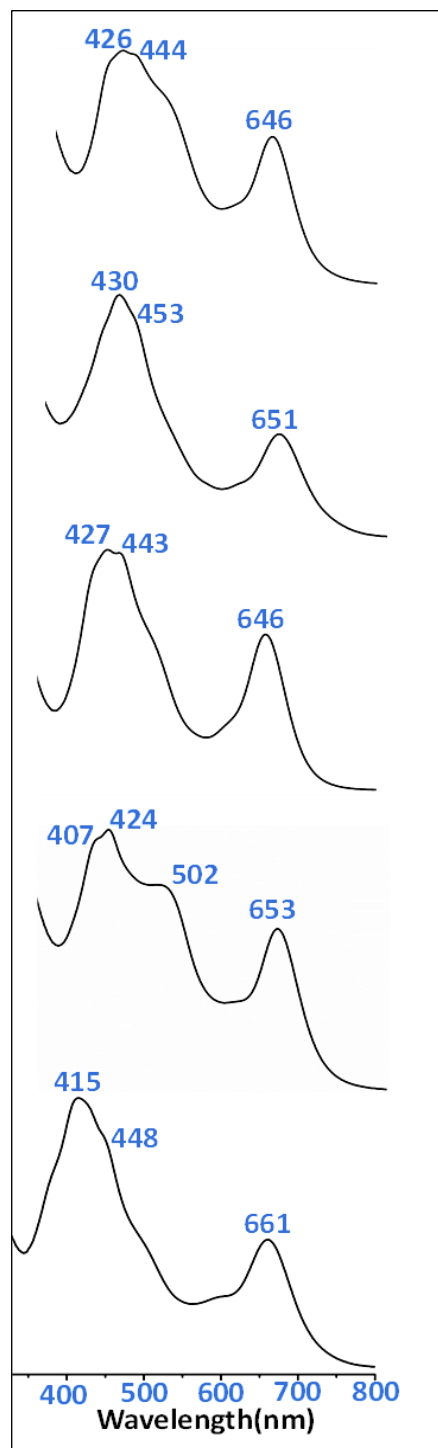


Figure 3.18 - UV-Visible spectra of **Co-(1-5)** in 10^{-5} M benzonitrile.

corrole complexes in 10⁻⁴ M DCM solution with pyridine. The titration was monitored by UV-Visible spectroscopy and at each step of pyridine addition, the UV-Visible spectra of solution was recorded, and the Hill equation (eq 3.1) was employed to calculate the logK₂ values.

The spectral changes observed during titration as well as the Hill plot for Co-(1-5) are depicted in Figure 3.19. A strong Q-band appearance

Table 3.3. Pyridine binding constants for cobalt corroles in CH₂Cl₂

Compound	Binding constant (logK ₂)
Co-1	5.1
Co-2	4.9
Co-3	4.9
Co-4	4.8
Co-5	4.5

accompanied by the reduction of intensity in Soret band was observed at the end point. The slope determined for every complex was one and the binding constant values were found to be in the 4.5-5.1 range. (Table 3.3) The resulting slope value of one, meant that the titration consisted of one step, i.e., one pyridine ligand was bounded at axial position. This behavior is found in good accordance with the previous concentration dependent study explained above, in which the complex initially showed no spectral bands at ~640 nm but after the introduction of a coordinating ligand in solution, a significant behavioral shift easily identified by UV-Visible spectroscopy was found.

One key point was the binding constant values trend for the synthesized complexes i.e., the maximum logK₂ value was observed for Co-1 complex consisted of highly electron withdrawing group (pentafluorophenyl) at the C_{10-meso} position while the lowest was observed for Co-5 onto which the group present is electron donating in nature (3,4,5-

trimethoxyphenyl). This corresponds to the fact that as the electron density on the central metal decreases, the ligand binding potential enhances.

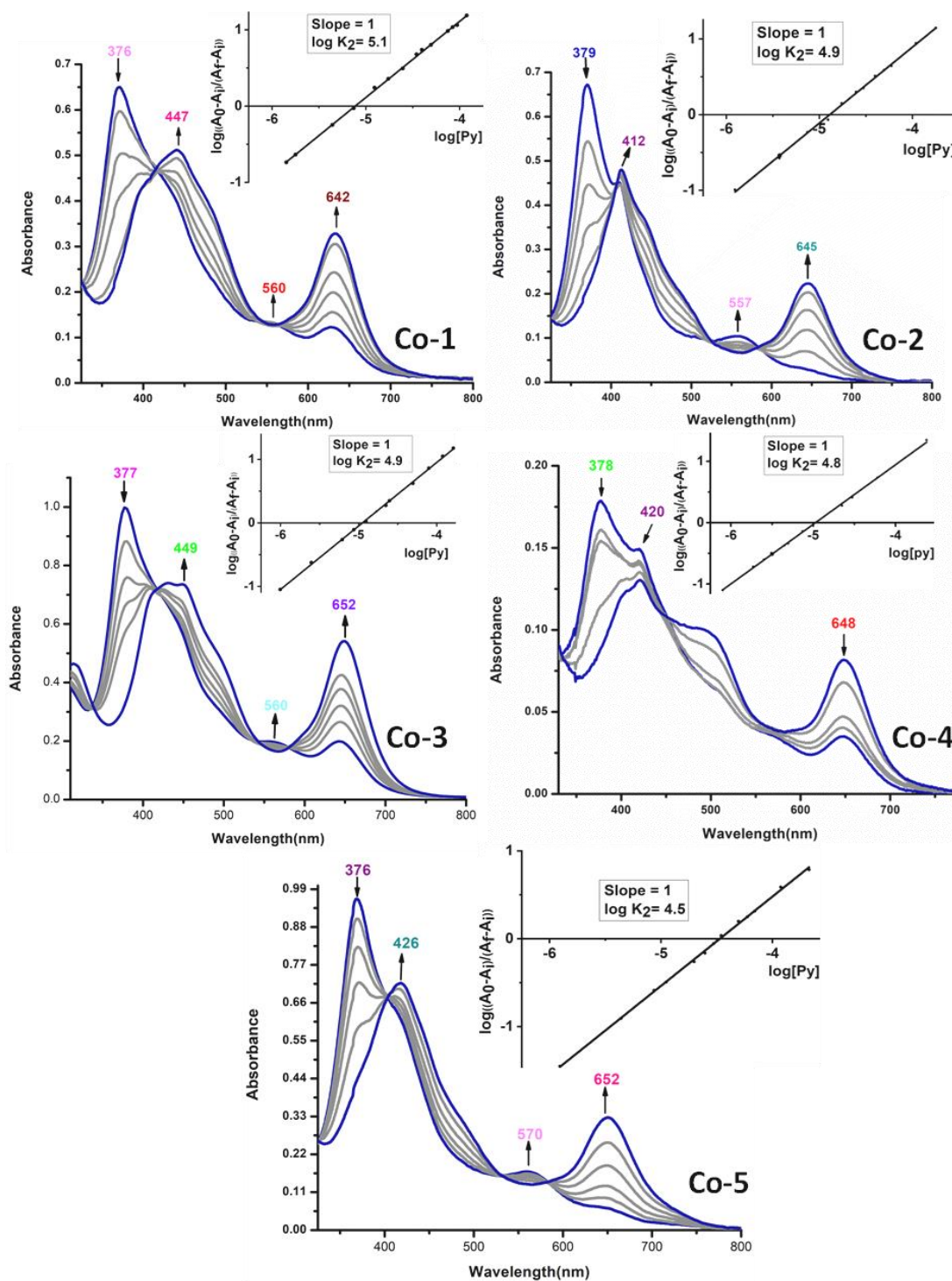


Figure 3.19. Titration of Co-(1 to 5) with pyridine. Hill plots for the binding constant analysis are shown in inset.

3.4 CONCLUSION

A series of A₂B type cobalt(III) corroles was prepared and studied regarding various aspects. The complexes were characterized through UV-Visible spectroscopy when present in 10⁻⁴ M DCM, 10⁻⁶ M DCM, 10⁻⁵ M pyridine and 10⁻⁵ M PhCN solution. A behavioral analysis with different solvent conditions determined the coordination number of the complexes, which is 5 in highly dilute solution or in the absence of a coordinating ligand and 6 in high concentration of DCM or in presence of coordinating ligand. Benzonitrile is also able to show 6- coordinated form, hence acting as a binding ligand. The binding constant data also revealed the binding of only one pyridine molecule to all the synthesized cobalt corrole since in very dilute solution cobalt(III) corroles exist in 5-coordinated form and hence resulting in 6-coordinated form in high concentration. These complexes are present in the 6-coordinated form in the presence of coordinating ligand such as pyridine and benzonitrile. The sharp and well resolved peaks in the ¹H NMR spectra proved that the complexes are present in Co^{III} form. The similar results were gathered from X-ray crystallographic study of the **Co-2** complex in which the equatorial i.e., Co–N_{pyrrolic} and axial i.e., Co–N_{pyridine} bond distances obtained were 1.8845(3) Å (on average) and 2.013(3) Å respectively. The X-ray crystallographic and ¹H NMR studies hence have confirmed that bispyridine complex of cobalt triarylcorroles are authentic diamagnetic Co^{III} complexes.

References-

- [1] V. Quesneau, W. Shan, N. Desbois, S. Brandès, Y. Rousselin, M. Vanotti, V. Blondeau-Patissier, M. Naitana, P. Fleurat-Lessard, E. Van Caemelbecke, K.M. Kadish, C.P. Gros, Cobalt Corroles with Bis-Ammonia or Mono-DMSO Axial Ligands. Electrochemical, Spectroscopic Characterizations and Ligand Binding Properties, *Eur. J. Inorg. Chem.* 2018 (2018) 4265–4277. <https://doi.org/10.1002/ejic.201800897>.
- [2] X. Jiang, W. Shan, N. Desbois, V. Quesneau, S. Brandès, E. Van Caemelbecke, W.R. Osterloh, V. Blondeau-Patissier, C.P. Gros, K.M. Kadish, Mono-DMSO ligated cobalt nitrophenylcorroles: Electrochemical and spectral characterization, *New J. Chem.* 42 (2018) 8220–8229. <https://doi.org/10.1039/c8nj00300a>.
- [3] X. Jiang, M.L. Naitana, N. Desbois, V. Quesneau, S. Brandès, Y. Rousselin, W. Shan, W.R. Osterloh, V. Blondeau-Patissier, C.P. Gros, K.M. Kadish, Electrochemistry of Bis(pyridine)cobalt (Nitrophenyl)corroles in Nonaqueous Media, *Inorg. Chem.* 57 (2018) 1226–1241. <https://doi.org/10.1021/acs.inorgchem.7b02655>.
- [4] W. Sinha, A. Mizrahi, A. Mahammed, B. Tumanskii, Z. Gross, Reactive Intermediates Involved in Cobalt Corrole Catalyzed Water Oxidation (and Oxygen Reduction), *Inorg. Chem.* 57 (2018) 478–485. <https://doi.org/10.1021/acs.inorgchem.7b02696>.
- [5] K.M. Kadish, J. Shen, L. Frémond, P. Chen, M. El Ojaimi, M. Chkounda, C.P. Gros, J.M. Barbe, K. Ohkubo, S. Fukuzumi, R. Guilard, Clarification of the oxidation state of cobalt corroles in heterogeneous and homogeneous catalytic reduction of dioxygen, *Inorg. Chem.* 47 (2008) 6726–6737. <https://doi.org/10.1021/ic800458s>.
- [6] K.M. Kadish, J. Shao, Z. Ou, L. Frémond, R. Zhan, F. Burdet, J.M. Barbe, C.P. Gros, R. Guilard, Electrochemistry, spectroelectrochemistry, chloride binding, and O₂ catalytic reactions of free-base porphyrin - Cobalt corrole dyads, *Inorg. Chem.* 44 (2005) 6744–6754. <https://doi.org/10.1021/ic050738n>.
- [7] W. Sinha, A. Mahammed, N. Fridman, Y. Diskin-Posner, L.J.W. Shimon, Z. Gross, Superstructured metallocorroles for electrochemical CO₂ reduction, *Chem. Commun.* 55 (2019) 11912–11915. <https://doi.org/10.1039/c9cc06645d>.

- [8] W. Lee, X. Zhan, J. Palma, J. Vestfrid, Z. Gross, D.G. Churchill, Minding our P-block and Q-bands: paving inroads into main group corrole research to help instil broader potential, *Chem. Commun.* 57 (2021) 4605–4641. <https://doi.org/10.1039/D1CC00105A>.
- [9] W.R. Osterloh, V. Quesneau, N. Desbois, S. Brandès, W. Shan, V. Blondeau-Patissier, R. Paolesse, C.P. Gros, K.M. Kadish, Synthesis and the Effect of Anions on the Spectroscopy and Electrochemistry of Mono(dimethyl sulfoxide)-Ligated Cobalt Corroles, *Inorg. Chem.* 59 (2020) 595–611. <https://doi.org/10.1021/acs.inorgchem.9b02855>.
- [10] W.R. Osterloh, N. Desbois, V. Quesneau, S. Brandès, P. Fleurat-Lessard, Y. Fang, V. Blondeau-Patissier, R. Paolesse, C.P. Gros, K.M. Kadish, Old Dog, New Tricks: Innocent, Five-coordinate Cyanocobalt Corroles, *Inorg. Chem.* 59 (2020) 8562–8579. <https://doi.org/10.1021/acs.inorgchem.0c01037>.
- [11] P.E. Ellis, J.E. Linard, T. Szymanski, R.D. Jones, J.R. Budge, F. Basolo, Axial Ligation Constants of Iron(II) and Cobalt(II) “Capped” Porphyrins, *J. Am. Chem. Soc.* 102 (1980) 1889–1896. <https://doi.org/10.1021/ja00526a022>.
- [12] R. Guillard, C.P. Gros, F. Bolze, F. Jérôme, Z. Ou, J. Shao, J. Fischer, R. Weiss, K.M. Kadish, Alkyl and aryl substituted corroles. 1. Synthesis and characterization of free base and cobalt containing derivatives. X-ray structure of (Me₄Ph₅Cor)Co(py)₂, *Inorg. Chem.* 40 (2001) 4845–4855. <https://doi.org/10.1021/ic010177+>.
- [13] R. Guillard, F. Jérôme, J.M. Barbe, C.P. Gros, Z. Ou, J. Shao, J. Fischer, R. Weiss, K.M. Kadish, Alkyl and aryl substituted corroles. 2. Synthesis and characterization of linked “face-to-face” biscalloles. X-ray structure of (BCA)Co₂(py)₃, where BCA represents a biscallole with an anthracenyl bridge, *Inorg. Chem.* 40 (2001) 4856–4865. <https://doi.org/10.1021/ic0101782>.
- [14] B. Koszarna, D.T. Gryko, Efficient synthesis of meso-substituted corroles in a H₂O-MeOH mixture, *J. Org. Chem.* 71 (2006) 3707–3717. <https://doi.org/10.1021/jo060007k>.

- [15] I.G. and Z.G. Atif Mahammed Ilona Giladi, Synthesis and Structural Characterization of a novel Covalently-Bound Corrole Dimer, *Chem. Eur. J.* 2001., 723 (2001) 4259–4265. <https://doi.org/0947-6539/01/0719-4259> \$ 17.50+.50/0.
- [16] O. V. Dolomanov, L.J. Bourhis, R.J. Gildea, J.A.K. Howard, H. Puschmann, OLEX2: A complete structure solution, refinement and analysis program, *J. Appl. Crystallogr.* 42 (2009) 339–341. <https://doi.org/10.1107/S0021889808042726>.
- [17] L.J. Bourhis, O. V. Dolomanov, R.J. Gildea, J.A.K. Howard, H. Puschmann, The anatomy of a comprehensive constrained, restrained refinement program for the modern computing environment - Olex2 dissected, *Acta Crystallogr. Sect. A Found. Crystallogr.* 71 (2015) 59–75. <https://doi.org/10.1107/S2053273314022207>.
- [18] G.M. Sheldrick, Crystal structure refinement with SHELXL, *Acta Crystallogr. Sect. C Struct. Chem.* 71 (2015) 3–8. <https://doi.org/10.1107/S2053229614024218>.
- [19] S. Ganguly, J. Conradie, J. Bendix, K.J. Gagnon, L.J. McCormick, A. Ghosh, Electronic Structure of Cobalt–Corrole–Pyridine Complexes: Noninnocent Five-Coordinate Co(II) Corrole–Radical States, *J. Phys. Chem. A.* 121 (2017) 9589–9598. <https://doi.org/10.1021/acs.jpca.7b09440>.
- [20] L. Simkhovich, N. Galili, I. Saltsman, I. Goldberg, Z. Gross, Coordination chemistry of the novel 5,10,15-tris(pentafluorophenyl)corrole: Synthesis, spectroscopy, and structural characterization of its cobalt(III), rhodium(III), and iron(IV) complexes, *Inorg. Chem.* 39 (2000) 2704–2705. <https://doi.org/10.1021/ic991342c>.
- [21] K. Sudhakar, A. Mahammed, N. Fridman, Z. Gross, Trifluoromethylation for affecting the structural, electronic and redox properties of cobalt corroles, *Dalt. Trans.* 48 (2019) 4798–4810. <https://doi.org/10.1039/c9dt00675c>.
- [22] S. Ooi, T. Tanaka, A. Osuka, Cobalt(III) and gallium(III) complexes of meso-free corroles with distinct position-dependent substituent effects, *J. Porphyr. Phthalocyanines.* 20 (2016) 274–281. <https://doi.org/10.1142/S1088424616500061>.

- [23] B. Mondal, K. Sengupta, A. Rana, A. Mahammed, M. Botoshansky, S.G. Dey, Z. Gross, A. Dey, Cobalt Corrole Catalyst for Efficient Hydrogen Evolution Reaction from H₂O under Ambient Conditions: Reactivity, Spectroscopy, and Density Functional Theory Calculations, *Inorg. Chem.* 52 (2013) 3381–3387. <https://doi.org/10.1021/ic4000473>.
- [24] H. Lei, A. Han, F. Li, M. Zhang, Y. Han, P. Du, W. Lai, R. Cao, Electrochemical, spectroscopic and theoretical studies of a simple bifunctional cobalt corrole catalyst for oxygen evolution and hydrogen production, *Phys. Chem. Chem. Phys.* 16 (2014) 1883–1893. <https://doi.org/10.1039/c3cp54361g>.
- [25] K.M. Kadish, Z. Ou, J. Shao, C.P. Gros, J.M. Barbe, F. Jérôme, F. Bolze, F. Burdet, R. Guilard, Alkyl and aryl substituted corroles. 3. Reactions of cofacial cobalt biscalcoroles and porphyrin-corroles with pyridine and carbon monoxide, *Inorg. Chem.* 41 (2002) 3990–4005. <https://doi.org/10.1021/ic020058+>.
- [26] V.A. Adamian, F. D'Souza, S. Licoccia, M.L. Di Vona, E. Tassoni, R. Paolesse, T. Boschi, K.M. Kadish, Synthesis, Characterization, and Electrochemical Behavior of (5,10,15-Tri-X-phenyl-2,3,7,8,12,13,17,18-octamethylcorrolato)cobalt(III) Triphenylphosphine Complexes, Where X = p-OCH₃, p-CH₃, p-Cl, m-Cl, o-Cl, m-F, o-F, or H, *Inorg. Chem.* 34 (1995) 532–540. <https://doi.org/10.1021/ic00107a003>.
- [27] W. Shan, N. Desbois, S. Pacquelet, Stéphane Brandès, Y. Rousselin, J. Conradie, A. Ghosh, C.P. Gros, K.M. Kadish, Ligand Noninnocence in Cobalt Dipyrrin-Bisphenols: Spectroscopic, Electrochemical, and Theoretical Insights Indicating an Emerging Analogy with Corroles, *Inorg. Chem.* 58 (2019) 7677–7689. <https://doi.org/10.1021/acs.inorgchem.8b03006>.
- [28] K.M. Kadish, P.W. Koh, Electrochemistry of Rhodium and Cobalt Corroles . Characterization of (OMC)Rh(PPh₃) and (OMC)Co(PPh₃) Where OMC is the Trianion of 2,3,7,8,12,13,17,18-Octamethylcorrole, *Am. Chem. Soc.* 31 (1992) 2305–2313. [https://doi.org/0020-1669/92/1331-2305\\$03.00/0](https://doi.org/0020-1669/92/1331-2305$03.00/0).

CHAPTER 4

STUDY THE INTERACTION OF ANIONS WITH A₂B COBALT CORROLES IN NON-AQUEOUS MEDIUM

4.1 INTRODUCTION

In this chapter, we have reported the interaction of **Co-(1-5)** (**Scheme 3.1**) with 14 different tetrabutyl ammonium salts of F⁻, CN⁻, CH₃COO⁻, NO₃⁻, AsO₃³⁻, AsO₄³⁻, Cl⁻, Br⁻, I⁻, ClO₄⁻, H₂PO₄⁻, S²⁻, HS⁻ and PF₆⁻. (**Figure 4.1**) Herein, the important feature of complexes i.e., the behaviour in presence of EWG or EDG on the peripheral corrole skeleton has been observed. The complexes containing strong electron withdrawing group such as pentafluoro phenyl, 2,6-difluoro phenyl and 2,6-dichloro phenyl at C_{10-*meso*} position have been found selective towards the three anions namely, fluoride, cyanide and acetate, when examined through spectroscopic and colorimetric approaches. Also, we have focused on the interacting effect of **Co-(1-5)** toward non-aqueous solvents. On changing the solvent, a dramatic shift in colour is observed for this series of complexes. Earlier, we focused on concentration dependence of these complexes in dichloromethane solutions, where the complexes were six co-ordinated at higher concentration and five in dilute solutions[1]. In present report the intermediary effects are observed in the acetonitrile solution of **Co-(1-5)**.

4.2 EXPERIMENTAL SECTION

The five Co[(p-NO₂Ph)₂RCor](py)₂ complexes were prepared with R as the desired electron withdrawing or electron donating substituent at the C_{10-*meso*} position. These were synthesized using the procedure described in literature and the resulting

complexes are outlined in **Scheme-3.1**. [2–5] The ¹H NMR, HRMS and UV–Visible data were found to be in agreement with the previously reported results for these complexes [1].

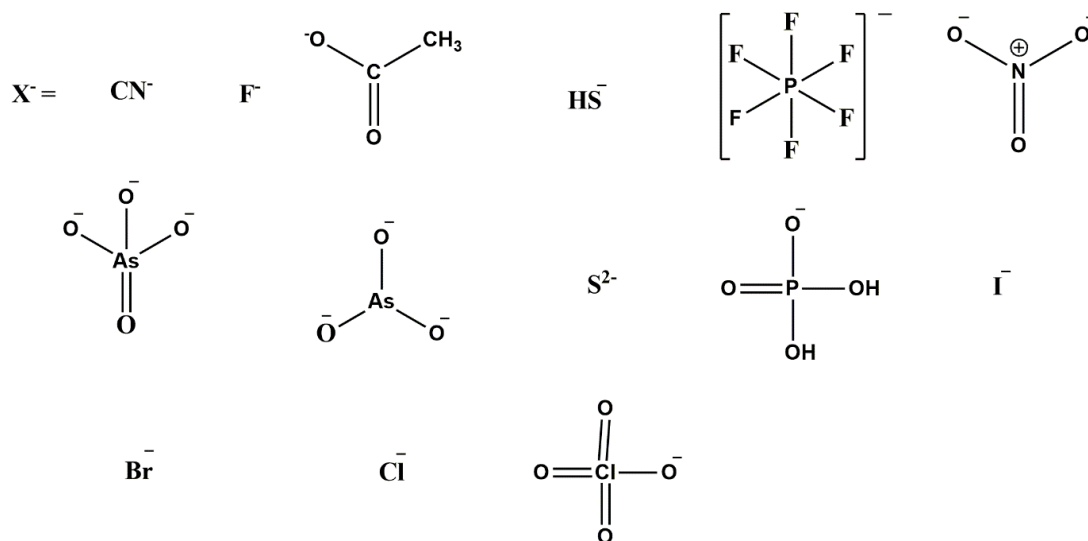


Figure 4.1. Tetrabutyl ammonium salts of anions (TBA⁺X⁻) used for interaction.

The reagents such as HPLC grade of acetonitrile, dichloromethane and benzonitrile, used as solvents, were purchased from Sigma-Aldrich chemical Co. and were used as such. The tetrabutyl ammonium salts of the following anions: F⁻, CN⁻, CH₃COO⁻, NO₃⁻, AsO₃³⁻, AsO₄³⁻, Cl⁻, Br⁻, I⁻, ClO₄⁻, H₂PO₄⁻, S²⁻, HS⁻ and PF₆⁻ for testing were purchased from Merck, Thermo fisher Scientific India and Avra synthesis private limited and used without further purification. (**Figure 4.1**)

UV-Visible spectroscopy: The optical absorption spectra were recorded in 1 cm path length quartz tube using a UV-1800 Shimadzu Spectrometer.

Procedure for UV-Visible Analysis: A solution of cobalt corroles, **Co-(1-5)** of 1×10⁻⁵ M was prepared in dichloromethane, benzonitrile and acetonitrile.

Binding constant determination: Hill equation (eq (3.1)) was used in order to obtain ease of attaching anionic ligands to the axial position of Co-(1-5) as well as the number of anionic ligands that could be attached. Co-(1-5) of concentration $\sim 1 \times 10^{-5} \text{M}$ were titrated with the appropriate anion and the results of each stage of the addition of anion were recorded in UV-Visible spectrometer. The resulting UV-plot data was then fitted into the Hill equation (eq (3.1)), which provided the binding constant and the number of ligands bound at the axial positions.

LOD determination: The straight-line plot obtained between absorption band at ~ 360 nm and concentration of anion used yielded the limit of detection using the eq (4.1).

$$\frac{3\sigma}{m} \quad \text{eq (4.1)}$$

This equation is based on σ (standard deviation of line) where 'm' represents slope of the line.

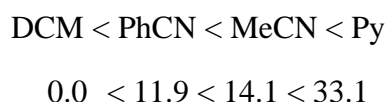
4.3 RESULTS AND DISCUSSION

4.3.1 UV-Visible response of Co-(1-5) towards solvents:

The spectra of Co-(1-5) in 10^{-5} M acetonitrile solution was investigated in this work. All of the compounds were characterized by the major absorption bands at around 380, 415, 575 and 635 nm. The bands at 380 and 415 nm are found due to the higher energy and more allowed Soret band and the latter two bands at 575 and 635 nm are ascribed to lower energy and symmetry-forbidden Q bands of the corrole core. As an example, in the Co-1, the bands were seen at 382 and 632 nm. On the other hand, for Co-3, the bands were appeared at 378, 410, 571 and 633 nm. (Figure 4.2) The only exception is

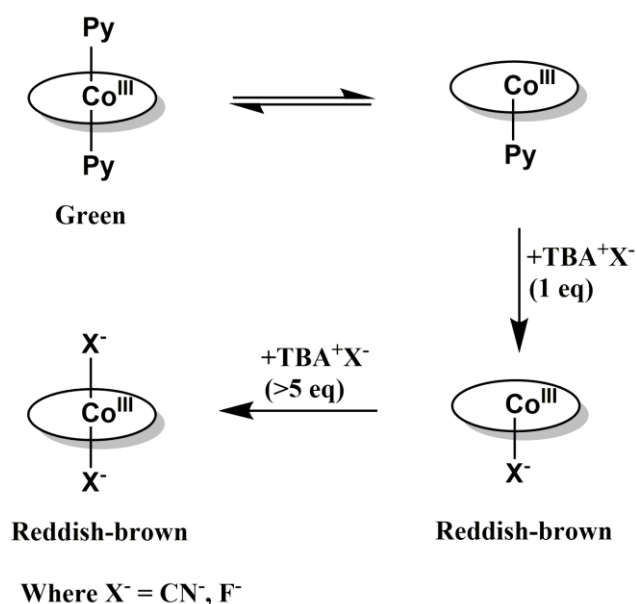
Co-4 corrole, where the acetonitrile solution exhibited a broad Soret band at 376 and 412 nm and a Q-band at 572 nm. These observations are in contrast to the neat benzonitrile and pyridine solutions of the same concentration of these complexes previously studied[1]. The absorption bands are varied substantially because in the benzonitrile and pyridine solutions of 10⁻⁵ M concentrations, the Soret band for all the complexes is located at ~426 nm. A strong Q-band at ~655 nm is also reported except for **Co-4** species. This strong Q-band at ~655 nm is associated with the presence of hexa co-ordinated form for these complexes. With the exception of **Co-4** and **Co-5**, the other three complexes appear green in the neat acetonitrile solution. As already discussed in earlier reports, the green colour is related to the presence of six co-ordinated species[1,6,7] and hence it highlights the co-ordinating behaviour of acetonitrile solvent ligated axially.

The co-ordination activity of the solvent seems to be related to the Gutmann donor number also[8,9]. The acetonitrile (MeCN) solvent has a donor number higher than that of benzonitrile (PhCN) but lower than that of pyridine. However, as previously studied, both the pyridine and benzonitrile behave as co-ordinating ligands. Hence, the acetonitrile (MeCN) donor number found intermediate between these two emphasizes its co-ordinating properties. The donor number for each of these solvents is given below.



In the Q-band region of the acetonitrile solutions of these complexes, the new prominent band at about 575 nm was observed, which is clearly absent in the pyridine

and benzonitrile solutions of the complexes. On the other hand, the band at around 655 nm was found to be intense in nature for benzonitrile and pyridine conditions but relatively very weak for acetonitrile solutions. This may be because in the acetonitrile solvent, certain 2nd axial sites are occupied by pyridine ligands and some are occupied by acetonitrile ligands. Whereas the band present at 575 nm signifies the five coordinated species. A similar spectral pattern of five and six coordinated species existing in equilibrium has been previously reported in DMSO solvent also.[10] The spectra for Co-(1) and Co-(3-4) also resembles well with the previously reported DCM solutions of these complexes.[1]



Scheme 4.1. Schematic representation of transformation of Co-(1) and Co-(3-4) into bisX⁻-cobalt corrole adducts.

The reported 10⁻⁴ and 10⁻⁵ M DCM solutions of the complexes have the spectra with the bands present at near 377 nm as the Soret band and at 566 and 637 nm as the Q-band and have been interpreted as the proof of five and six-coordinated species

coexisting in solution. In acetonitrile solvent also a very similar spectral behaviour is seen with no comparable shift in bands. Hence this can be predicted that the weak bands present at ~575 and ~655 nm in the **Co-(1)** and **Co-(3-4)** are indicative of the both five and six-coordinated species present in equilibrium where the sixth position of the complex is occupied by pyridine in the acetonitrile solvent (Scheme 1).[1,10] The green colour is intense in the first three corroles namely, **Co-(1-3)** which could be related to the presence of more electron withdrawing groups at C₁₀- *meso* position than in the **Co-(4-5)** corroles.

4.3.2 Colorimetric response of Co-(1-5) towards anions: Considering the fluctuation in UV-Visible absorption bands of the cobalt corrole complexes, when the solvent environment changes, it was hypothesized that these may also interact with anions. Anions acting as co-ordinating ligands may change the axial position environment. Hence, the activity of the cobalt-corrole-pyridine series **Co-(1-5)** in the presence of various anions was explored. All the complexes were studied individually with fourteen distinct anion salts in their 1:1 equivalent solution. The 1×10^{-5} M corroles complex acetonitrile solutions added with 1×10^{-5} M acetonitrile solutions of tetrabutyl ammonium salts of CN^- , F^- , CH_3COO^- , NO_3^- , AsO_3^- , AsO_4^- , Cl^- , Br^- , I^- , ClO_4^- , H_2PO_4^- , S_2^- , HS^- and PF_6^- were prepared. **Co-1** was initially green in its MeCN solution but turned reddish-brown when one equivalent concentration of CN^- , F^- or CH_3COO^- ion was added into it. While in the case of the addition of remaining anions, the solution remained green. **(Figure 4.3)** A similar shift in colour was found in the instance of the **Co-3**, but no such colour change was acknowledged in the case of the **Co-2**. The **Co-4** was initially yellowish-red in colour in its MeCN solution and on the addition of CN^- , F^- or CH_3COO^- a more intense colour was appeared that could be distinguished with

naked eye. The **Co-5** was yellowish-green in colour and no additional variations in appearance were observed after the addition of any anion. The appearance of colour change points towards the capability of the **Co-1**, **Co-3** and **Co-4** corroles to selectively recognize the CN^- , F^- or CH_3COO^- ion over other anions via the colorimetric approach.

4.3.3 UV-Visible response of Co-(1-5) towards anions: Earlier work on corrole complexes of cobalt with pyridine being at axial position confirmed that it acts as a labile ligand with these complexes. A systematic study of concentration and solvent dependence was conducted previously on this same series of complexes, uncovering that the co-ordination number of the complexes was five at 10^{-6} M concentration, which were reddish-brown in colour, and that there was an equilibrium between five and six co-ordination numbers at higher concentrations of dichloromethane, i.e., at 10^{-4} M[1]. Some solvents, such as pyridine or benzonitrile, have a co-ordinating character and hence also promote this six-coordinated form of these complexes, as supported by their green colour in solution[1,11]. The appearance of the Q-band in cobalt corroles at ~ 650 nm using UV-Visible spectroscopy has previously been determined as a marker band of hexa co-ordinated form of these complexes[7,11].

Hence, the variation in colour change with the addition of anions definitely raise the question of whether the complexes are either providing the space to change their geometry or the proximity. The behavior of the **Co-1** in a 1:1 equivalent solution with anions is shown in **Figure 4.2**, where except for three anions (cyanide, fluoride and acetate), all the other possess a spectral pattern similar to the blank solution. The Soret and Q-bands observed for neat MeCN solution and the 11 anions except CN^- , F^- or CH_3COO^- are at 382 and 632 nm, whereas there is a red shift in the Soret

band and it is found at 413 nm in the presence of CN^- , F^- or CH_3COO^- ion, and also the Q-band absorption at 573 nm is intensified while the band at 632 nm completely disappears. A fairly similar observation in the Soret band was also previously reported in F^- ion titration, with $(\text{Ar})_3\text{CoCo}(\text{DMSO})$ where Ar corresponds to the pentafluorophenyl group[12]. The enhancement in Q-band at 573 nm indicates that these three anions are strongly bound to the cobalt metal atom and the spectral data resembles well with the previous reports which indicates that the complexes are present in their five co-ordinated form and the CN^- anion binds at the axial position.[6,13] The complete disappearance of band at ~ 633 nm also states that the complex is exclusively present in its five coordinate form.[6,12,13] This process is closely observed through the titration of a MeCN solution of 1×10^{-5} M **Co-1** with CN^- anion solution, and throughout the titration, each CN^- addition step was monitored spectroscopically. The spectral changes are depicted in **Figure 4.4**. The band at ~ 633 nm weakens with the addition of CN^- anion. Later disappears entirely with the addition of CN^- at near 1 equivalent concentration, indicating the possibility of complete detachment of pyridine from the axial positions and hence giving rise to the formation of mono-cyano cobalt corroles only. The binding constant calculations also support these findings.(**Figure 4.4**) The slope and hence the number of binding species at axial position as found by the Hill equation, is close to one. This implies that the MeCN solution of the **Co-1** gives room for attachment of one CN^- ligand at its axial position, resulting in five co-ordinated forms. The outcomes were similar while titrating it with acetate and fluoride ions. The titrations of these two complexes are also shown in **Figure (4.4)**.

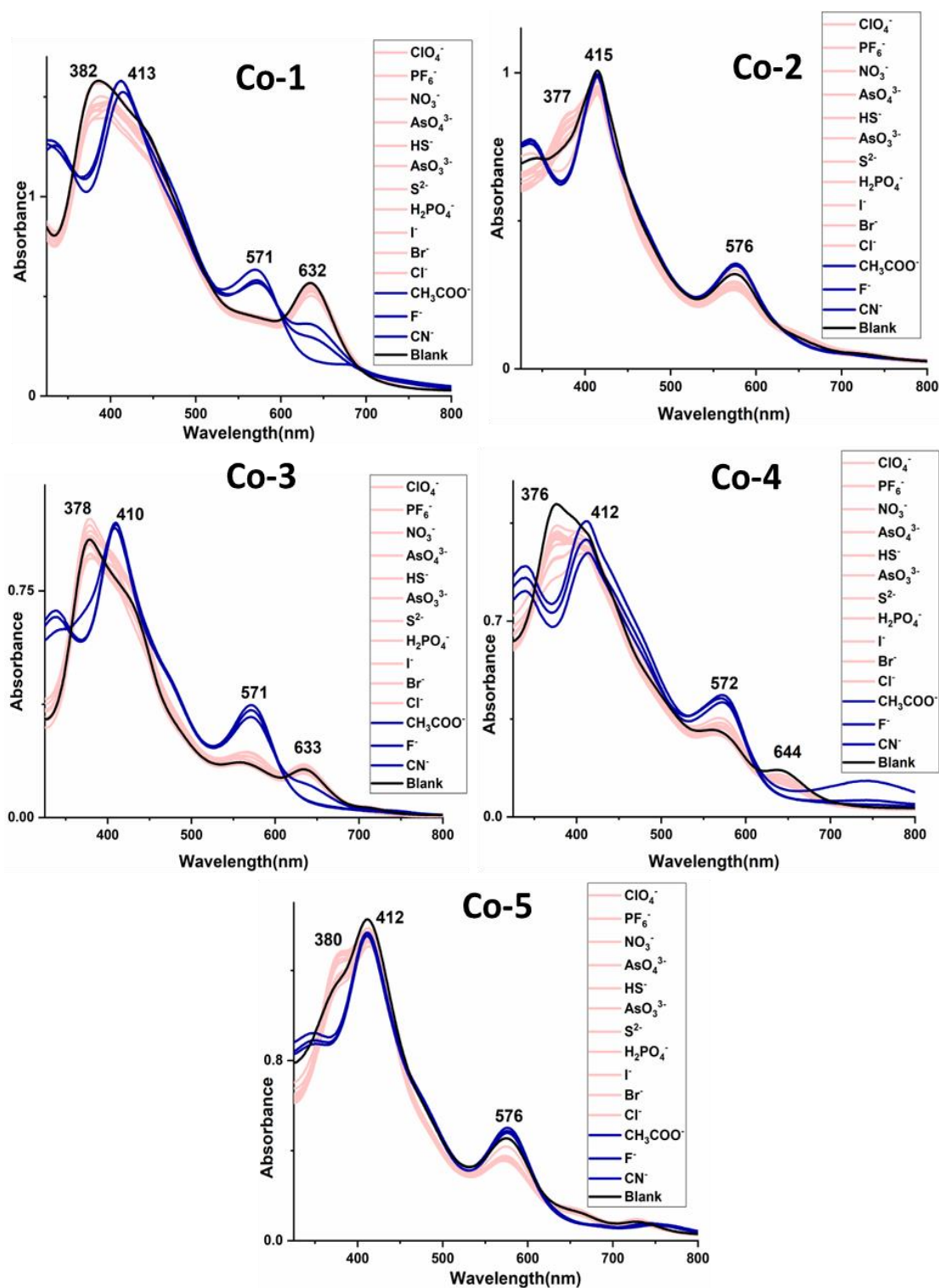


Figure 4.2. UV-vis spectra of Co-(1-5) at 10^{-5} M in acetonitrile containing anions
Cell path length = 10 dm.

Co-1**Co-2****Co-3****Co-4****Co-5**

Figure 4.3. The observed colour-change upon addition of 1.0 equivalent tetrabutylammonium salts of different anions into a solution of **Co-(1-5)** in acetonitrile. From left to right; **A**=Without anion, **B**= CN^- , **C** = F^- , **D** = CH_3COO^- , **E** = Cl^- , **F** = Br^- , **G** = I^- , **H** = NO_3^- , **I** = H_2PO_4^- , **J** = PF_6^- , **K** = AsO_3^{3-} , **L** = AsO_4^{3-} , **M**= ClO_4^- , **N** = S^{2-} , **O** = HS^- ,

In the case of the **Co-3**, a fairly similar spectral pattern of UV-Visible data was observed as in the **Co-1**. At 378, 571 and 633 nm the **Co-3** exhibits absorption bands without and with 11 anions at its 1 equivalent concentration. The three anions, CN⁻, F⁻ and CH₃COO⁻ ions, which are distinct from other anions, cause a red shift of 32 nm in the Soret band, leading it to appear at 410 nm. The band at 571 nm, on the other hand, grows stronger and no additional band at 633 nm was observed.

Table 4.1. Binding constant and limit of detection for addition of different anion on position six of mono-pyridine cobalt corrole **Co-1**, **Co-3** and **Co-4**

Complex	Anion	Binding Constant (logK ₂)	LOD(μM)
Co-1	CN ⁻	5.8	0.068
	F ⁻	5.7	0.149
	CH ₃ COO ⁻	4.8	0.127
Co-3	CN ⁻	5.9	0.013
	F ⁻	5.6	0.077
	CH ₃ COO ⁻	5.2	0.116
Co-4	CN ⁻	6.0	0.007
	F ⁻	6.0	0.008
	CH ₃ COO ⁻	5.8	0.018

For three anions (CN⁻, F⁻, and CH₃COO⁻) in particular, the **Co-4** also displayed a stronger Q-band at 572 nm in comparison to the other 11 anions and the colour of their solution with the **Co-4** was clearly identifiable from that of other anions, validating the stronger axial binding of these three anions to the central cobalt metal. The stronger absorption band appearance at 572 nm for these three specific anions, together with the red shift of around 32 nm in the band from 380 nm to 412 nm distinguishes and readily identifies them from the other eleven anions. The absorption spectrum of the **Co-2** in the presence of all of these fourteen anions is identical to that of the complex in the absence of these anions. (**Figure 4.2**) The Soret band is seen at 415 nm, and a similar observation in the Q-band is seen with

and without addition of anions, hence the complex preserves its original colour. The Q-band absorbs at 576 nm and is somewhat stronger for the three CN⁻, F⁻, and CH₃COO⁻ anions. However, it is not considerably stronger as in the case of the **Co-1**, **Co-3** and **Co-4**. The **Co-5** exhibited the similar property of not shifting the bands in the presence of CN⁻, F⁻ and CH₃COO⁻ anions. The major absorption bands in the case of the **Co-5** were spotted at 412 and 576 nm. (Figure 4.2) This highlights the two important causes of the complexes that favors colour change selectivity in certain anions but not in others. The apparent causes, as above emphasized, are the red shift of the Soret band for the CN⁻, F⁻, and CH₃COO⁻ anions and making the Q-band of ~577 nm stronger in respect of other anions. The colour and spectral alterations in the case of **Co-1**, **Co-2** and **Co-4** for different anions could be a good property of this series to be advanced further.

Table 4.2. UV-Visible spectral data of **Co-(1)** and **Co-(3-4)** summarizing λ_{\max} values of initial and final steps of titration with anions.

Complex	Anion	λ nm($\epsilon \times 10^{-4}$ cm ⁻¹ M ⁻¹)			
		Initial λ_{\max}		Final λ_{\max}	
		Soret band	Q-band	Soret band	Q-band
Co-1	Cyanide	379(7.3)	573(1.6), 633(1.4)	410(6.4)	573(1.9)
	Fluoride	377(7.1)	573(1.9), 630(1.3)	413(6.3)	573(1.8)
	Acetate	380(7.4)	571(1.5), 631(1.5)	410(5.8)	571(1.5)
Co-3	Cyanide	380(7.9)	573(1.5), 634(1.5)	413(7.2)	573(1.6)
	Fluoride	381(8.0)	572(1.6), 635(1.7)	412(7.9)	572(1.9)
	Acetate	381(7.9)	572(1.6), 635(1.6)	412(8.0)	572(1.9)
Co-4	Cyanide	379(6.9)	571(2.8), 645(1.6)	412(6.5)	571(2.6)
	Fluoride	378(7.1)	572(2.8), 650(1.5)	414(7.0)	572(2.5)
	Acetate	377(7.1)	572(2.4), 645(1.4)	413(6.8)	572(2.6)

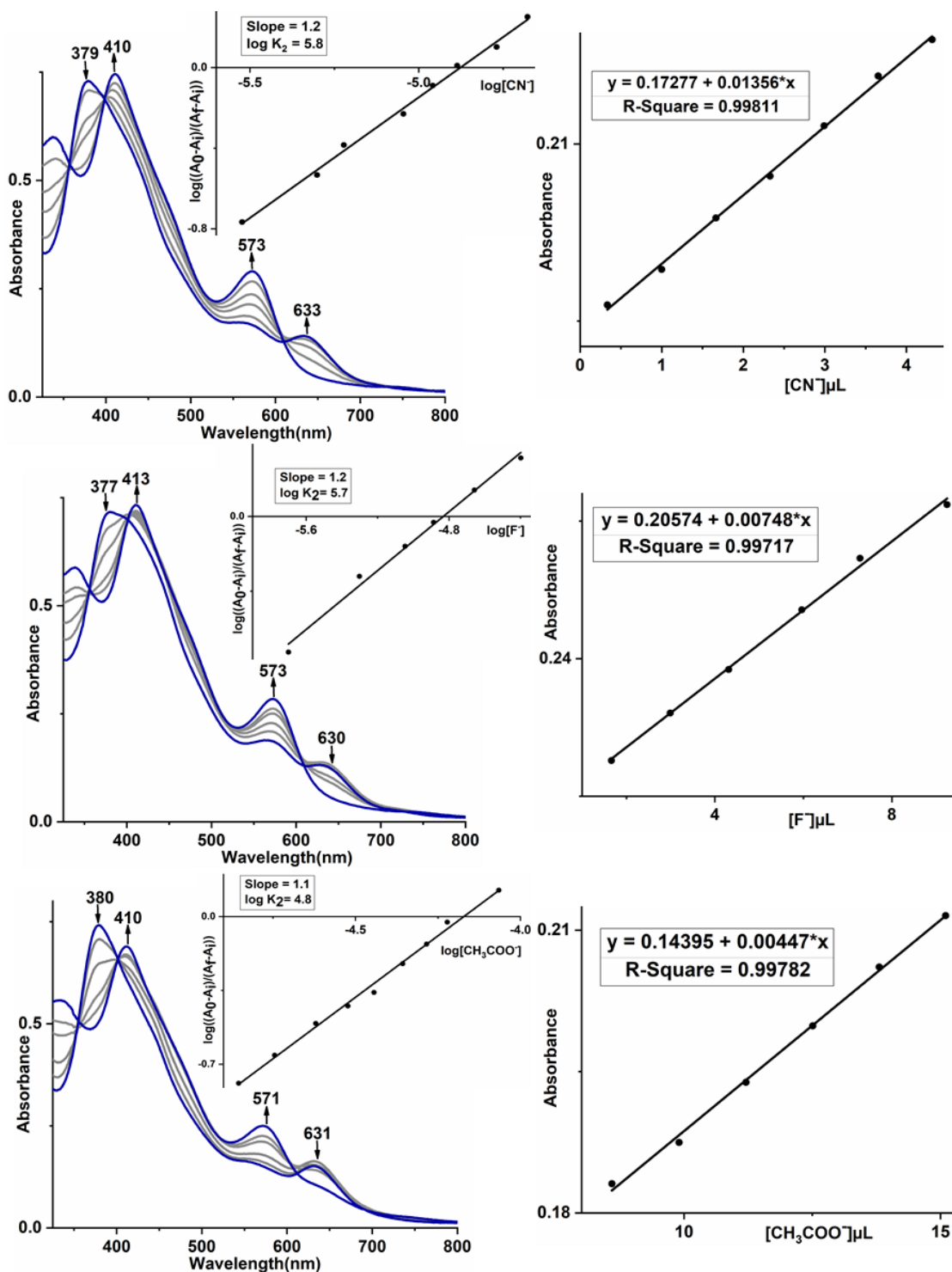


Figure 4.4. Left side: UV-Visible monitored titration of $\sim 1 \times 10^{-5}$ M Co-1 with CN^- , F^- and CH_3COO^- in CH_3CN , Right side: Plot to determine the LOD value for Co-1 towards CN^- , F^- and CH_3COO^- anions.

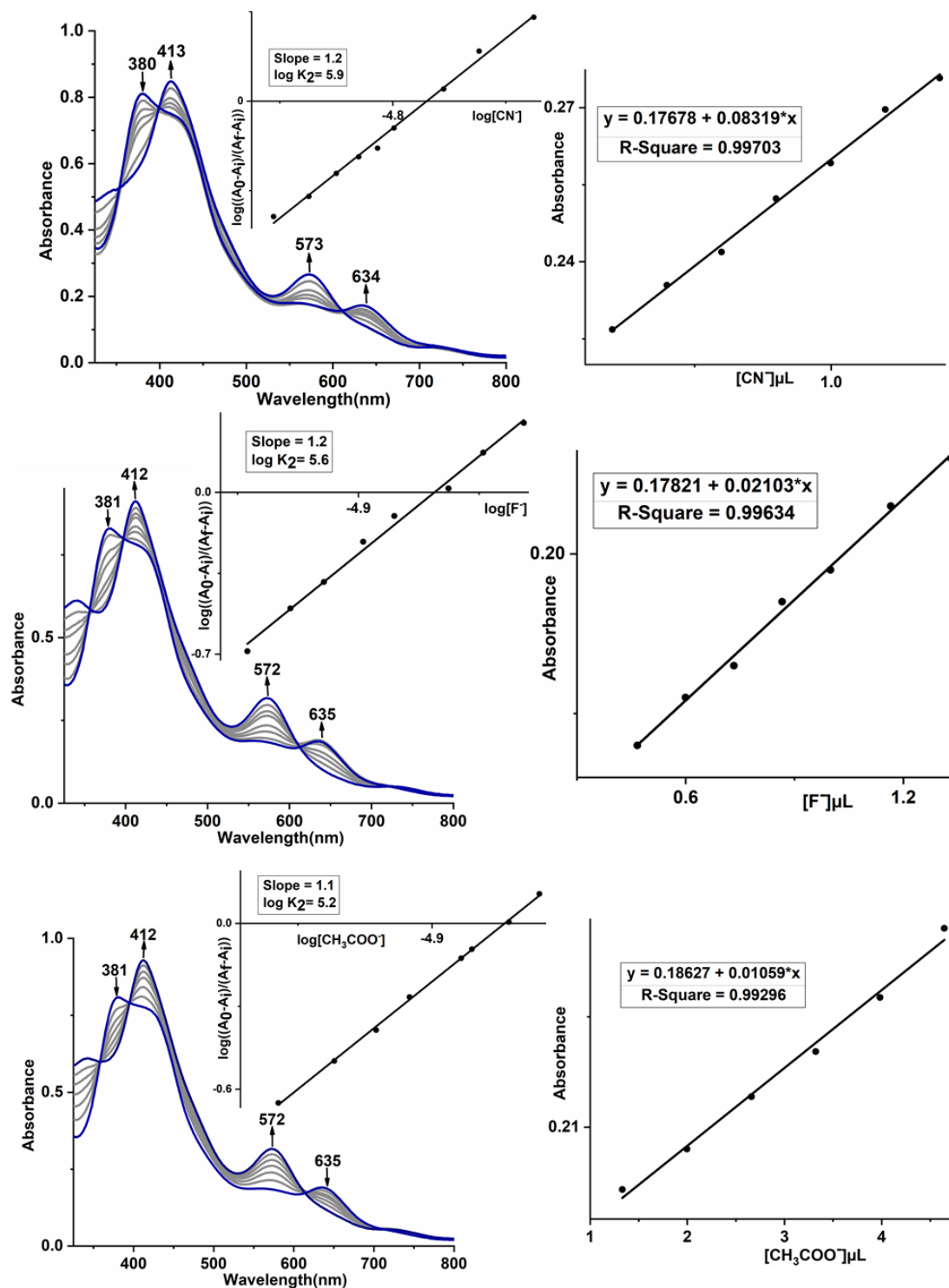


Figure 4.5. Left side: UV-Visible monitored titration of $\sim 1 \times 10^{-5}$ M *Co-3* with CN^- , F^- and CH_3COO^- in CH_3CN , Right side: Plot to determine the LOD value for *Co-2* towards CN^- , F^- and CH_3COO^- anions.

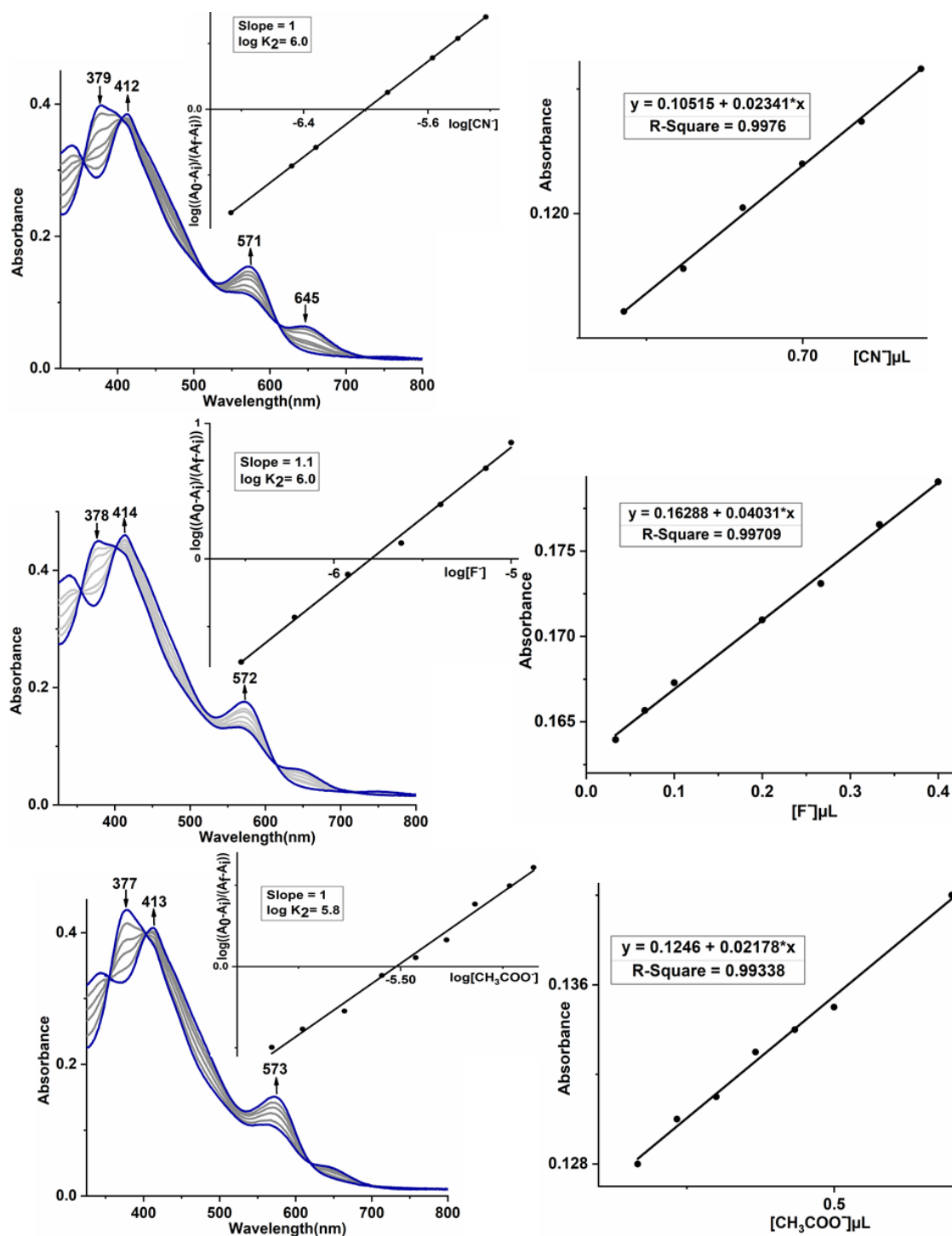


Figure 4.6. Left side: UV-Visible monitored titration of $\sim 1 \times 10^{-5}$ M Co-4 with CN⁻, F⁻ and CH₃COO⁻ in CH₃CN, Right side: Plot to determine the LOD value for Co-4 towards CN⁻, F⁻ and CH₃COO⁻ anions.

4.4 LIMIT OF DETECTION OF CYANIDE, FLUORIDE AND ACETATE ANIONS:

The corrole compounds **Co-1**, **Co-3**, **Co-4** are sensitive towards the anions cyanide, fluoride and acetate. Their sensitivity has been detected by titrating the complexes with TBA⁺CN⁻, TBA⁺F⁻ and TBA⁺OAc⁻ anions and recording their UV-Visible spectra at each step to characterize the variation. For **Co-1**, the variation in spectral changes caused by stepwise addition of TBA⁺CN⁻, TBA⁺F⁻ or TBA⁺OAc⁻ are depicted in **Figure 4.4**. The bands displayed a clear steady minimization in absorption at 379 nm with the addition of TBA⁺CN⁻ and concurrently enhanced the peak absorption at 410 nm. The absorption band at 573 nm increased linearly with an increase in CN⁻ ion concentration. The detection limit was determined to be 0.0682 μM using the **eq (4.1)** in ~10⁻⁵ M MeCN solution. The absorption pattern of **Co-1** in MeCN titration with F⁻ and CH₃COO⁻ ion exactly matches with it, and so the bands at 377 nm for TBA⁺F⁻ and 380 nm for TBA⁺OAc⁻ in its Soret band region also progressively decreased, followed by an elevation in absorption bands of 413 and 410 nm, respectively. All of these variations are accompanied by a shift in the colour of the solution from green to red with each step. F⁻ and CH₃COO⁻ ion detection limits obtained were 0.149 and 0.127 μM, respectively. (**Table (4.2)**) Similarly, the detection limit of **Co-3** for these three anions was computed, and the results are summarized in **Table (4.1)**. (**Figure 4.5**) The **Co-4** displayed the best detection limit among the three complexes (**Figure 4.6**) The complex shows the detection of 0.0068 μM for the CN⁻ ion. (**Table 4.1**) After conducting the titration with ~10⁻⁵ M concentration of complexes with the above-mentioned anions, the absorbance values were fitted in **eq (3.1)**. Even though **Co-4** has less electron withdrawing substituents at the *meso* position than **Co-1** and **Co-3**, it provides the best limit of detection and this is supported by the binding of the anions, which is also

highest for **Co-4**. For all three complexes, CN⁻ anion had higher logK values than the other two examined anions.

Table 4.3. UV–Visible spectra at 10⁻⁵ M concentration of the bis-X adducts in CH₃CN solvent of **Co-(1)** and **Co-(3-4)**.

Complex	Anion	λ nm($\epsilon \times 10^{-4}$ cm ⁻¹ M ⁻¹)	
		Soret band	Q-band
Co-1	Cyanide	427(7.9)	545(4.2), 732(4.7)
	Fluoride	418(6.8)	579(2.8), 730(1.1)
	Acetate	412(9.2), 473(5.3)	572(3.2)
Co-3	Cyanide	431(6.8), 493(4.2)	550(2.7), 743(3.7)
	Fluoride	418(5.4)	568(2.5), 740(1.7)
	Acetate	430(7.7), 477(3.7)	571(2.8)
Co-4	Cyanide	422(6.5)	551(2.9), 742(2.9)
	Fluoride	412(6.5)	573(2.7)
	Acetate	411(6.4)	571(2.4)

The spectral behaviour changes dramatically after the addition of greater than ten equivalents of these anions. (**Figure 4.7**) In the **Co-1** solution of acetonitrile, the continue addition of CN⁻ ion at higher than 1 equivalent concentration continuously red shifted the Soret band and also resulted in the emergence of a new band at ~730 nm as shown in **Figure 4.7**. The band becomes more intense until it approaches the 12-15 equivalent of CN⁻ addition. This band is consistent with the previously

reported spectroscopic data, which revealed a bis-CN adduct formed in situ after the addition of CN^- at higher equivalent conditions.[12,14] Hence, it indicates that the **Co-1** is transformed into bis-CN cobalt corrole by occupying the 2nd axial position. As a result, with less than one equivalent of CN^- addition, the binding constant ($\log K_2$) is appeared to be greater than one but less than two. The addition of a higher concentration of F^- also led to the appearance of a band at 730 nm,

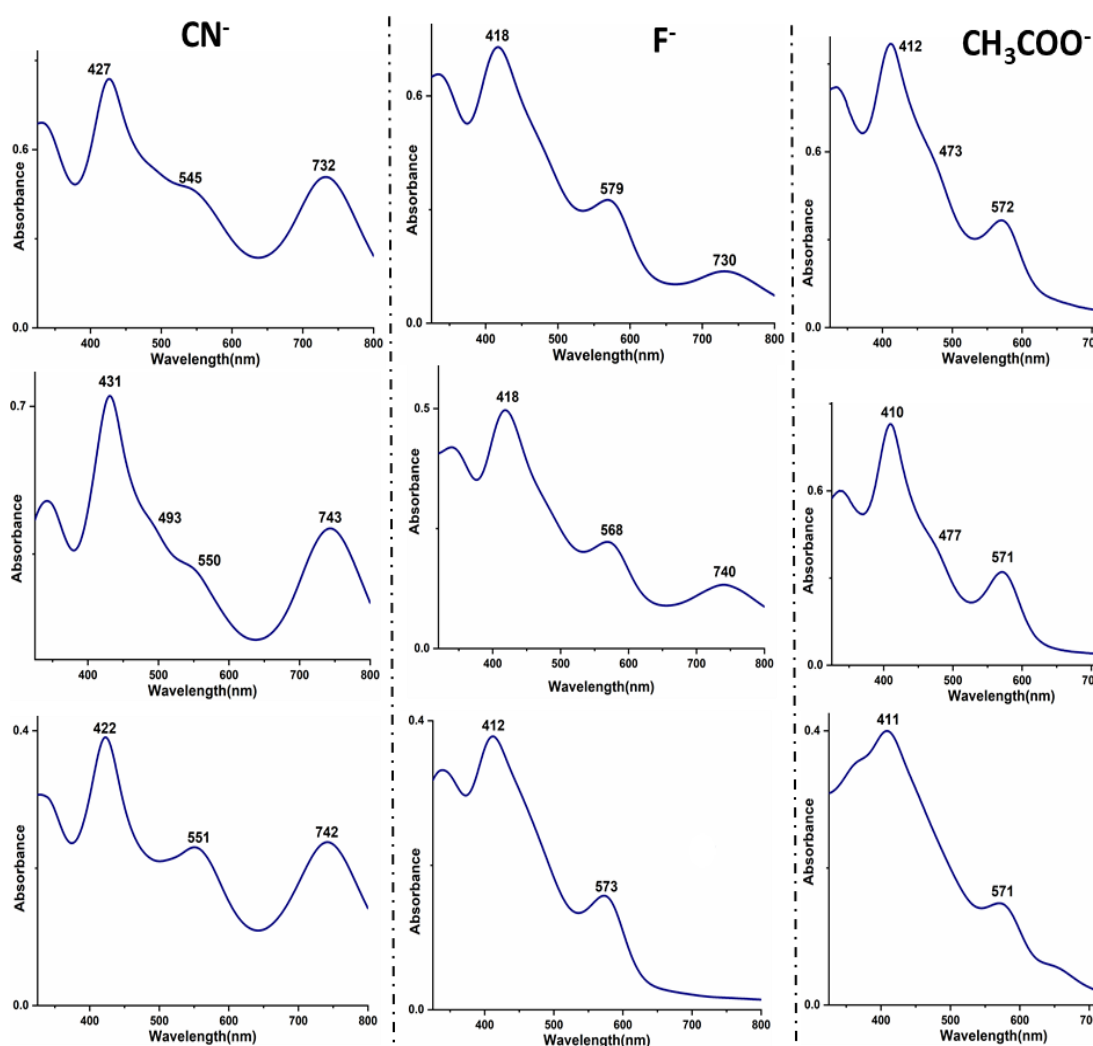


Figure 4.7. UV-Visible spectra at 10^{-5} M of the bis-X adducts in CH_3CN solvent of **Co-(1-2)** and **Co-4** where $\text{X} = \text{CN}^-$, F^- , CH_3COO^- ion at >10 equivalents.

although it was not as intense as obtained with CN⁻ anions. In the case of acetate anions, however, no such appearance in the band was observed even after the addition of 20 equivalents of it. (Figure 4.7) (Table 4.3) A similar observation for **Co-3** was made, where addition of CN⁻ ions results in an intensified band at ~740 nm resembling the bis-CN adduct formation described above, however no such band was identified for acetate ion. The F⁻ anion addition on the other side, produced a weaker band which was comparable to what was observed for **Co-1** complex. A conclusion that can be drawn from these findings is that the **Co-1** and **Co-3** are clearly capable of exhibiting selectivity for acetate anions at >20 equivalent amount, whereas at 5-10 equivalent addition, the CN⁻ anion is detected selectively.

In the case of the **Co-4**, there is a substantial presence of bis-CN adduct. The complex is highly susceptible to CN⁻ ion and it emerges the band near 740 nm even addition of nearly 1 equivalent amount of CN⁻ anion. While for other two anions, namely F⁻ and OAc⁻ ions, the **Co-4** does not possess a marker band at 740 nm. This implies that the **Co-4** is selective towards the detection of CN⁻ anions.

4.5 CONCLUSION

In summary, we adopted spectroscopic and colorimetric techniques to investigate a series of five *A₂B* cobalt corroles possessing different electron withdrawing and electron donating *meso* position substituents. The complexes are found to be solvent dependent and hence their behaviour with different non-aqueous media has been closely observed. Three complexes **Co-1**, **Co-2** and **Co-3** were found green in their acetonitrile solutions, which indicated that the acetonitrile solvent shows binding properties. A considerable shift in absorption bands was also detected, which supported the solvent-

dependent behaviour of the complexes. The **Co-1** in MeCN solution displayed the absorption bands at 382 and at 632 nm, but in its benzonitrile and pyridine solutions, the Soret band is located at ~426 nm and the Q-band at ~655 nm. These complexes were also tested with various anions where the complexes exhibited unique behaviour toward different anions. As an instance, in a 1:1 equivalent solution of fourteen separate anions, the **Co-1** was shown to be selective towards F⁻, CN⁻ and CH₃COO⁻ accompanied by a change in color from green to reddish-brown. Similarly, **Co-3** and **Co-4** also displayed selectivity as shown by **Co-1**. At higher concentrations of anions, the **Co-1** and **Co-3** preferentially displayed the characteristic absorption band at ~735 nm for F⁻ and CN⁻ anion, however no such band was appeared in the case of acetate anion, which made these complexes selective for acetate anion at >10 equivalent of anions. The **Co-4**, on the other hand, has been found CN⁻ anion selective. In this way, the cobalt corroles have meaningful outcomes for various ligands present, encouraging further research in this domain.

References-

- [1] Jyoti, N. Fridman, A. Kumar, S.G. Warkar, Synthesis, structural characterization and binding ability of A₂B cobalt(III) corroles with pyridine, *Inorganica Chim. Acta.* 527 (2021) 120580. <https://doi.org/10.1016/j.ica.2021.120580>.
- [2] B. Koszarna, D.T. Gryko, Efficient synthesis of meso-substituted corroles in a H₂O-MeOH mixture, *J. Org. Chem.* 71 (2006) 3707–3717. <https://doi.org/10.1021/jo060007k>.
- [3] I.G. and Z.G. Atif Mahammed Ilona Giladi, Synthesis and Structural Characterization of a novel Covalently-Bound Corrole Dimer, *Chem. Eur. J.* 2001,. 723 (2001) 4259–4265. <https://doi.org/0947-6539/01/0719-4259> \$ 17.50+.50/0.
- [4] R. Kubba, O. Yadav, P. Yadav, N. Fridman, A. Kumar, Penta -hexa coordination behaviour of ABA-P(V) corrole, *J. Mol. Struct.* 1243 (2021) 130857. <https://doi.org/10.1016/j.molstruc.2021.130857>.
- [5] A. Varshney, A. Kumar, S. Yadav, Catalytic activity of bis p-nitro A₂B (oxo)Mn(V) corroles towards oxygen transfer reaction to sulphides, *Inorganica Chim. Acta.* 514 (2021) 120013. <https://doi.org/10.1016/j.ica.2020.120013>.
- [6] V. Quesneau, W. Shan, N. Desbois, S. Brandès, Y. Rousselin, M. Vanotti, V. Blondeau-Patissier, M. Naitana, P. Fleurat-Lessard, E. Van Caemelbecke, K.M. Kadish, C.P. Gros, Cobalt Corroles with Bis-Ammonia or Mono-DMSO Axial Ligands. Electrochemical, Spectroscopic Characterizations and Ligand Binding Properties, *Eur. J. Inorg. Chem.* 2018 (2018) 4265–4277. <https://doi.org/10.1002/ejic.201800897>.
- [7] K.M. Kadish, Z. Ou, J. Shao, C.P. Gros, J.M. Barbe, F. Jérôme, F. Bolze, F. Burdet, R. Guillard, Alkyl and aryl substituted corroles. 3. Reactions of cofacial cobalt biscalcoroles and porphyrin-corroles with pyridine and carbon monoxide, *Inorg. Chem.* 41 (2002) 3990–4005. <https://doi.org/10.1021/ic020058+>.
- [8] K.M. Kadish, P.W. Koh, Electrochemistry of Rhodium and Cobalt Corroles . Characterization of (OMC)Rh(PPh₃) and (OMC)Co(PPh₃) Where OMC is the Trianion of 2,3,7,8,12,13,17,18-Octamethylcorrole, *Am. Chem. Soc.* 31 (1992) 2305–2313. [https://doi.org/0020-1669/92/1331-2305\\$03.00/0](https://doi.org/0020-1669/92/1331-2305$03.00/0).

- [9] U. Mayer, V. Gutmann, W. Gerger, The acceptor number - A quantitative empirical parameter for the electrophilic properties of solvents, *Monatshefte Für Chemie*. 106 (1975) 1235–1257. <https://doi.org/10.1007/BF00913599>.
- [10] X. Jiang, W. Shan, N. Desbois, V. Quesneau, S. Brandès, E. Van Caemelbecke, W.R. Osterloh, V. Blondeau-Patissier, C.P. Gros, K.M. Kadish, Mono-DMSO ligated cobalt nitrophenylcorroles: Electrochemical and spectral characterization, *New J. Chem.* 42 (2018) 8220–8229. <https://doi.org/10.1039/c8nj00300a>.
- [11] X. Jiang, M.L. Naitana, N. Desbois, V. Quesneau, S. Brandès, Y. Rousselin, W. Shan, W.R. Osterloh, V. Blondeau-Patissier, C.P. Gros, K.M. Kadish, Electrochemistry of Bis(pyridine)cobalt (Nitrophenyl)corroles in Nonaqueous Media, *Inorg. Chem.* 57 (2018) 1226–1241. <https://doi.org/10.1021/acs.inorgchem.7b02655>.
- [12] W.R. Osterloh, V. Quesneau, N. Desbois, S. Brandès, W. Shan, V. Blondeau-Patissier, R. Paolesse, C.P. Gros, K.M. Kadish, Synthesis and the Effect of Anions on the Spectroscopy and Electrochemistry of Mono(dimethyl sulfoxide)-Ligated Cobalt Corroles, *Inorg. Chem.* 59 (2020) 595–611. <https://doi.org/10.1021/acs.inorgchem.9b02855>.
- [13] W.R. Osterloh, N. Desbois, V. Quesneau, S. Brandès, P. Fleurat-Lessard, Y. Fang, V. Blondeau-Patissier, R. Paolesse, C.P. Gros, K.M. Kadish, Old Dog, New Tricks: Innocent, Five-coordinate Cyanocobalt Corroles, *Inorg. Chem.* 59 (2020) 8562–8579. <https://doi.org/10.1021/acs.inorgchem.0c01037>.
- [14] L. Lvova, G. Pomarico, F. Mandoj, F. Caroleo, C. Di Natale, K.M. Kadish, S. Nardis, Smartphone coupled with a paper-based optode: Towards a selective cyanide detection, *J. Porphyr. Phthalocyanines*. 1088424620 (2020). <https://doi.org/10.1142/S1088424620500091>.

CHAPTER 5

HYDROGEN EVOLUTION ACTIVITY OF COBALT CORROLES

5.1 INTRODUCTION

Recently, metallocorroles have been extensively studied, including their multiple routes of synthesis, functionalisation at the periphery, and insertion of metal in the macrocyclic corrole core. All of this has led us to the novel corrole compositions that are widely employed in a range of applications. Thus, Corrole is a versatile macrocycle with several modification options. Since the very beginning, the introduction of cobalt metal into corrole has been a recognised phenomenon. Cobalt corroles have been frequently known to exhibit a number of redox reactions. This property has led us to the use of cobalt corroles for a variety of applications, including ORR[1–8], HER[9–13], OER[14], CO₂ reduction [15–17] and various sensing applications where these are used to prepare different sensing materials.[18–24]

In our current study, we have focused on the impact of substituting electron withdrawing or electron donating groups (**Co-(1-5)**) on the overall oxidation or reduction potential. For this, the cyclic voltammetry experiments were performed using dichloromethane as a solvent. Firstly, the DFT methods have been used to structurally optimize all the geometries using Gaussian09W software and the 6-31G(d,p) basis set. A penta-coordinated Triphenylphosphine ligated with [10-(2,6-difluorophenyl)-5,15-bis(4-nitrophenyl)corrolato]Cobalt(III) was also synthesised and well characterized using different spectroscopic techniques. The X-ray crystals of this complex were also obtained in good quality, which further confirmed the proof of composition and the

insertion of cobalt metal as well. The hydrogen evolution ability of two of the complexes was also assessed through cyclic voltammetry.

5.2 EXPERIMENTAL SECTION

5.2.1 Materials:

All reagents were of highest purity and were purchased from commercial sources. These were used as received without further purification. Silica gel (230-440 mesh) was used for the Column chromatography. HPLC grade Hexane and DCM were used as eluent. Trifluoroacetic acid and acetonitrile were purchased from Merck. Triphenylphosphine and Pyridine were purchased from Avra chemicals. Tetrabutylammonium perchlorate (TBAP) was obtained from Alfa Aesar.

5.2.2 Instrumentation:

UV–Vis spectroscopy: UV-1800 Shimadzu Spectrophotometer was utilized to record the UV-Visible spectra. Cuvettes made up of Quartz with optical path lengths of 1 cm were used.

Nuclear magnetic resonance spectroscopy: A Bruker Avance spectrometer set at 400 MHz for ^1H NMR and 377 MHz for ^{19}F NMR was used to record the spectra. Chemical shifts are reported in ppm relative to residual solvent peaks of chloroform ($\delta = 7.26$ ppm) in the ^1H NMR spectra. The obtained spectra were evaluated by using MestRenova software.

Mass Spectrometry: High-resolution mass spectra (HRMS) of complexes were recorded by Maxis Impact HD Mass Spectrometer. As a direct probe, APCI (atmospheric pressure chemical ionisation) was utilised in either positive or negative mode.

X-ray crystallography: Slow evaporation of heptane/dichloromethane solutions yielded single crystals of $C_{73}H_{49}CoF_2N_6O_4P$. An appropriate crystal was selected and mounted on a diffractometer at 293 K. With the number of indicated reflections, precise cell parameters were obtained. Data collection was performed using monochromated $MoK\alpha$ radiation and the λ was 0.71073 Å, using ϕ and ω scans to cover the Ewald sphere. A Using Olex2[25], the structure was solved with the olex2.solve[26] structure solution program using Charge Flipping and refined with the SHELXL[27] refinement package using Least Squares minimization. All non-hydrogen atoms were refined with anisotropic displacement parameters.

Crystallographic Data for $C_{73}H_{49}CoF_2N_6O_4P$ (Co-6) (M = 1202.08 g/mol): : triclinic, space group P-1, a = 13.4789(2) Å, b = 13.9042(3) Å, c = 16.4431(3) Å, α = 95.7823(15)°, β = 100.6753(15)°, γ = 105.2753(16)°, V = 2884.75(9) Å³, Z = 2, T = 293 K, 13311 independent reflections measured ($4.522^\circ \leq 2\theta \leq 60.34^\circ$), ($R_{int} = 0.0427$, $R_{\sigma} = 0.0452$), The final R_1 was 0.0481 and $wR_2 = 0.1204$ for ($I > 2\sigma(I)$). $R_1 = 0.0661$, $wR_2 = 0.1305$ (all data), $\mu(MoK\alpha) = 0.391 \text{ mm}^{-1}$, $\rho_{calc} = 1.384 \text{ g/cm}^3$.

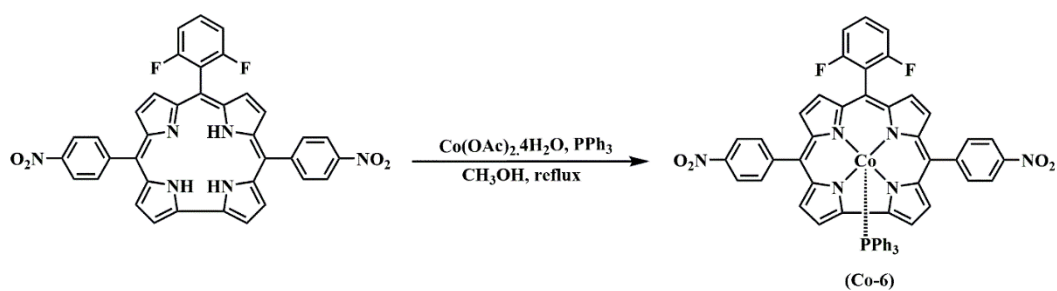
Cyclic Voltammetry: Cyclic voltammetry experiments were performed using CH instruments (CHI 620E) equipped with a three-electrode system viz. a platinum wire counter electrode, a glassy carbon working electrode, and a saturated calomel reference electrode (SCE). For the CV recordings, HPLC-grade acetonitrile and dichloromethane were employed as the solvents, and 0.1 M tetrabutylammonium perchlorate (TBAP) was chosen as the supporting electrolyte. The concentration of corrole was maintained approximately 1 mM during electrochemical analysis. The scan rate was 0.1 V/s.

Theoretical Calculations: The geometry optimisation and all the calculations were carried out with Gauss View06 W software.[28] A 6-31G(d,p) basic set was used throughout for geometry optimization.[29] The crystal coordinates of **Co-2** have been used as a fundamental structure and all the subsequent input structures have been produced by varying the substituents.

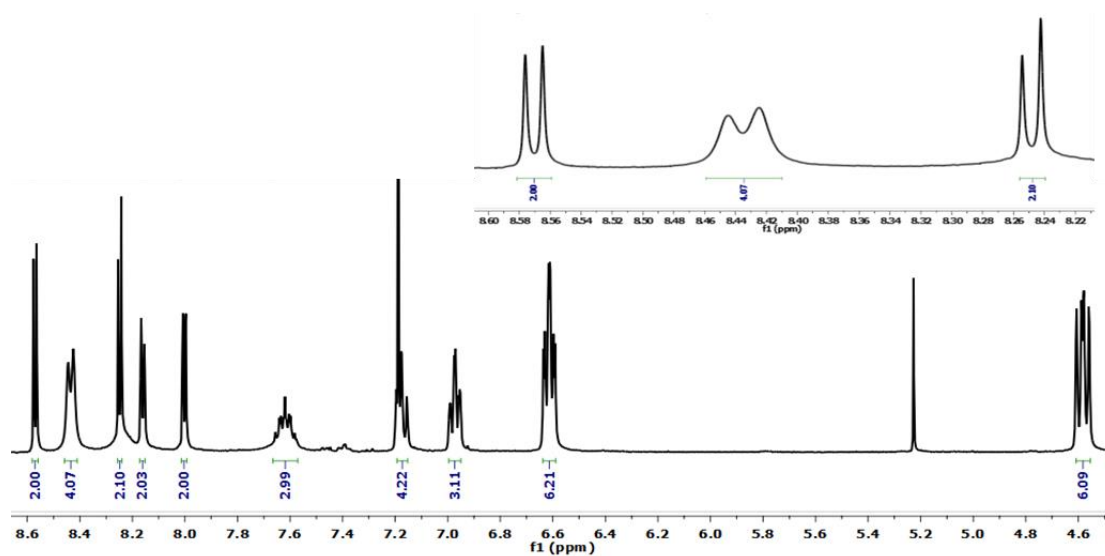
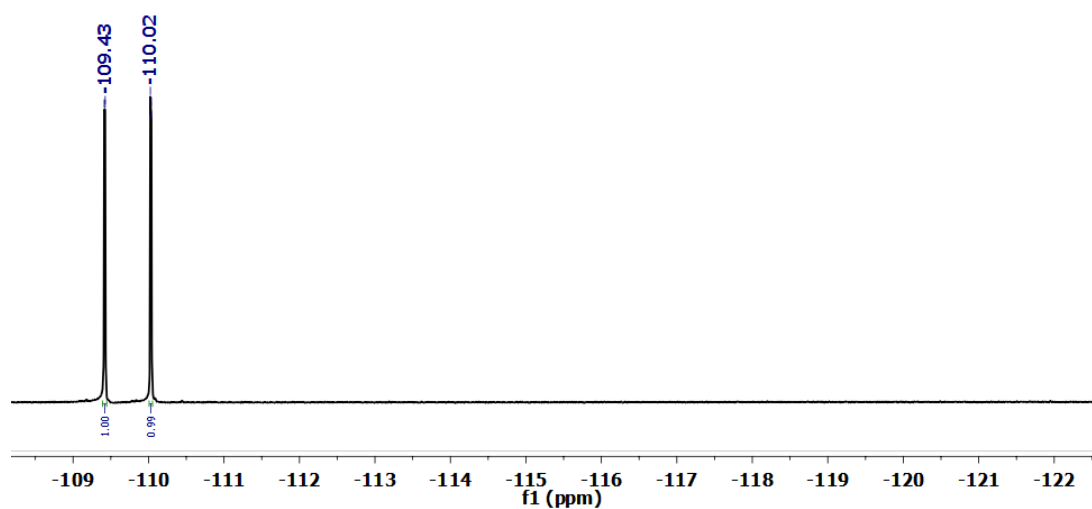
5.2.3 Synthesis of the Complexes:

Co-(1-5) were prepared as reported in our previous literature.[30] A procedure for synthesis of **(Co-6)** is provided in this section.(**Scheme 5.1**) The prepared free base corrole was treated at 60 °C with $\text{Co}(\text{oAc})_2 \cdot 4\text{H}_2\text{O}$, using PPh_3 as a solvent. The obtained crude complex underwent column chromatography and the mixture containing DCM and hexane were used as eluent to obtain the pure product.

10-(2,6-difluorophenyl)-5,15-bis(4-nitrophenyl)corrolato]Cobalt(III)Triphenylphosphine (Co-6) was obtained through silica gel chromatography with DCM:Hexane (40:60) as eluent in 76 % yield (46.6 mg, 0.0275 mmol). ^1H NMR(400 MHz, CDCl_3) δ 8.57 (d, $^3J_{\text{H-H}} = 4.5$, 2H), 8.43 (d, $^3J_{\text{H-H}} = 7.9$ Hz, 4H), 8.25 (d, $^3J_{\text{H-H}} = 4.8$ Hz, 2H), 8.16 (d, $^3J_{\text{H-H}} = 4.8$ Hz, 2H), 8.00 (d, $^3J_{\text{H-H}} = 4.5$ Hz, 2H), 7.55-7.69 (m, 3H), 7.19 – 7.15 (m, 4H), 7.00 – 6.95 (m, 3H), 6.61 (m, 6H), 4.61 – 4.56 (m, 6H).(**Figure 5.1**) ^{19}F NMR (377 MHz, CDCl_3) δ -110.02 (s, F), -109.43 (s, F).(**Figure 5.2**) HRMS: Calcd for $\text{C}_{55}\text{H}_{34}\text{CoF}_2\text{N}_6\text{O}_4\text{P}$ ($[\text{M-PPh}_3]^+$) m/z 708.077 m/z found 708.033($[\text{M-PPh}_3]^+$). (**Figure 5.3**)



Scheme 5.1 – Synthesis scheme of Co-6.

Figure 5.1 - ^1H NMR spectrum of Co-6 in CDCl_3 .Figure 5.2 – ^{19}F NMR spectrum of Co-6 in CDCl_3 .

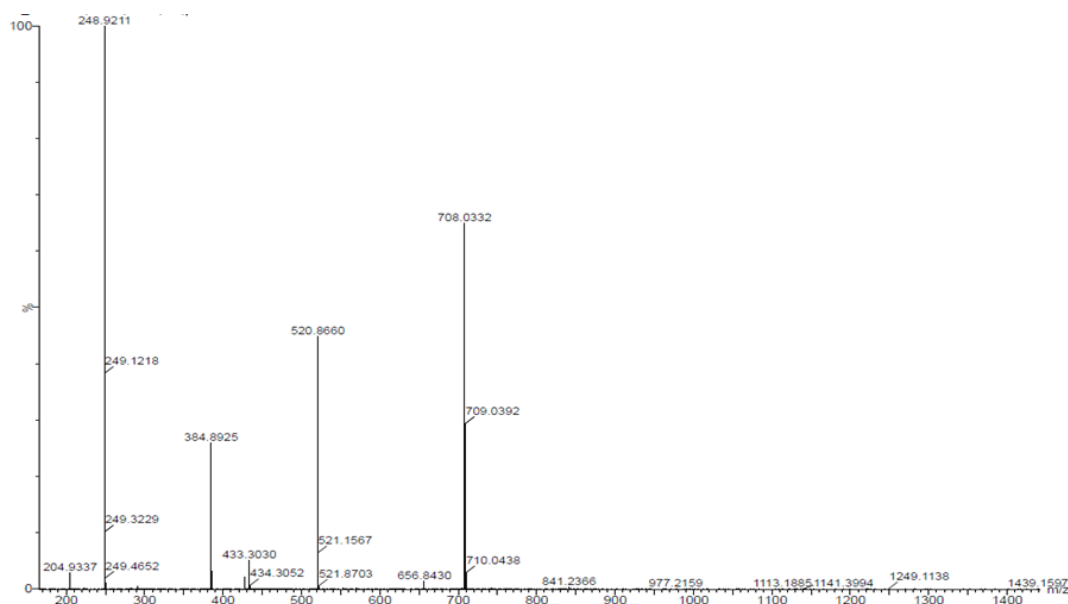


Figure 5.3 - HRMS spectra of Co-6.

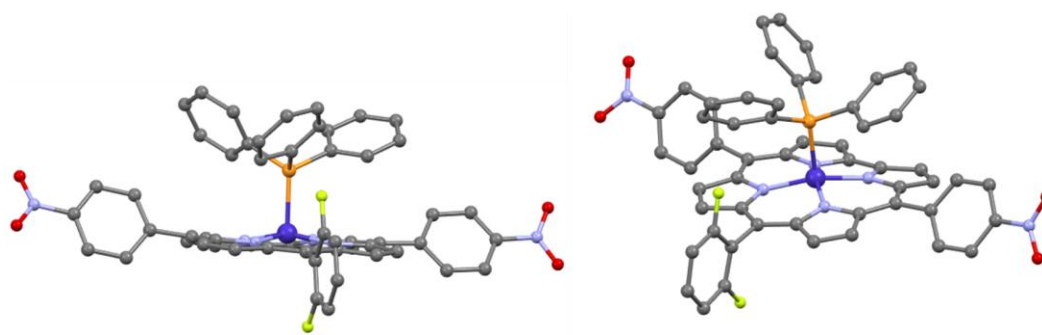


Figure 5.4 - X-ray single crystal structure of (Co-6), side (left) and top view (right).

5.3 RESULTS AND DISCUSSION

5.3.1 Synthesis:

A series of cobalt corroles (**Co-1 to 5**) already reported was synthesized in good yield by following the procedure described in literature.[30–32] A new complex of triphenylphosphine ligated cobalt corrole (**Co-6**) was also synthesised and obtained in good yield. TLC, $^1\text{H-NMR}$, $^{19}\text{F-NMR}$ spectra and HRMS were used to validate the purity of the compound synthesised. The X-ray quality crystals of 10-(2,6-

difluorophenyl)-5,15-bis(4-nitrophenyl)corrolato]Cobalt(III)Triphenylphosphine (Co-6) were also obtained in good quality which further confirmed the proof of composition and insertion of cobalt metal as well as attachment of PPh₃ group at axial position. (Figure 5.4)

5.3.2 NMR Spectroscopy:

The ¹H-NMR spectra of (Co-6) displayed sharp peaks for β-pyrrolic protons within 8.2-8.6 ppm range.(Figure 5.1) The signals found in 7.00 – 4.56 ppm range integrated as 6:6:3 can be assigned due to three different sets of protons of three phenyl rings present axially. The extent of the lower δ values have been attributed to the diamagnetic ring current effect of corrole macrocycle.[33–35] ¹⁹F-NMR spectra of (Co-6) displayed two signals due to two fluorine atoms of C₁₀ meso-difluorophenyl group at near -110 ppm.(Figure 5.2) The well resolved two peaks obtained reflects that the fluorine atoms are not coordinated symmetrically. The spectral range and nature of spectra of both the ¹H-NMR and ¹⁹F-NMR is indicative of the existence of the diamagnetic Co^{III} oxidation state of complexes.[35,36]

5.3.3 X-ray Crystallography:

Single crystals of the structure of Co-6 were unambiguously elucidated through an X-ray structural analysis.(Figure 5.4) The crystal adopts the P-1 space group and Triclinic crystal system. (Table 5.1) The carbon framework of the corrole macrocycle is found to be slightly non-planar. The cobalt atom lies 0.2968 Å above the 4-nitrogen atoms mean plane. While, cobalt atom is displaced by 0.3896 Å above the 23-atom mean

plane. The mean Co-N bond distance is found to be 1.8755 Å which is quite comparable to the reported square pyramidal Co-corroles in the literature.[37–39] The Co-P distance obtained is 2.1980 Å which is in good agreement with the other observed typical metallocorroles.[37]

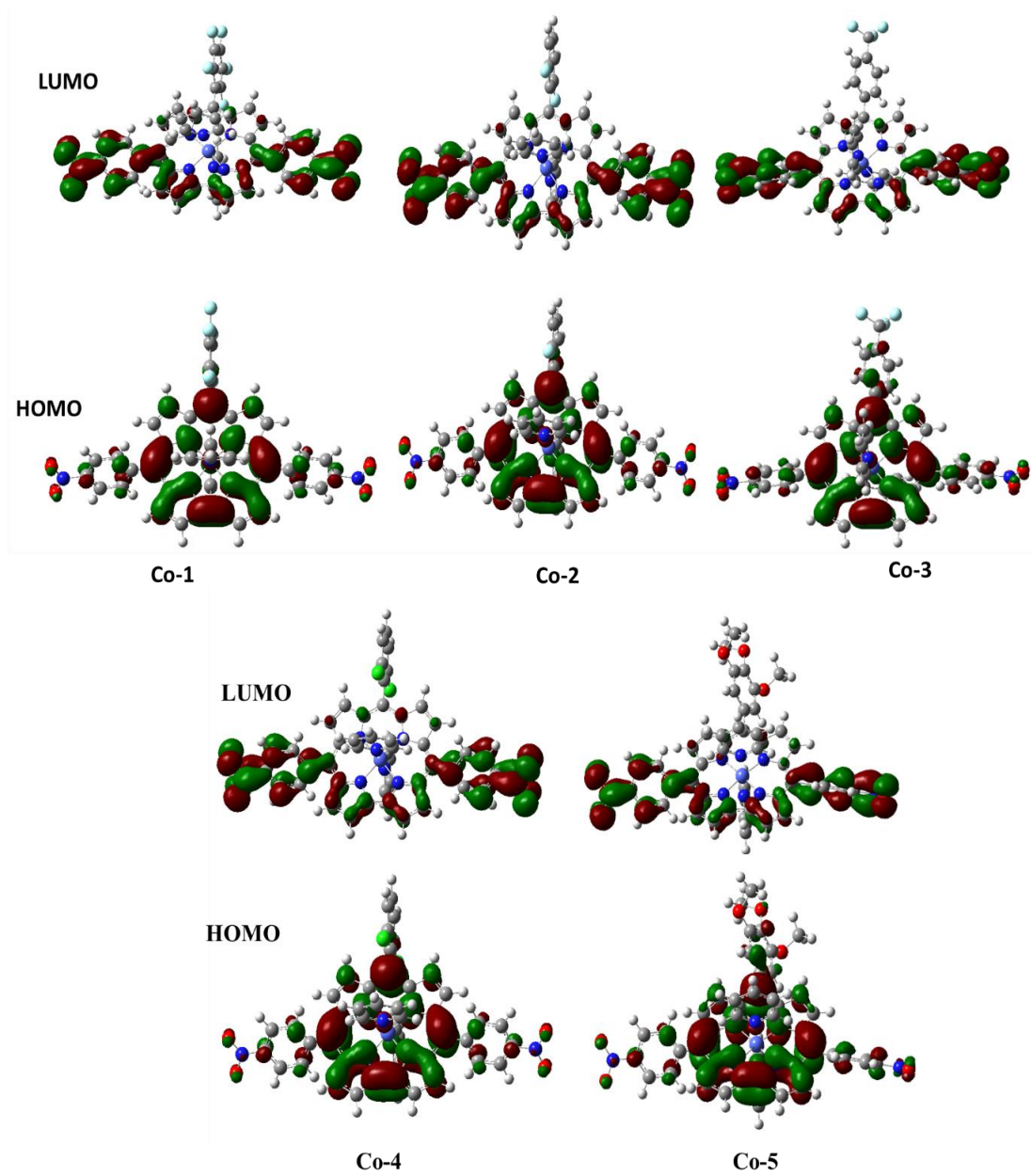


Figure 5.5 - HOMO-LUMO of Co-(1-5).

5.4 DFT STUDIES:

DFT calculations for **Co-(1-5)** were carried out using B3LYP/LANL2DZ level and using Gauss View06 W. The HOMO and LUMO of all these complexes are shown in **Figure 5.5**. In HOMO, the electron π -cloud in all the complexes is largely concentrated on the corrole macrocycle, whereas in LUMO, it is dispersed across the *meso*-carbons. **Figure 5.6** shows the variation in the computed energy gap between the frontier molecular orbitals over the series of **Co-(1-5)** compounds. The variation in energy gap for these compounds depends upon the behaviour of groups present at *meso*- positions. It is usually assumed that increasing the number of electron- withdrawing groups, such as fluorine, would reduce the energy of HOMO by attracting the electrons towards the ring. In contrast, the empty LUMO will be affected less, thereby making the HOMO-LUMO gap larger in the case of pentafluoro substituted **Co-1**. Methoxy groups having electron donating characteristics on the other hand, should have a reverse effect and have lower HOMO-LUMO gap. Therefore, the smallest energy gap is seen in the case of **Co-5**.

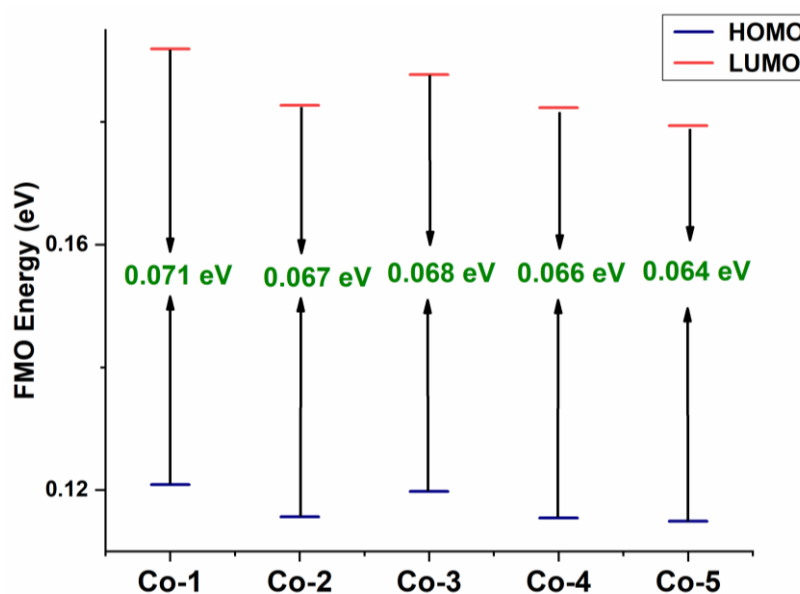


Figure 5.6 – Variation in HOMO-LUMO gap of **Co-(1-5)**.

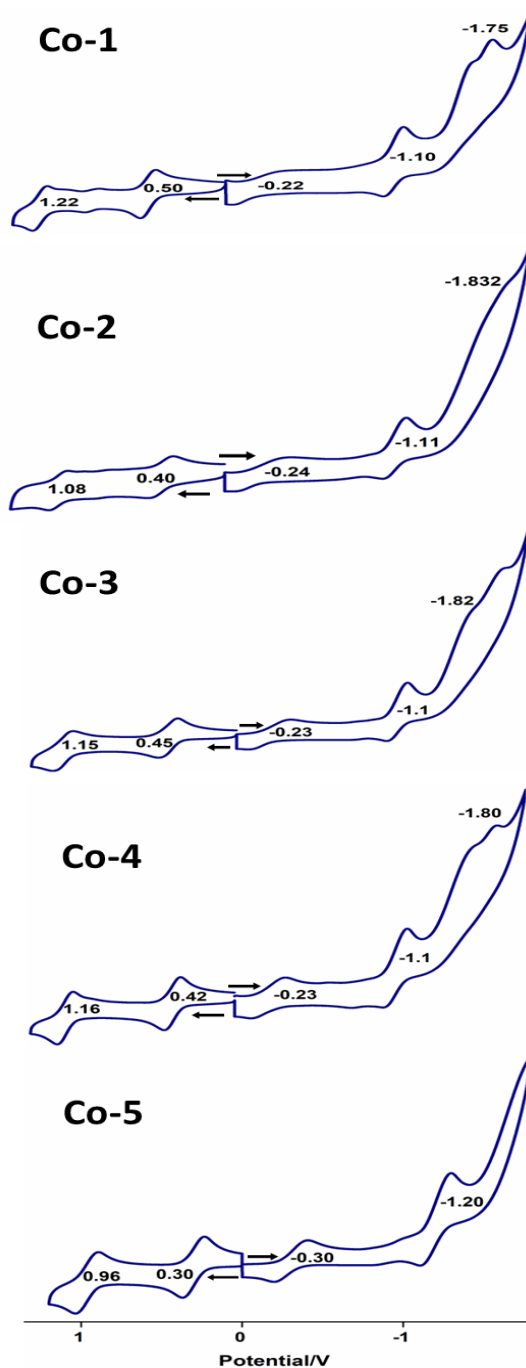


Figure 5.7- Cyclic voltammograms of Co-(1-5) in DCM containing 0.1 M TBAP and at scan rate of 100 mV.

5.5 Electrochemistry:

The impact of substituting electron withdrawing or electron donating substituents on the overall oxidation/reduction potential was examined by cyclic voltammetry. In

general, it is anticipated that the addition of more electron withdrawing group would cause the redox potential to shift towards more positive direction. The cyclic voltammetric experiments were carried out in the presence of a non-coordinating solvent i.e., dichloromethane without the addition of pyridine and using 0.1 M TBAP.

Cyclic voltammograms of **Co-(1–5)** in CH₂Cl₂ are displayed in **Figure 5.7** and a summary of recorded half-wave and peak potentials is provided in **Table 5.1**. The complexes undergo a number of oxidation and reductions processes, as illustrated in **Figure 5.7**. All the five complexes exhibit two oxidation steps, and they also display two to three reductions. There is a continuous shifting in the electrode potential on moving from **Co-5** to **Co-1**. For an instance, the E_{1/2} for **Co-5** possessing penta-fluorophenyl substituent at *meso*-position is located at -0.22V while **Co-3**, having 2,6-difluorophenyl group has an E_{1/2} value of -0.23V. The **Co-5** complex substituted with tri-methoxy groups on the *meso*-phenyl corrole has the Co(III/II) E_{1/2} at the most negative potential i.e., at -0.30V.

The nitrobenzene group is found to be reduced at -1.08 V. All the *meso*-nitrophenyl substituted porphyrin or corrole complexes provides the nitro group reduction potential in a range of -1.1- -1.25 V.[36,40–42] These findings demonstrates the independency of the reduction potential of nitrophenyl groups from the nature of metal or ring substituents. A similar observation has been seen for the **Co-(1-5)** complexes. The complexes undergo one electron reduction at -1.1 to -1.2 V. In addition, the current is also seen to be increasing approximately two times on comparison of preceding Co(III/II) reduction. Hence the second reduction peak situated at -1.1V has been considered as the peak responsible for the reduction of *meso*-nitrophenyl groups. Once

the reduction is occurred at -1.1 V, a second reversible reduction occurs there in at the E_p from -1.75 to -1.80 V. (**Figure 5.7**) The results resemble very well with the previously observed literature.

The electronic effect of different complexes could be easily observed from the cyclic voltammograms. The **Co-1** to **Co-4** have the initial reversible one electron reduction on the -0.22, -0.24, -0.23 and -0.23 V, respectively. The three-electron donating -OCH₃ groups on **Co-5** make the complex harder to reduce and easiest to oxidise among this series pertaining the first reduction potential at -0.30V and first oxidation potential at less positive position i.e., at 0.30V. The hardest to reduce complex **Co-5** have the second E_{pc} at -1.3V but the E_{pa} is observed at -1.1 V only. This indicates the lack of interaction of *meso*-nitrophenyl groups on the overall activity of the macrocycle. Although the nitrophenyl groups do not shift their redox potentials under the influence of different metal or ring substituents, but these groups surely shift the redox potential of the compounds in the positive direction by exerting the electron withdrawing effect on the overall ring. It is generally found that the presence of one nitro-phenyl ring on the *meso*-position shifts the redox potential by 30–100 mV in the case of corroles and porphyrins. Kadish and coworkers shows that the insertion of per nitrophenyl ring shifted redox potential by 80 mV in DCM solvent.[30,36]

5.6 HER ACTIVITY ANALYSIS:

Analysis of the electrocatalyzed HER was carried out for **Co-3** (**Figure 8c**). The electrochemical properties were observed in CH₃CN solvent using 0.1M TBAP as a supporting electrolyte. As it has been found from cyclic voltammetry experiments, those complexes can attain a +1-oxidation state and hence could be used for the process

that leads to the evolution of hydrogen. The most important parameters to take into account when considering the efficiency of the HERs are the kinetic reactivity ($i_{\text{cat}}/i_{\text{p}}$) and onset potentials. The addition of TFA, serving as a proton source, to

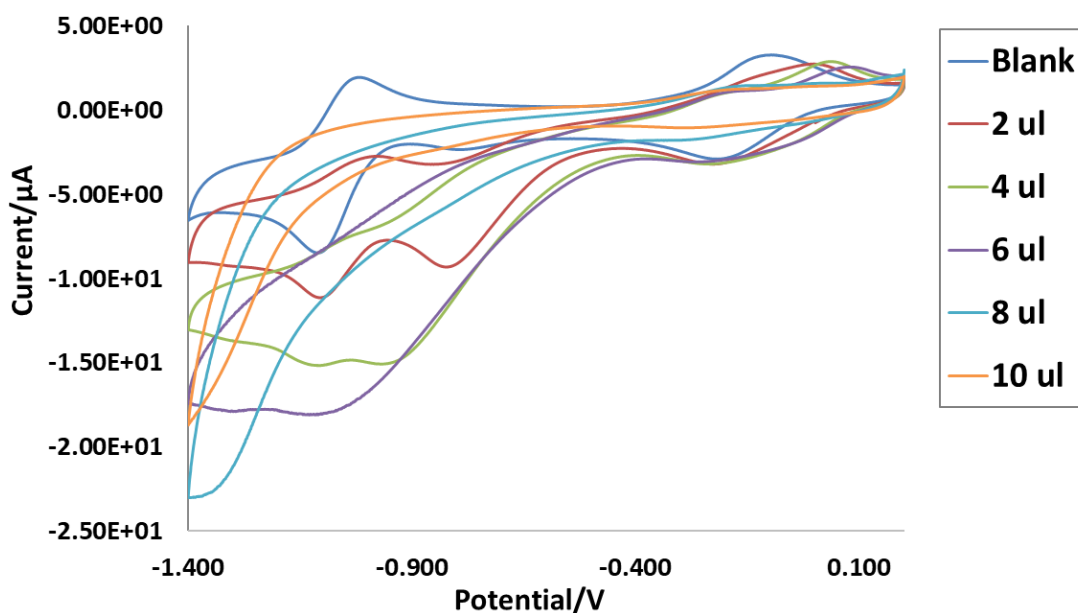


Figure 5.8 - Reductive cyclic voltammetry of **Co-3** in acetonitrile in the presence of 1.0–10.0 μl of 10^{-3} M TFA with 0.1 M TBAP as the supporting electrolyte.

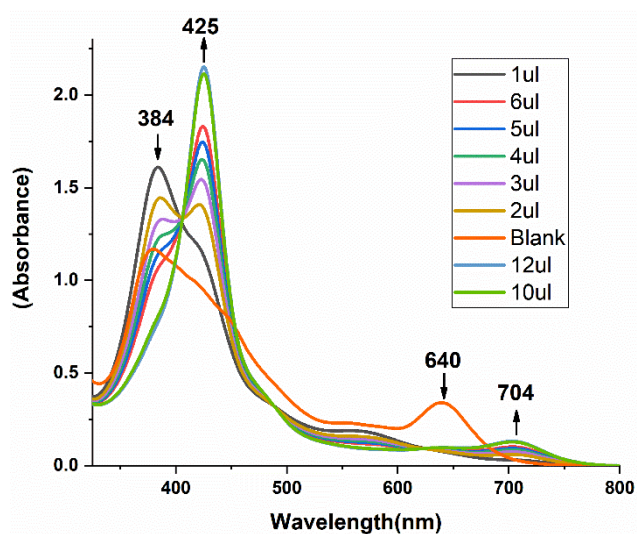


Figure 5.9 - Titration of 10^{-3} M **Co-3** at different conc. of trifluoroacetic acid.

Co-3 solutions in CH₃CN induced the catalytic waves close to the first (Co^{III}/Co^{II}) and third (Co^{II}/Co^I) reduction potentials. When the concentration of TFA is increased in the **Co-3** solution, a clear increase in the catalytic wave is observed at first. However, no significant current enhancement was subsequently found, indicating that the complex was not as effective for HER catalytic properties as earlier reported complexes have shown.

The titration experiment was then performed in the presence of UV-Visible spectroscopy, and it was found that the complexes spectra were altered continually with each step of addition of TFA (**Figure 8d**). The intensity of the Soret band initially present at 384 nm was reduced, and a new band at 425 nm emerged, which has a higher intensity when compared to the previous Soret band. Additionally, at 704 nm, a new, yet not so strong, Q-band appeared. This suggests the formation of a new species instead of the evolution of hydrogen by the cobalt corroles.

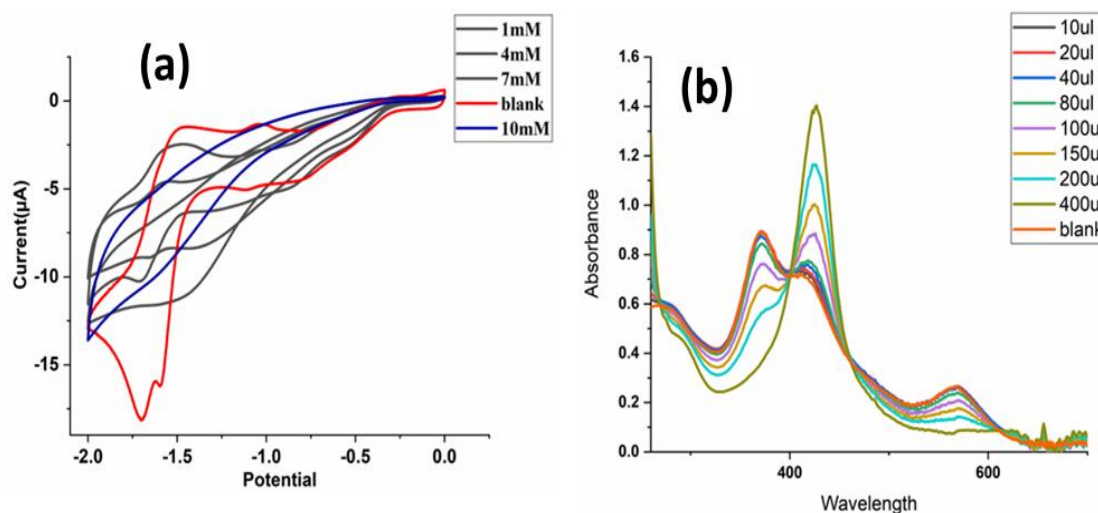


Figure 5.10 – (a) Reductive cyclic voltammetry of **Co-3** in acetonitrile in the presence of 1.0–10.0 μl of 10⁻³ M TFA using 0.1 M of TBAP as the supporting electrolyte (b) Titration of 10⁻³ M **Co-3** at different conc. of trifluoroacetic acid.

Cobalt triphenylphosphine corroles are frequently found as good electrocatalysts. A number of PPh_3 ligated complexes of cobalt corroles are reported by now. As electrocatalysts for hydrogen evolution processes, oxygen evolution reactions, and oxygen reduction reactions, many nitrophenyl-substituted cobalt corroles have been reported.[12,40,43–47] A_3 nitrophenyl corroles and even corroles with A_2B substitutes have previously shown excellent activity for the HER process.[12,40,43,44,48] Therefore, we prepared A_2B type PPh_3 ligated cobalt corroles possessing two p-nitrophenyl groups at C_5 and C_{15} positions and 2,6-difluorophenyl group at C_{10} positions (**Co-6**), to investigate the impact of an axially co-ordinated ligand on the overall activity of cobalt corroles. The HER activity was determined upon gradual addition of TFA to the **Co-6** solution using CH_3CN solvent, and no abrupt current enhancement was observed. This further demonstrates the lack of efficacy of **Co-6** for the HER process. The complex undergoes structural modifications instead of the evolution of hydrogen by the cobalt corroles. This is proved by the titration data shown in Figure 5.10 (b), which provides evidence for this proposition.

Table 5.1: Half wave and peak potentials of **Co-(1-5)** ($E_{1/2}$ or E_p , V vs SHE) for two oxidations and two-three reduction processes in CH_2Cl_2 using 0.1 M of TBAP.

Complex	Oxidation		Reduction			
	2 nd	1 st	E_{pc}	1 st	2 nd / NO_2Ph^*	3 rd
Co-1	1.22	0.50	-0.35	-0.04	-1.10	-1.75
Co-2	1.08	0.40	-0.4	-0.07	-1.11	
Co-3	1.15	0.45	-0.36	-0.1	-1.10	-1.82
Co-4	1.16	0.42	-0.34	-0.13	-1.11	-1.8
Co-5	0.96	0.30	-0.41	-0.19	-1.2	

5.7 CONCLUSION

In summary, electrochemistry of a series of five A₂B type bis-pyridine ligated cobalt complexes $\text{Co}[(p\text{-NO}_2\text{Ph})_2\text{RCor}](\text{py})_2$, where R belong to different electron withdrawing or electron donating substituent at *meso*- position for different complexes (**Co-1(1-5)**), has been assessed using Cyclic voltammetry. DFT calculations have also been employed, highlighting the effect of *meso*-carbon substituents in corroles, upon HOMO-LUMO gap variation. A new complex, $\text{Co}[(p\text{-NO}_2\text{Ph})_2(2,6\text{-DiFPh})\text{Cor}]\text{PPh}_3$, possessing triphenylphosphine ligand at axial position is synthesised and characterised using ¹H-NMR, ¹⁹F-NMR and Mass Spectrometry. The complex was identified as a penta-coordinated Co^{III} species by x-ray crystallography. The electrochemical study of synthesised **Co-3** and **Co-6** reveals that cobalt corroles are inactive towards the HER process under homogenous conditions for both PPh₃ and pyridine ligated complexes.

References-

- [1] K.M. Kadish, J. Shen, L. Frémond, P. Chen, M. El Ojaimi, M. Chkounda, C.P. Gros, J.M. Barbe, K. Ohkubo, S. Fukuzumi, R. Guilard, Clarification of the oxidation state of cobalt corroles in heterogeneous and homogeneous catalytic reduction of dioxygen, *Inorg. Chem.* 47 (2008) 6726–6737. <https://doi.org/10.1021/ic800458s>.
- [2] J.P. Collman, M. Kaplun, R.A. Decréau, Metal corroles as electrocatalysts for oxygen reduction, *Dalt. Trans.* (2006) 554–559. <https://doi.org/10.1039/b512982f>.
- [3] V.A. Adamian, F. D'Souza, S. Licoccia, M.L. Di Vona, E. Tassoni, R. Paolesse, T. Boschi, K.M. Kadish, Synthesis, Characterization, and Electrochemical Behavior of (5,10,15-Tri-X-phenyl-2,3,7,8,12,13,17,18-octamethylcorrolato)cobalt(III) Triphenylphosphine Complexes, Where X = p-OCH₃, p-CH₃, p-Cl, m-Cl, o-Cl, m-F, o-F, or H, *Inorg. Chem.* 34 (1995) 532–540. <https://doi.org/10.1021/ic00107a003>.
- [4] J.H. Palmer, Transition Metal Corrole Coordination Chemistry, in: Springer-Verlag Berlin Heidelb., 2011: pp. 49–90. https://doi.org/10.1007/430_2011_52.
- [5] A. Ghosh, Electronic Structure of Corrole Derivatives: Insights from Molecular Structures, Spectroscopy, Electrochemistry, and Quantum Chemical Calculations, *Chem. Rev.* 117 (2017) 3798–3881. <https://doi.org/10.1021/acs.chemrev.6b00590>.
- [6] K.M. Kadish, L. Frémond, Z. Ou, J. Shao, C. Shi, F.C. Anson, F. Burdet, C.P. Gros, J.M. Barbe, R. Guilard, Cobalt(III) corroles as electrocatalysts for the reduction of dioxygen: Reactivity of a monocorrole, biscalcorroles, and porphyrin-corrole dyads, *J. Am. Chem. Soc.* 127 (2005) 5625–5631. <https://doi.org/10.1021/ja0501060>.
- [7] Z. Ou, A. Lü, D. Meng, S. Huang, Y. Fang, G. Lu, K.M. Kadish, Molecular Oxygen Reduction Electrocatalyzed by meso -Substituted Cobalt Corroles Coated on Edge-Plane Pyrolytic Graphite Electrodes in Acidic Media, *Inorg. Chem.* 51 (2012) 8890–8896. <https://doi.org/10.1021/ic300886s>.
- [8] A. Mahammed, Z. Gross, Metallocorroles as Electrocatalysts for the Oxygen Reduction Reaction (ORR), *Isr. J. Chem.* 56 (2016) 756–762. <https://doi.org/10.1002/ijch.201600027>.

- [9] H. Lin, M.S. Hossain, S.Z. Zhan, H.Y. Liu, L.P. Si, Electrocatalytic hydrogen evolution using triaryl corrole cobalt complex, *Appl. Organomet. Chem.* (2020) 1–10. <https://doi.org/10.1002/aoc.5583>.
- [10] H. Sun, Y. Han, H. Lei, M. Chen, R. Cao, Cobalt corroles with phosphonic acid pendants as catalysts for oxygen and hydrogen evolution from neutral aqueous solution, *Chem. Commun.* 53 (2017) 6195–6198. <https://doi.org/10.1039/c7cc02400b>.
- [11] X. Li, H. Lei, J. Liu, X. Zhao, S. Ding, Z. Zhang, X. Tao, W. Zhang, W. Wang, X. Zheng, R. Cao, Carbon Nanotubes with Cobalt Corroles for Hydrogen and Oxygen Evolution in pH 0–14 Solutions, *Angew. Chemie - Int. Ed.* 57 (2018) 15070–15075. <https://doi.org/10.1002/anie.201807996>.
- [12] A. Kumar, S. Sujesh, P. Varshney, A. Paul, S. Jeyaraman, Aminophenyl-substituted cobalt(III) corrole: A bifunctional electrocatalyst for the oxygen and hydrogen evolution reactions, *Dalt. Trans.* 48 (2019) 11345–11351. <https://doi.org/10.1039/c9dt02339a>.
- [13] D. Dolui, S. Ghorai, A. Dutta, Tuning the reactivity of cobalt-based H₂ production electrocatalysts via the incorporation of the peripheral basic functionalities, *Coord. Chem. Rev.* 416 (2020) 213335. <https://doi.org/10.1016/j.ccr.2020.213335>.
- [14] H. Lei, X. Li, J. Meng, H. Zheng, W. Zhang, R. Cao, Structure Effects of Metal Corroles on Energy-Related Small Molecule Activation Reactions, *ACS Catal.* 9 (2019) 4320–4344. <https://doi.org/10.1021/acscatal.9b00310>.
- [15] W. Sinha, A. Mahammed, N. Fridman, Y. Diskin-Posner, L.J.W. Shimon, Z. Gross, Superstructured metallocorroles for electrochemical CO₂ reduction, *Chem. Commun.* 55 (2019) 11912–11915. <https://doi.org/10.1039/c9cc06645d>.
- [16] J. Grodkowski, P. Neta, E. Fujita, A. Mahammed, L. Simkhovich, Z. Gross, Reduction of cobalt and iron corroles and catalyzed reduction of CO₂, *J. Phys. Chem. A.* 106 (2002) 4772–4778. <https://doi.org/10.1021/jp013668o>.
- [17] S. Gonglach, S. Paul, M. Haas, F. Pillwein, S.S. Sreejith, S. Barman, R. De, S. Müllegger, P. Gerschel, U.P. Apfel, H. Coskun, A. Aljabour, P. Stadler, W. Schöfberger, S. Roy, Molecular cobalt corrole complex for the heterogeneous electrocatalytic reduction of carbon dioxide, *Nat. Commun.* 10 (2019) 1–10. <https://doi.org/10.1038/s41467-019-11868-5>.

- [18] S. Brandès, V. Quesneau, O. Fonquernie, N. Desbois, V. Blondeau-Patissier, C.P. Gros, Porous organic polymers based on cobalt corroles for carbon monoxide binding, *Dalt. Trans.* 48 (2019) 11651–11662. <https://doi.org/10.1039/c9dt01599j>.
- [19] J.M. Barbe, G. Canard, S. Brandès, R. Guillard, Synthesis and physicochemical characterization of meso-functionalized corroles: Precursors of organic-inorganic hybrid materials, *European J. Org. Chem.* (2005) 4601–4611. <https://doi.org/10.1002/ejoc.200500374>.
- [20] Y. Wang, J. Akhigbe, Y. Ding, C. Brückner, Y. Lei, Meso-Tritolylcorrole-Functionalized Single-walled Carbon Nanotube Donor-Acceptor Nanocomposites for NO₂ Detection, *Electroanalysis*. 24 (2012) 1348–1355. <https://doi.org/10.1002/elan.201200077>.
- [21] S. Yang, M.E. Meyerhoff, Study of cobalt(III) corrole as the neutral ionophore for nitrite and nitrate detection via polymeric membrane electrodes, *Electroanalysis*. 25 (2013) 2579–2585. <https://doi.org/10.1002/elan.201300400>.
- [22] X. Sheng, H. Zhao, L. Du, Selectivity of Cobalt Corrole for CO vs. O₂ and N₂ in Indoor Pollution, *Sci. Rep.* 7 (2017) 14536. <https://doi.org/10.1038/s41598-017-15228-5>.
- [23] E. Jaworska, G. Pomarico, B.B. Berna, K. Maksymiuk, R. Paolesse, A. Michalska, All-solid-state paper based potentiometric potassium sensors containing cobalt(II) porphyrin/cobalt(III) corrole in the transducer layer, *Sensors Actuators, B Chem.* 277 (2018) 306–311. <https://doi.org/10.1016/j.snb.2018.08.090>.
- [24] M. Vanotti, S. Poisson, V. Soumann, V. Quesneau, S. Brandès, N. Desbois, J. Yang, L. André, C.P. Gros, V. Blondeau-Patissier, Influence of interfering gases on a carbon monoxide differential sensor based on SAW devices functionalized with cobalt and copper corroles, *Sensors Actuators, B Chem.* 332 (2021). <https://doi.org/10.1016/j.snb.2021.129507>.
- [25] O. V. Dolomanov, L.J. Bourhis, R.J. Gildea, J.A.K. Howard, H. Puschmann, OLEX2: A complete structure solution, refinement and analysis program, *J. Appl. Crystallogr.* 42 (2009) 339–341. <https://doi.org/10.1107/S0021889808042726>.

- [26] L.J. Bourhis, O. V. Dolomanov, R.J. Gildea, J.A.K. Howard, H. Puschmann, The anatomy of a comprehensive constrained, restrained refinement program for the modern computing environment - Olex2 dissected, *Acta Crystallogr. Sect. A Found. Crystallogr.* 71 (2015) 59–75. <https://doi.org/10.1107/S2053273314022207>.
- [27] G.M. Sheldrick, Crystal structure refinement with SHELXL, *Acta Crystallogr. Sect. C Struct. Chem.* 71 (2015) 3–8. <https://doi.org/10.1107/S2053229614024218>.
- [28] R. Dennington, T.A. Keith, John M. Millam, GaussView, version 6.0. 16, Semichem Inc Shawnee Mission KS. (2016).
- [29] C. Lee, W. Yang, R.G. Parr, Development of the Colle-Salvetti correlation-energy formula into a functional of the electron density, *Phys. Rev. B.* 37 (1988) 785–789. <https://doi.org/10.1103/PhysRevB.37.785>.
- [30] Jyoti, N. Fridman, A. Kumar, S.G. Warkar, Synthesis, structural characterization and binding ability of A₂B cobalt(III) corroles with pyridine, *Inorganica Chim. Acta.* 527 (2021) 120580. <https://doi.org/10.1016/j.ica.2021.120580>.
- [31] B. Koszarna, D.T. Gryko, Efficient synthesis of meso-substituted corroles in a H₂O-MeOH mixture, *J. Org. Chem.* 71 (2006) 3707–3717. <https://doi.org/10.1021/jo060007k>.
- [32] I.G. and Z.G. Atif Mahammed Ilona Giladi, Synthesis and Structural Characterization of a novel Covalently-Bound Corrole Dimer, *Chem. Eur. J.* 2001, 723 (2001) 4259–4265. [https://doi.org/0947-6539/01/0719-4259 \\$ 17.50+.50/0](https://doi.org/0947-6539/01/0719-4259 $ 17.50+.50/0).
- [33] S. Ganguly, J. Conradie, J. Bendix, K.J. Gagnon, L.J. McCormick, A. Ghosh, Electronic Structure of Cobalt–Corrole–Pyridine Complexes: Noninnocent Five-Coordinate Co(II) Corrole–Radical States, *J. Phys. Chem. A.* 121 (2017) 9589–9598. <https://doi.org/10.1021/acs.jpca.7b09440>.
- [34] K. Sudhakar, A. Mahammed, N. Fridman, Z. Gross, Trifluoromethylation for affecting the structural, electronic and redox properties of cobalt corroles, *Dalt. Trans.* 48 (2019) 4798–4810. <https://doi.org/10.1039/c9dt00675c>.
- [35] L. Simkhovich, N. Galili, I. Saltsman, I. Goldberg, Z. Gross, Coordination chemistry of the novel 5,10,15-tris(pentafluorophenyl)corrole: Synthesis, spectroscopy, and structural characterization of its cobalt(III), rhodium(III), and iron(IV) complexes, *Inorg. Chem.* 39 (2000) 2704–2705. <https://doi.org/10.1021/ic991342c>.

- [36] X. Jiang, M.L. Naitana, N. Desbois, V. Quesneau, S. Brandès, Y. Rousselin, W. Shan, W.R. Osterloh, V. Blondeau-Patissier, C.P. Gros, K.M. Kadish, Electrochemistry of Bis(pyridine)cobalt (Nitrophenyl)corroles in Nonaqueous Media, *Inorg. Chem.* 57 (2018) 1226–1241. <https://doi.org/10.1021/acs.inorgchem.7b02655>.
- [37] R. Paolesse, L. Jaquinod, D.J. Nurco, S. Mini, F. Sagone, T. Boschi, K.M. Smith, 5,10,15-Triphenylcorrole: A product from a modified Rothmund reaction, *Chem. Commun.* 2 (1999) 1307–1308. <https://doi.org/10.1039/a903247i>.
- [38] P.B. Hitchcock, G.M. McLaughlin, Five-co-ordinate cobalt(III): Crystal and molecular structure of corrole(triphenylphosphine)cobalt(III), *J. Chem. Soc. Dalt. Trans.* (1976) 1927–1930. <https://doi.org/10.1039/DT9760001927>.
- [39] K.E. Thomas, J. Conradie, L.K. Hansen, A. Ghosh, Corroles cannot ruffle, *Inorg. Chem.* 50 (2011) 3247–3251. <https://doi.org/10.1021/ic1017032>.
- [40] Y. Niu, M. Li, Q. Zhang, W. Zhu, J. Mack, G. Fomo, T. Nyokong, X. Liang, Halogen substituted A2B type Co(III)triarylcorroles: Synthesis, electronic structure and two step modulation of electrocatalyzed hydrogen evolution reactions, *Dye. Pigment.* 142 (2017) 416–428. <https://doi.org/10.1016/j.dyepig.2017.02.049>.
- [41] V. Quesneau, W. Shan, N. Desbois, S. Brandès, Y. Rousselin, M. Vanotti, V. Blondeau-Patissier, M. Naitana, P. Fleurat-Lessard, E. Van Caemelbecke, K.M. Kadish, C.P. Gros, Cobalt Corroles with Bis-Ammonia or Mono-DMSO Axial Ligands. Electrochemical, Spectroscopic Characterizations and Ligand Binding Properties, *Eur. J. Inorg. Chem.* 2018 (2018) 4265–4277. <https://doi.org/10.1002/ejic.201800897>.
- [42] B. Li, Z. Ou, D. Meng, J. Tang, Y. Fang, R. Liu, K.M. Kadish, Cobalt triarylcorroles containing one, two or three nitro groups. Effect of NO₂ substitution on electrochemical properties and catalytic activity for reduction of molecular oxygen in acid media, *J. Inorg. Biochem.* 136 (2014) 130–139. <https://doi.org/10.1016/j.jinorgbio.2013.12.014>.
- [43] H. Chen, D.L. Huang, M.S. Hossain, G.T. Luo, H.Y. Liu, Electrocatalytic activity of cobalt tris(4-nitrophenyl)corrole for hydrogen evolution from water, *J. Coord. Chem.* 72 (2019) 2791–2803. <https://doi.org/10.1080/00958972.2019.1671588>.

- [44] X. Liang, Y. Qiu, X. Zhang, W. Zhu, The post-functionalization of Co(III)PPh₃ triarylcorroles through Suzuki-Miyaura couplings and their tunable electrochemically-catalyzed hydrogen evolution and oxygen reduction, *Dalt. Trans.* 49 (2020) 3326–3332. <https://doi.org/10.1039/c9dt04917g>.
- [45] C.M. Lemon, D.K. Dogutan, D.G. Nocera, Porphyrin and Corrole Platforms for Water Oxidation, Oxygen Reduction, and Peroxide Dismutation, in: *Handb. Porphyr. Sci.*, 2012: pp. 1–143. https://doi.org/10.1142/9789814397605_0001.
- [46] A. Friedman, I. Saltsman, Z. Gross, L. Elbaz, Electropolymerization of PGM-free molecular catalyst for formation of 3D structures with high density of catalytic sites, *Electrochim. Acta.* 310 (2019) 13–19. <https://doi.org/10.1016/j.electacta.2019.04.096>.
- [47] W. Tang, Y. Qiu, X. Li, R.C. Soy, J. Mack, T. Nyokong, L. Xu, pH-Dependent Electrochemically Catalyzed Oxygen Reduction Behaviors of o-Substituted Co(III) Corroles, *Macroheterocycles.* 13 (2020) 7–13. <https://doi.org/10.6060/mhc2001831>.
- [48] H. Lei, A. Han, F. Li, M. Zhang, Y. Han, P. Du, W. Lai, R. Cao, Electrochemical, spectroscopic and theoretical studies of a simple bifunctional cobalt corrole catalyst for oxygen evolution and hydrogen production, *Phys. Chem. Chem. Phys.* 16 (2014) 1883–1893. <https://doi.org/10.1039/c3cp54361g>.

CHAPTER 6

CONCLUSION AND FUTURE PROSPECTS

6.1 CONCLUSION

Cobalt corrole complexes have been the subject of attention since the very beginning. This is because, in general, cobalt complexes exist in the Co^{III} oxidation state, but when coordinated in a corrole macrocycle, they exhibit complex redox chemistry. These complexes offer both, metal- and ring-centred reactions depending on the reaction parameters, such as the type and number of substituents on in the *meso*-, β - and axial positions. This fundamental trait has been assessed by the use of various spectroscopic techniques, and all of these characteristics have been proven to be important when used in diverse contexts. We have also focused on one of the series of A₂B-type cobalt corroles. In the first chapter, an in-depth look at the evolution of corroles and metallocorroles has been taken. The importance of these complexes has also been discussed. provides a comprehensive overview of the history and significance of corroles and metallocorroles. In chapter two, the objectives of the current research are explained and justified. In chapter three, we have discussed the synthesis scheme of the A₂B-type bispyridine cobalt corroles. Various characterization techniques through which these were characterized, such as ¹H-NMR, ¹⁹F- NMR, UV-Visible, High Resolution, and Mass Spectrometry have been mentioned along with the data. The single-crystal XRD data of the complex is also displayed. The Pyridine binding properties of all the complexes have been thoroughly studied. Chapter four comprises the study of the interaction and sensing properties of cobalt corroles with fourteen different anions. Three complexes exclusively bind CN⁻, F⁻, and OAc⁻ anions at their

axial positions. The binding constant determination gives the number of binding species (n) >1 at less than one equivalent concentration of anions in the acetonitrile solution of the complex. Although the complexes detect all three anions at less than 1 equivalent of the anion addition, **Co-1** and **Co-2** are more selective towards CH_3COO^- ion, whereas **Co-4** selectively detects the CN^- ion at larger equivalents of these anions. Chapter 5 presents an analysis of the electrochemical characteristics of bis-pyridine cobalt corroles in dichloromethane (DCM), employing TBAP as the supporting electrolyte. With the help of Cyclic voltammetry and DFT calculations, the influence of electron withdrawing or electron donating substituents on the overall potential have been examined. $\text{Co}[(p\text{-NO}_2\text{Ph})_2(2,6\text{-DiFPh})\text{Cor}]\text{PPh}_3$ is successfully synthesized and subsequently characterised through NMR, Mass, and X-ray spectroscopic techniques. The electrochemical study of the considered cobalt corroles is inactive towards the HER process under homogenous conditions.

6.2 FUTURE PROSPECTS

The investigation of A_2B type bispyridine cobalt corroles is unquestionably a step in the right direction towards a better understanding of the characteristics of cobalt corroles. Theoretical calculations into cobalt corroles might be a forward step towards a more in-depth understanding of the characteristics of cobalt corroles. More research into the effects of other axial ligands on cobalt corroles is something that may be noticed. It is possible to see the effect that anions had on the other series of cobalt corrosion products. In addition to this, the efficiency of hydrogen evolution may be seen under heterogeneous conditions. Additional research might be done on the use of cobalt corroles for additional applications, such as ORR, OER, the reduction of CO_2 and so on.

LIST OF PUBLICATIONS

1. **Jyoti**, N. Fridman, A. Kumar, S.G. Warkar, Synthesis, structural characterization and binding ability of A₂B cobalt(III) corroles with pyridine, *Inorganica Chim. Acta.* 527 (2021) 120580. <https://doi.org/10.1016/j.ica.2021.120580>.
2. **Jyoti**, S.G. Warkar, A. Kumar, Study on the interaction of anions with A₂B cobalt corroles in non-aqueous medium, *J. Porphyr. Phthalocyanines.* 26 (2022) 719–731. <https://doi.org/10.1142/S1088424622500560>.
3. **Jyoti**, Churchill D., Gross Z., Warkar SG and Kumar A., Synthesis and Applications of Cobalt Corroles. (To be Submitted)
4. **Jyoti**, Warkar SG and Kumar A., Hydrogen Evolution Activity of Cobalt Corroles? (Under revision)
5. A. Varshney, D. Ahluwalia, R. Kubba, **Jyoti**, A. Kumar, Recent developments in corroles as an ion sensor, *J. Indian Chem. Soc.* 99 (2022) 100708. <https://doi.org/10.1016/j.jics.2022.100708>.
6. R. Kubba, M. Kumar Singh, **Jyoti**, O. Yadav, A. Kumar, Förster resonance energy transfer (FRET) between CdSe quantum dots and ABA phosphorus(V) corroles, *Spectrochim. Acta - Part A Mol. Biomol. Spectrosc.* 291 (2023) 122345. <https://doi.org/10.1016/j.saa.2023.122345>.
7. S. Kumar, **Jyoti**, D. Gupta, A. Kumar G. Singh, A Decade of Exploration of Transition-Metal-Catalyzed Cross-Coupling Reactions: An Overview, Synopen Thieme (Accepted)

CONFERENCES AND WORKSHOPS

1. Presented Poster at “Indian Analytical Congress (IAC-2019), an **International Conference** jointly Organised by Indian Society of Analytical Scientists, Delhi Chapter & FICCI during 12-14 December, 2019.
2. Presented Poster in the **International Conference** on Chemistry for sustainable Development organised by Dept. of Chemistry, Central University of Jharkhand, Ranchi, India, held from 2nd to 4th July 2021.
3. Participated in Virtual Conference on ‘Recent Advances in Bis and Tetra-Pyrrolic Molecular Materials’ organized by Department of Chemistry, Central University of Kerala during 24-26th August, 2020.
4. Attended Workshop on Computational Chemistry of Materials: Molecule, Solids, Nanoparticles and Biological Activity (CCM-2022) organised by Centre for Advanced Computational Chemistry Studies, Delhi held from 19th – 25th October, 2022.
5. Participated in five-day online short term course on “Electrochemistry-Fundamentals and Applications in Engineering (EFA22)” organized by Department of Chemical Engineering, NIT Rourkela held from 23rd – 27th December, 2022.

ABOUT THE AUTHOR

Name: Jyoti

Father's Name: Dharpal Singh

Mother's Name: Sunita

Nationality: Indian



The author completed her schooling from Hardayal Public School, Bahadurgarh, Haryana. She then pursued her bachelor's degree in Chemistry from the University of Delhi and her master's degree from Maharishi Dayanand University. She qualified the CSIR-UGC-NET JRF exam in Chemical Sciences in 2017 and joined DTU as a CSIR-JRF in 2018. She started her Ph.D. journey in July 2018 under the supervision of Prof. Sudhir G. Warkar and Prof. Anil Kumar at the Department of Applied Chemistry, DTU. Her research work revolves around the synthesis and applications of Cobalt corroles. During her Ph.D., she received a commendable research excellence award, in year 2021, from Delhi Technological University. She has also presented her research work at both National and International conferences during her Ph.D. tenure. She wishes to work as an academician along with exploring the wider perspectives of macrocyclic chemistry in her future.